Statistical Mechanics of Self-Avoiding Tethered Membranes

by

Damin Liu

B.Sc., University of Science and Technology of China, 1984

M.Sc., Simon Fraser University, 1987

A THESIS SUBMITTED IN PARTIAL FULFILLMENT
OF THE REQUIREMENTS FOR THE DEGREE OF
DOCTOR OF PHILOSOPHY
in the Department
of
Physics

SIMON FRASER UNIVERSITY
October 1992

ISBN 0-315-91070-4

APPROVAL

Name: Damin Liu

Degree: Doctor of Philosophy

Title of thesis: Statistical Mechanics of Self-Avoiding Tethered Membranes

Examining Committee: Dr. Barbara J. Frisken
Chair

Prof. Michael Plischke
Senior Supervisor

Prof. Leslie E. Ballentine

Prof. David H. Boal

Prof. Michael Wortis

Dr. Daniel M. Kroll
External Examiner
Research Staff Member
Institut für Festkörperforschung
KFA Jülich
Germany

Date Approved: October 30, 1992

PARTIAL COPYRIGHT LICENSE

I hereby grant to Simon Fraser University the right to lend my thesis, project or extended essay (the title of which is shown below) to users of the Simon Fraser University Library, and to make partial or single copies only for such users or in response to a request from the library of any other university, or other educational institution, on its own behalf or for one of its users. I further agree that permission for multiple copying of this work for scholarly purposes may be granted by me or the Dean of Graduate Studies. It is understood that copying or publication of this work for financial gain shall not be allowed without my written permission.

Title of Thesis/Project/Extended Essay

Statistical Mechanics of Self-Avoiding Tethered Membranes

Author:

(signature)

DAMIN LIU

(name)

Nov. 25, 1992

(date)

ABSTRACT

I report the results of Monte Carlo studies on self-avoiding tethered membranes. Similar to one-dimensional polymers, two-dimensional tethered membranes have the essential feature that at moderate temperatures the crosslinks between the constituent particles remain in place. The conformation of the membranes in equilibrium is the focus of these studies.

Analytical calculations for the tethered membranes are first reviewed. I start with the generalized Edwards Hamiltonian for a D-dimensional manifold ($D = 1$ for polymers and $D = 2$ for membranes) embedded in d-dimensional space and perform dimensional analysis. The concept of upper critical dimension (above which self-avoidance is irrelevant) is introduced and a generalized Flory theory is constructed. I describe a perturbative renormalization-group analysis which treats the excluded-volume effect as a perturbation to an ideal manifold. The theory, at the lowest order of expansion, predicts a crumpled phase for self-avoiding tethered membranes.

I have performed Monte Carlo simulations on a model tethered membrane embedded in three-dimensional space. Two studies are reported in this thesis. The role of self-avoidance in determining the shape of tethered membranes at infinite temperature is first studied by varying the diameter of the particles on the network. For the strongly self-avoiding membranes, we find a flat but rough phase: The sizes of the network in the two long directions scale linearly with the maximum linear size of the network while the size in the short direction scales with this maximum size with an exponent smaller than 1. There is no evidence for the existence of a crumpled phase. For the weakly self-avoiding membrane, the study suggests that, for any finite diameter, self-avoiding membranes are flat in three dimensions in the thermodynamic limit.

I have also studied a model tethered membrane in which the particles interact

through hard-core repulsion as well as a longer range attractive potential. As the temperature is decreased, the membrane undergoes a phase transition from the usual high-temperature flat phase to a low-temperature crumpled phase. The crumpled phase, which seems to exist over a range of temperatures, is isotropic and is characterized by a fractal dimension close to the Flory estimate $D_{\mathrm{f}} = 2.5$. At still lower temperatures the membrane is in a collapsed phase.

ACKNOWLEDGEMENTS

First and foremost, I would like to thank my academic supervisor, Professor Michael Plischke. I thank him, first of all, for being a friend who is caring and understanding. During the years of my graduate studies, he has always been there for me when I needed his support and advice in times of difficulty.

I feel extremely lucky to have been his student: He is accessible and very helpful, patient and always encouraging. He guided me, every step of the way, not only in the thesis research but also in preparing for the future. And he did so with great care and support. My working with him has been a most pleasant experience.

I am grateful to Professor David H. Boal for his generosity in providing me with his program for analyzing data and his other help in my thesis research.

A special thank is given to Dr. Edward Levinson for useful discussions and for the moral support from him in the final days of my graduate studies.

I would also like to thank my friends who have made my life, on and off campus, so much more enjoyable.

Finally, I express my deepest gratitude to my wife for her constant support.

The financial support from Simon Fraser University and a scholarship from the University of Science and Technology of China are gratefully acknowledged.

Dedicated to my mother and father.

Contents

List of Tables

List of Figures

Chapter 1

Introduction

Membranes are thin and highly flexible surfaces found in various branches of science, such as biology, chemistry, engineering, physics, and interdisciplinary sciences [1, 2]. For example, bilayer membranes composed of amphiphilic lipid molecules are found naturally in most biological systems such as cells. Other membranes, such as surfactant bilayers, can be found in chemical solutions.

Physical studies of membranes have focussed on their conformational behavior. These studies are necessarily done on a length scale large compared to the size of constituent molecules and, thus, the details of the molecules on short length scales can be ignored. On such a length scale, membranes can be regarded as two-dimensional surfaces embedded in three-dimensional space and undergoing thermally excited fluctuations in this space.

A biological membrane such as a red blood cell membrane is very complex, having many different structural components. The simplest model membrane may be a lipid bilayer which resembles the most elementary component of a biological membrane and can be prepared artificially in the laboratory by dispersing amphiphilic biological lipids in aqueous fluids. This two-dimensional system can exhibit a variety of phases, corresponding to different states of the internal degrees of freedom associated with

the in-plane translational motion of the constituent molecules. For example, the bilayer may exhibit liquid crystalline and hexatic phases at low temperatures. At high temperatures, the membrane is in the fluid phase, in which the molecules diffuse freely within the plane with zero shear modulus. Such a membrane, referred to as a fluid membrane, shows large out-of-plane shape fluctuations in the absence of external lateral forces. Since these membranes do not resist shear, it is generally believed that surface conformations are governed only by the bending rigidity. A surface which has only a bending rigidity is characterized by a persistence length, defined to be the distance over which unit vectors normal to the surface become uncorrelated [3, 4]. This persistence length is a rapidly varying function of temperature,

$$\xi_p \approx a \exp(c\kappa/k_B T) ,$$

where a and c are constants and κ is the bending rigidity. This formula for the persistence length was derived from a linear theory. A more detailed renormalization-group analysis [5, 6] has shown that short-wavelength transverse undulations significantly reduce the effective bending rigidity of the membrane on length scales large compared to the persistence length. Thus, when viewed on a length scale larger than the persistence length, the membranes may appear convoluted or crumpled.[1]

Polymerized membranes are quite different from liquid membranes. The constituent molecules (or more generally, monomers) of polymerized membranes are tethered together to form a network of a certain connectivity. With this crosslinking, in-plane fluid phases are no longer possible. An example of such a network can be found in red blood cells [10]. Under the bilayers of the cells, there exists a cytoskeleton composed of protein spectrins knotted by actins at the vertices of the network. This network is anchored to the lipid bilayers of the cells through ankyrins and can be isolated in the laboratory. The essential point of distinction between this network

[1]Self-avoiding fluid membranes are difficult to study analytically. Early computer simulation [7] indicated that a self-avoiding fluid vesicle was crumpled. Other recent simulations [8, 9] suggest that for zero bending rigidity a self-avoiding fluid membrane behaves like a branched polymer.

and a liquid membrane is that at moderate temperatures the connections between the spectrin chains remain in place.

The connectivity of polymerized networks can be considered fixed on the time scale on which shape fluctuations take place, and this is an essential feature of polymerized membranes. Polymerized membranes may be regarded as thin elastic sheets. Bending and stretching of a polymerized membrane induce a surface tension which strongly suppresses the out-of-plane fluctuations. In fact, even for a fluid membrane, it can be shown that on applying a lateral tension the out-of-plane fluctuations are drastically reduced [2, and references therein]. The geometric constraints imposed by the network are responsible for the significantly different behavior of tethered membranes as compared with fluid membranes [11].

While there have been few experiments on polymerized (or tethered) membranes, extensive analytical and numerical studies have been carried out during the past few years. In this thesis I discuss some of these studies as well as my own.

1.1 Linear polymers and the Flory theory

Two-dimensional polymerized membranes are natural generalizations of one-dimensional polymers. I will in this section first review some of the properties of linear polymers[2] that are relevant to my thesis. Linear polymers are formed by interconnecting a large number of monomers into a linear structure. Each monomer unit is a group of molecules.

Consider a polymer chain embedded in a d-dimensional space. One of the simplest idealizations of a flexible polymer chain is a non-self-avoiding (ideal) random walk on a lattice (eg. see Fig. 1.1). A polymer of degree of polymerization, N, then becomes a random walk of N steps. Denote by $\hat{\mathbf{a}}_i$ the i-th step of the walk. All steps are

[2]Reference: [12].

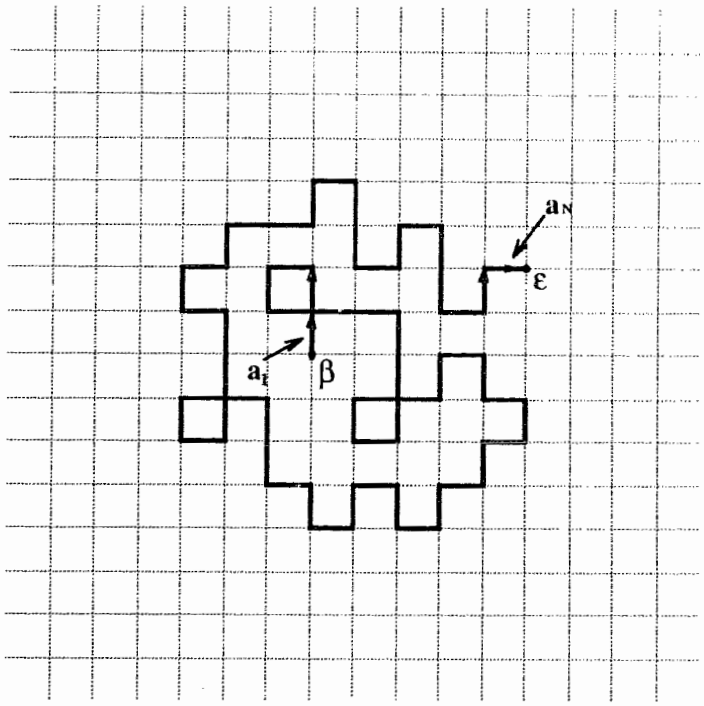

Figure 1.1: A random walk on a square lattice. The walk, starting from site β, steps toward any of the four nearest neighbors with equal probability and ends up at some random location ϵ on the lattice after N steps. All steps, denoted by $\hat{\mathbf{a}}_i$, $i = 1, 2, \cdots, N$, are uncorrelated.

uncorrelated and $\langle \hat{\mathbf{a}}_i \cdot \hat{\mathbf{a}}_j \rangle = \delta_{ij} a^2$ where a is the step size. The angular brackets denote an average over configurations. The position of the walk at the i-th step is simply $\vec{\mathbf{r}}_i = \hat{\mathbf{a}}_1 + \hat{\mathbf{a}}_2 + \cdot + \hat{\mathbf{a}}_i = \sum_{l=1}^{i} \hat{\mathbf{a}}_l$. The radius of gyration of the walk, R_g, is defined as

$$
\begin{aligned}
R_g^2 &\equiv \frac{1}{N^2} \left\langle \sum_{i<j}^{N} (\vec{\mathbf{r}}_i - \vec{\mathbf{r}}_j)^2 \right\rangle \qquad (1.1) \\
&= \frac{1}{N^2} \left\langle \sum_{i<j}^{N} \left(\sum_{l=1}^{i} \hat{\mathbf{a}}_l - \sum_{l=1}^{j} \hat{\mathbf{a}}_l \right)^2 \right\rangle = \frac{1}{N^2} \left\langle \sum_{i<j}^{N} \left(\sum_{l=1}^{j-i} \hat{\mathbf{a}}_{i+l} \right)^2 \right\rangle \\
&= \frac{1}{N^2} \sum_{i<j}^{N} (j-i) a^2 = \frac{a^2}{N^2} \sum_{j=1}^{N} j(j-1)
\end{aligned}
$$

$$= \frac{a^2}{N^2}\left[\frac{1}{6}N(N+1)(2N+1) - \frac{1}{2}N(N+1)\right]$$

$$= \frac{a^2}{6N}(N^2-1) \overset{N\to\infty}{\simeq} \frac{Na^2}{6} .$$

The end-to-end distance (between ends β and ϵ in Fig. 1.1), R_0, can be similarly obtained,

$$R_0^2 \equiv \left\langle (\vec{\mathbf{r}}_N - \vec{\mathbf{r}}_0)^2 \right\rangle = \left\langle \sum_l^N \hat{\mathbf{a}}_l \cdot \sum_m^N \hat{\mathbf{a}}_m \right\rangle = \sum_{l,m}^N \langle \hat{\mathbf{a}}_l \cdot \hat{\mathbf{a}}_m \rangle = Na^2 , \tag{1.2}$$

and we see that R_0 has the same scaling behavior as the radius of gyration. In contrast to this behavior, a fully directed or stretched 'random' walk has the behavior $R_0 \sim N$, whereas an unconstrained random walk has $R_0 \sim N^{1/2}$, with an exponent less than 1. We call the conformation of the random walk *crumpled.*

The conformation of an ideal random walk is self-similar in the sense that a segment of the chain behaves the same statistically as any other part of the chain. In particular, if we group g consecutive steps into subunits, as shown in Fig. 1.2, each subunit is then of size $\sqrt{g}a$ according to (1.2). The end-to-end distance of the chain should be invariant under coarse-graining, and (1.2) shows that it is,

$$R_0^2\,(N/g, \sqrt{g}a) = \left(\frac{N}{g}\right)(\sqrt{g}a)^2 = R_0^2(N,a) = Na^2 .$$

Clearly, such a grouping procedure can be carried out repeatedly. This is exactly the Kadanoff block-spin transformation. If the coarse-grained chain is appropriately shrunk, then, at least statistically, the resultant chain looks similar to a portion of the original chain. This scaling transformation combined with the Kadanoff transformation is called the renormalization-group (RG) transformation. In the language of the RG theory, we may say that the ideal random walk is characterized by a fixed point which gives an exponent $\nu_0 = 1/2$ where $R_0 \sim N^{\nu_0}$.

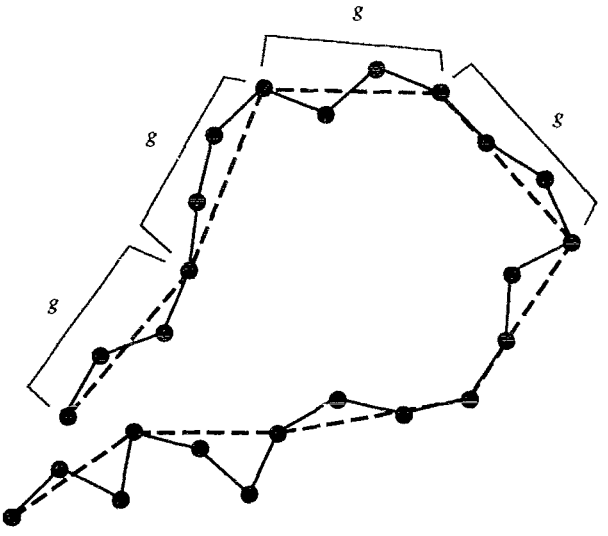

Figure 1.2: Grouping random-walk steps into subunits. Every g consecutive steps are grouped together to form a subunit and each subunit is of size $\sqrt{g}a$. The solid lines represent the steps of a random walk and the bullets mark the joints of the chain. The dashed lines represent the subunits. The end-to-end distance of the chain is invariant under this grouping procedure.

The entropy of such a random walk can also be calculated exactly. The entropy $S(\vec{\mathbf{r}})$ associated with all chain conformations starting from an origin and ending at a distance $\vec{\mathbf{r}}$ is related to the number of routes, $\mathcal{N}(\vec{\mathbf{r}})$, that the random walker can take in going from the origin to $\vec{\mathbf{r}}$ in N steps

$$S(\vec{\mathbf{r}}) = k_B \ln \mathcal{N}(\vec{\mathbf{r}}) \tag{1.3}$$

where k_B is the Boltzmann constant. Since all directions of the random walk are completely uncorrelated, $\mathcal{N}(\vec{\mathbf{r}})$ can be written as the product of d one-dimensional binary distribution functions which approach Gaussian distributions when N is large. Thus we have $\mathcal{N}_N(\vec{\mathbf{r}}) \sim \exp\left[-dr^2/\left(2R_0^2\right)\right]$ and $S(\vec{\mathbf{r}}) = S(\vec{\mathbf{0}}) - k_B dr^2/(2R_0^2)$. If the internal energy E of the polymer is constant, the free energy can be written as

$$F(r) = E - TS = F(0) + k_B T \frac{dr^2}{2R_0^2}\,, \tag{1.4}$$

and, formally, an ideal polymer behaves like a spring with a spring constant proportional to temperature T.

These properties of an ideal polymer are universal properties of a Markov chain and do not depend on the binding potential between the neighboring monomers of the chain. If we take into account only the interactions between neighboring monomers in the chain, such as those which restrict the angles or provide bending forces between successive bonds, and ignore interactions between monomers far apart in their sequence in the chain, as we have done for ideal polymers, we will always get the same properties, whatever the microscopic structure of the chain is. This can be clearly seen from the Kadanoff transformation. If we choose the subunits large enough so that the neighboring subunits are separated by a distance greater than the correlation length of the monomers, the chain can be treated as an ideal polymer consisting of independent subunits. Our previous results remain valid if we replace a by an effective length of the subunits and replace N by the number of the subunits.

When such a coarse graining is done for a chain and the chain is then treated as an ideal chain, the free energy can be written as a sum of the contributions from the subunits,

$$F = \frac{1}{2}\kappa_0 \sum_x [\vec{\mathbf{r}}(x+c) - \vec{\mathbf{r}}(x)]^2 \ , \tag{1.5}$$

where $\kappa_0 = k_B T d/c^2$, x is the index of a subunit and c is the distance between neighboring units. Since we are not interested in things happening on the scale of monomers, for simplicity of analysis we adopt a continuum version of (1.5),

$$F = \frac{1}{2}\kappa \int dx \left(\frac{d\vec{\mathbf{r}}}{dx}\right)^2 \ . \tag{1.6}$$

The validity of the above results depends on the omission of interactions between monomers far apart in the chain sequence. While this is perfectly appropriate for an ideal polymer, it is incorrect for a real polymer in which no two monomers can overlap regardless of their sequence in the chain. In other words, although the interactions

between neighboring monomers are of short range in space, they are of long range in terms of distance along the chain. The idea of a RG analysis, however, still applies in this case. In Chapter 2, I shall discuss perturbative RG approach for polymers and membranes.

For a real polymer, one would expect its radius of gyration to be greater than that of an ideal polymer ($R_g \sim N^\nu$ with $\nu \geq 1/2$) and its entropy to be smaller than the entropy for an ideal polymer, as a result of the excluded-volume effects due to self-avoidance. However, the hard-core repulsion is not the only interaction present between monomers. The interaction between monomers is an effective one mediated by the solvent. Monomers interact with each other through van der Waals potential and attract each other at larger distances. There may be screened Coulomb interactions as well. In a mean-field type theory, Flory [12, 13] calculated the effective pair interaction between monomers. This effective interaction is found to be, in most experimental situations, an increasing function of temperature. The effective interaction is repulsive in a 'good' solvent and is attractive in a 'poor' solvent at experimentally relevant temperatures. At a particular temperature, $T = \theta$, the short-range effective repulsion and van der Waals attraction between monomers overcome each other and the effective interaction vanishes. A polymer chain is nearly ideal (quasi ideal) at this temperature θ which is referred to as the (Flory) θ-point. For a polymer chain in a good solvent, Flory devised a scheme to find the scaling behavior of the chain. He constructed two terms for the total free energy of a polymer. One of these terms is the free energy contributed by entropic effects. In the Flory scheme, this term is simply borrowed from (1.4) for the ideal polymer chain. The other term is the effective repulsive energy. The situation of a chain in poor solvent is more complicated than this and we shall not discuss it until in Chapter 5.

Consider a polymer occupying a certain volume in a d-dimensional embedding space. The linear size of this volume is R_g and c is the local concentration of

monomers ($c \cong N/R_g^d$). The repulsive energy is proportional to the probability that two monomers occupy the same space of unit volume, namely c^2, and to the strength of effective repulsion v. The total repulsive energy is the integration of $\frac{1}{2}vT\langle c^2\rangle$ over a volume R_g^d. If we ignore fluctuations in concentration c (a typical mean field theory approach), $\langle c^2\rangle$ can be written as $\langle c\rangle^2 \sim \left(N/R_g^d\right)^2$, and the total repulsive energy is given by $\frac{1}{2}vTN^2/R_g^d$. The total free energy is, therefore,

$$F_{\text{total}} = k_B T \frac{dR_g^2}{2R_0^2} + T\frac{vN^2}{2R_g^d} , \tag{1.7}$$

where R_0 is the end-to-end distance for the polymer chain when the interaction is ignored. The two terms in (1.7) compete with each other: The repulsive energy favors a large R_g and the entropy term favors the opposite. The competition results in an R_g which minimizes the total free energy. We carry out the minimization and obtain the formula

$$R_g \sim N^\nu ,$$

where

$$\nu = \frac{3}{d+2} . \tag{1.8}$$

The Flory formula works remarkably well for polymers for all d dimensions ($d \leq 4$) despite its apparent deficiencies and the fact that a mean-field theory neglects fluctuations and usually does not yield accurate values for exponents. It is exact for $d = 1$, $d = 2$ [14], and is within a percent of the most accurate numerical results for $d = 3$. The Flory formula can also be used to predict correctly the upper critical dimension of an embedding space, i.e., the dimension above which a self-avoiding polymer behaves just like an ideal polymer. Such good agreement is considered unfortunate by some people, who argue that it delayed the progress of polymer physics [15]. I shall discuss the topic of upper critical dimensions and revisit the Flory prediction in Chapter 2.

1.2 The tethered membrane model

1.2.1 The Gaussian network

Consider first a 'phantom' membrane network of a certain connectivity in which only nearest-neighbor (NN) monomers interact with each other. The Hamiltonian of the network in this approximation is

$$\mathcal{H} = \sum_{i,j\,(\mathrm{NN})} \mathrm{V}\left(|\vec{\mathbf{r}}_i - \vec{\mathbf{r}}_j|\right) = \sum_{i,j\,(\mathrm{NN})} \mathrm{V}\left(r_{ij}\right) \ , \tag{1.9}$$

where V is some interaction potential.

A natural generalization of an ideal linear polymer is a network of springs in which $\mathrm{V}(r_{ij}) = \kappa r_{ij}^2/2$ and

$$\mathcal{H} = \frac{1}{2} \sum_{i,j\,(\mathrm{NN})} \kappa \left(\vec{\mathbf{r}}_i - \vec{\mathbf{r}}_j\right)^2 \ . \tag{1.10}$$

It is convenient to work with the continuum version of the above expression for a D-dimensional Gaussian network,

$$\mathcal{H} = \frac{1}{2}\kappa \int d^D\mathbf{x}\, (\nabla\vec{\mathbf{r}})^2 \tag{1.11}$$

where

$$(\nabla\vec{\mathbf{r}})^2 = \sum_{i=1}^{D} \left(\frac{\partial\vec{\mathbf{r}}}{\partial x_i}\right)^2 \tag{1.12}$$

and the D-dimensional vector $\mathbf{x} = (x_1, x_2, \ldots, x_D)$ is the position of an element in the internal space of the network. In this thesis, I use boldface to denote a vector in the internal space, whereas a vector in the external (embedding) space is denoted by the conventional notation—an arrow on top of a letter.

For the Gaussian network with the Hamiltonian (1.11), one can easily calculate the end-to-end (or side-to-side, more precisely) distance and the radius of gyration of the network. For calculating the root-mean-square separation in the embedding space

for two points $\mathbf{x}$ and $\mathbf{x}'$ on the network, it is convenient to introduce the generating function,

$$\begin{aligned}\Phi(\vec{\mathbf{k}},\mathbf{x},\mathbf{x}') &= \left\langle \exp\left\{i\vec{\mathbf{k}}\cdot[\vec{\mathbf{r}}(\mathbf{x})-\vec{\mathbf{r}}(\mathbf{x}')]\right\}\right\rangle \\ &= \frac{1}{\mathcal{Z}_0}\int \mathcal{D}\vec{\mathbf{r}}\,\exp\left\{i\vec{\mathbf{k}}\cdot[\vec{\mathbf{r}}(\mathbf{x})-\vec{\mathbf{r}}(\mathbf{x}')]\right\}\exp\left(-\beta\mathcal{H}\right)\,, \qquad (1.13)\end{aligned}$$

where $\mathcal{Z}_0$ is the partition function,

$$\mathcal{Z}_0 = \int \mathcal{D}\vec{\mathbf{r}}\,\exp\left(-\beta\mathcal{H}\right)\,, \qquad (1.14)$$

and where the integration is over all possible configurations of the membrane network. Henceforth, we set $\beta = 1$ for convenience.

More generally, one can show [16] that

$$\begin{aligned}\left\langle \exp\left[i\int d^D\mathbf{x}\,\vec{\mathbf{k}}(\mathbf{x})\cdot\vec{\mathbf{r}}(\mathbf{x})\right]\right\rangle &= \frac{1}{\mathcal{Z}_0}\int\mathcal{D}\vec{\mathbf{r}}\,\exp\left\{-\int d^D\mathbf{x}\left[\frac{1}{2}\kappa(\nabla\vec{\mathbf{r}})^2 - i\vec{\mathbf{k}}(\mathbf{x})\cdot\vec{\mathbf{r}}(\mathbf{x})\right]\right\} \\ &= \frac{1}{2\kappa}\int d^D\mathbf{x}\,d^D\mathbf{y}\,\mathrm{G}_D(\mathbf{x}-\mathbf{y})\,\vec{\mathbf{k}}(\mathbf{x})\cdot\vec{\mathbf{k}}(\mathbf{y})\,, \qquad (1.15)\end{aligned}$$

where

$$\mathrm{G}_D(\mathbf{x}) = -\int\frac{d^D\boldsymbol{\theta}}{(2\pi)^D}\frac{e^{i\boldsymbol{\theta}\cdot\mathbf{x}}}{\boldsymbol{\theta}^2} \qquad (1.16)$$

is a Green's function satisfying

$$\nabla^2\mathrm{G}_D(\mathbf{x}) = \delta^D(\mathbf{x})\,. \qquad (1.17)$$

$\mathrm{G}_D(\mathbf{x})$ is exactly like the Coulomb potential in D-dimensional space. The solution has spherical symmetry and therefore $\mathrm{G}_D(\mathbf{x}) = \mathrm{G}_D(x)$ where $x = |\mathbf{x}|$.

Using (1.15), we can write $\Phi(\vec{\mathbf{k}},\mathbf{x},\mathbf{x}')$ as

$$\Phi(\vec{\mathbf{k}},\mathbf{x},\mathbf{x}') = \exp\left[-\frac{k^2}{\kappa}\mathrm{G}_D(\mathbf{x}-\mathbf{x}')\right]\,. \qquad (1.18)$$

Integrating both sides of (1.17) over a hypersphere of linear size y and applying Gauss' law, we find

$$1 = \int_V d^D\mathbf{x}\nabla^2\mathrm{G}_D(\mathbf{x}) = \int_S d\mathbf{S}\cdot\nabla\mathrm{G}_D(\mathbf{x}) = S_D y^{D-1}\frac{d\mathrm{G}_D(y)}{dy}\,.$$

Thus,

$$\mathrm{G}_D(x) = \int^x \frac{d\mathrm{G}(y)}{dy} dy = \frac{1}{S_D} \int^x y^{1-D} dy = \frac{1}{S_D(2-D)} |x|^{2-D} \tag{1.19}$$

for $D \neq 2$, where $S_D = 2\pi^{D/2}/\Gamma(D/2)$ is the surface area of a D-dimensional unit hypersphere. For $D = 2$, the integral is well defined and $\mathrm{G}_D(x) = \frac{1}{S_D} \ln |x|$.

The average-squared distance is given by

$$\left\langle [\vec{\mathbf{r}}(\mathbf{x}) - \vec{\mathbf{r}}(\mathbf{x}')]^2 \right\rangle = -\nabla_{\vec{\mathbf{k}}}^2 \, \Phi(\vec{\mathbf{k}}, \mathbf{x}, \mathbf{x}') \Big|_{\vec{\mathbf{k}}=0} \, . \tag{1.20}$$

By using (1.18) and (1.19), we derive the two-point distance,

$$\left\langle |\vec{\mathbf{r}}(\mathbf{x}) - \vec{\mathbf{r}}(\mathbf{x}')|^2 \right\rangle = \frac{2d}{\kappa} \mathrm{G}_D(\mathbf{x} - \mathbf{x}') \tag{1.21}$$

$$= \frac{2d}{S_D(2-D)\kappa} |\mathbf{x} - \mathbf{x}'|^{2-D} \, . \tag{1.22}$$

From this formula, we observe that the average distance between two points near opposite sides on the boundary, in analogy with the end-to-end distance in a polymer, scales like $R \sim L^{(2-D)/2}$. One can easily show that the radius of gyration of a manifold of linear size L scales in the same way for large L,

$$R_g^2(L) = \frac{1}{L^{2D}} \iint d^D\mathbf{x} \, d^D\mathbf{x}' \left\langle [\vec{\mathbf{r}}(\mathbf{x}) - \vec{\mathbf{r}}(\mathbf{x}')]^2 \right\rangle \tag{1.23}$$

$$\sim \frac{L^{2-D}}{\kappa(2-D)} \sim L^{2\nu_0} \, .$$

Thus,

$$\nu_0 = \frac{2-D}{2} \, . \tag{1.24}$$

For a membrane ($D = 2$), $\nu_0 = 0$ and $R_g \sim (\ln L)^{1/2}$.

One naturally asks whether or not the scaling law for the radius of gyration of a Gaussian network is universal, i.e., independent of the nature of the interactions, as in the case for polymers. In the same spirit of coarse-graining, a Migdal-Kadanoff renormalization-group analysis was carried out by Kantor *et al.* [17]. They found

numerically that several central-force potentials converge to a Gaussian spring potential under renormalization. For these potentials, at least, the aforementioned scaling behavior is universal. The Gaussian network may, therefore, be considered a generic model for non-self-avoiding membranes.

1.2.2 Self-avoiding network and bounds on the exponent ν

Most studies of tethered membranes have focused on the possible phases of membranes and the exponent ν which governs the scaling behavior of the radius of gyration. The value of the exponent ν is bounded by physical limits. Consider a D-dimensional manifold. When it is fully stretched, the radius of gyration R_g scales as L which is the linear size of the manifold. When the manifold has the most compact conceivable isotropic conformation in d-dimensional space, its mass occupies a volume of R_g^d in the embedding space, namely $L^D \sim R_g^d$. Thus $R_g \sim L^{D/d}$. The value of ν is therefore bounded by the exponents for these two limiting cases, $D/d \leq \nu \leq 1$. Clearly, the Flory prediction for polymers [(1.8)] satisfies these bounds. For a membrane in three-dimensional space, ν is bounded by a lower limit of $2/3$ and an upper limit of 1. Previous researchers have found a flat phase with $\nu = 1$ and a collapsed phase with $\nu = 2/3$. The crumpled phase with an intermediate exponent was not observed numerically before my simulations.

The fact that a collapsed phase is achieved by computer simulation is highly nontrivial, since the numerous constraints on a tethered surface make it very difficult to compress such an object. Kantor *et al.* [17] carried out a 'table-top experiment' by crumpling sheets of foil and measured the exponent ν. They found that a crumpled phase with $\nu \approx 0.8$, close to the generalized Flory prediction (see Chapter 2), is generally achieved by randomly crumpling the sheets. Only an 'intelligent' folding procedure will yield a collapsed phase. It should be pointed out that such a table-top experiment uses an irreversible process to produce the 'crumpled' phase and, thus, is

not necessarily indicative of what happens in an equilibrium process.

The Hamiltonian of a self-avoiding network is usually taken to be the Edwards model [18],

$$\mathcal{H} = \frac{1}{2}\kappa \int d^D\mathbf{x}\,(\nabla\vec{\mathbf{r}})^2 + \frac{1}{2}v \iint_{|\mathbf{x}_1-\mathbf{x}_2|\geq a} d^D\mathbf{x}_1\, d^D\mathbf{x}_2\, \delta^d\left[\vec{\mathbf{r}}(\mathbf{x}_1) - \vec{\mathbf{r}}(\mathbf{x}_2)\right] . \qquad (1.25)$$

The lower cutoff parameter a eliminates the unphysical self-intersections and represents the microscopic scale of description of the network. If we change a, other parameters in the Hamiltonian should be readjusted accordingly. This point will become clear when I discuss renormalization-group analysis in Chapter 2.

1.3 Some studies on tethered membranes

In early work on the tethered membrane, Kantor, Kardar, and Nelson [19] studied a 'phantom' membrane model with bending rigidity in which excluded-volume effects are neglected except for nearest neighbors. The effects of bending rigidity for a phantom membrane prove to be drastically different from what they would be for polymers. Bending rigidity favors a flat phase, while the entropy effect favors a crumpled phase. Kantor *et al.* found a high-temperature crumpled phase with $R_g \sim (\ln L)^{1/2}$, consistent with the result for a Gaussian membrane, and a low-temperature flat or stretched phase with $R_g \sim L$ ($\nu = 1$), which is not present for linear polymers. In the case of polymers, bending rigidity modifies the persistence length but does not give rise to a stretched phase.

The excluded-volume effect, in fact, is the most important factor in determining the shape of a membrane. Contrary to the earlier belief that a self-avoiding membrane was crumpled in the absence of bending rigidity, more extensive computer simulations [20, 21, 22, 23, 24], including my own which I shall report in this thesis, showed that a self-avoiding membrane is always flat when in equilibrium, at least for particles with sufficiently large hard cores. In fact, for such a membrane embedded in three

dimensional space, it is found that the membrane may be flat no matter how small the hard cores. In higher embedding dimension the situation is less clear, and there is some indication that self-avoiding membranes may crumple for $d \geq 5$ [25]. These results are in marked contrast to the predictions of the Flory theory described above. This will be discussed further in Chapter 2.

The effects of the tethering constraints on the entropy have been studied by randomly cutting a fraction of the bonds to reduce the geometrical constraints [26, 27]. The entropy of the membrane is increased in the process and, therefore, the possibility of a crumpled phase is enhanced. These studies showed that a membrane remains flat up to the point where it falls apart at the site or bond percolation point, indicating that connectivity is an essential feature of tethered membranes.

Other studies have been carried out on the effect of long-range interactions between particles on the network [28, 29]. After all, physical membranes or solid sheets cannot be described only in terms of connectivity and hard-core interactions. One expects that the particles on the network will interact through van der Waals or screened Coulomb interactions at longer distances, and such interactions, if attractive, will at sufficiently low temperatures overcome the effective bending rigidity due to the hard cores and lead to a collapsed or crumpled phase.

Concurrently with my research [29], Abraham and Kardar studied [28] self-avoiding membranes with van der Waals interactions between particles using the molecular dynamics technique. At high temperatures they found that the membrane is flat. At intermediate temperatures the membrane folds once onto itself. On further cooling a doubly-folded configuration develops. The membrane undergoes successive folding transitions towards the fully collapsed phase at very low temperatures.

I studied (see Chapter 5) a tethered membrane model in which the particles on the network interact through a potential which is hard-core repulsive and square-well attractive. This interaction potential differs in form and range from the interaction

used in Ref. [28]. My Monte Carlo simulations indicate a transition from the flat phase to an isotropically crumpled phase as the temperature is lowered. This crumpled phase is characterized by an exponent very close to the Flory prediction and seems to persist over a range of temperatures. At very low temperatures, a collapsed phase is found.

These results are consistent with recent experimental data. Hwa *et al.* [30] and Wen *et al.* [31] performed experiments on carefully prepared exfoliated sheets of graphite oxide (GO). In these experiments, sheets of GO were suspended in aqueous solutions at different pH and the structure factor was obtained by light scattering measurements. Remarkably, the exponent ν remained constant at roughly the Flory value for a considerable range of pH, analogously to the persistence of the crumpled phase observed in our simulation for a range of temperatures. These workers also found a collapsed phase with fractal dimension $D_f = 3$ when the sheets were suspended in an acetone solution, in which the effective intrasheet interaction was presumably stronger.

Our work is complementary to that of Abraham and Kardar [28]. Although we see evidence of folding in isolated configurations in our simulation, we have not been able to identify equilibrium states characterized by a discrete number of folds, or a sequence of folding transitions.

1.4 Organization of the thesis

In this thesis, I shall report the results of the research which I have done on the properties of self-avoiding tethered membranes. In Chapter 2, I review some of the analytical calculations for the tethered membranes. I shall start from the generalized continuous Edwards Hamiltonian for a D-dimensional manifold and first of all perform dimensional analysis. From this, the concept of upper critical dimensions will be

introduced and a generalized Flory theory constructed. The excluded-volume effects on a self-avoiding membrane will be treated as a perturbation to an ideal Gaussian manifold and a perturbative renormalization-group analysis will be outlined. Chapter 3 contains the description of the Monte Carlo procedure and related topics which we will encounter in the simulations reported in Chapters 4 and 5. A few physical quantities which characterize the shapes of membranes will be introduced as well. My early studies on the role of self-avoidance in the structure of tethered membranes are reported in Chapter 4. More recent simulational work of mine on a self-avoiding membrane model with attractive interactions between particles on the network is presented in Chapter 5.

Chapter 2

Theory of Tethered Membranes

2.1 Dimensional analysis and critical dimensions

For the discussion of this chapter,[1] we adopt the Edwards Hamiltonian, (1.25)

$$\mathcal{H} = \frac{1}{2}\kappa \int d^D\mathbf{x}\,(\nabla\vec{\mathbf{r}})^2 + \frac{1}{2}v \iint_{|\mathbf{x}_1-\mathbf{x}_2|\geq a} d^D\mathbf{x}_1\, d^D\mathbf{x}_2\, \delta^d\left[\vec{\mathbf{r}}(\mathbf{x}_1) - \vec{\mathbf{r}}(\mathbf{x}_2)\right] .$$

If we rescale the external space by a factor of $\kappa^{1/2}$, we can eliminate κ from the first term of the above Hamiltonian and obtain a new Hamiltonian,

$$\mathcal{H} = \frac{1}{2}\int d^D\mathbf{x}\,(\nabla\vec{\mathbf{r}})^2 + \frac{1}{2}v\kappa^{d/2} \iint_{|\mathbf{x}_1-\mathbf{x}_2|\geq a} d^D\mathbf{x}_1\, d^D\mathbf{x}_2\, \delta^d[\vec{\mathbf{r}}(\mathbf{x}_1) - \vec{\mathbf{r}}(\mathbf{x}_2)] , \qquad (2.1)$$

where the length unit of the external space is set by $\kappa^{-1/2}$. In the case of a Gaussian manifold, this can be seen from (1.22). The strength of interaction is measured by

$$u \equiv v\kappa^{d/2} . \qquad (2.2)$$

We shall in Section 2.2 use u as an expansion parameter.

Dimensional analysis is carried out on (2.1) by rescaling variable $\mathbf{x}$ of the internal space by a length l,

$$\mathbf{x}' = \frac{\mathbf{x}}{l} .$$

[1] References: [1, 33, 34]

Assuming that the membrane is isotropic we rescale $\vec{\mathbf{r}}(\mathbf{x})$ in the following way:

$$\vec{\mathbf{r}}' = \frac{\vec{\mathbf{r}}}{l^{\nu}} ,$$

where ν is the exponent characterizing the scaling behavior of the manifold in the embedding space. With these substitutions (2.1) becomes

$$\mathcal{H} = \frac{1}{2} l^{D-2+2\nu} \int d^D\mathbf{x}\, (\nabla\vec{\mathbf{r}})^2 + \frac{1}{2} u l^{2D-d\nu} \iint_{|\mathbf{x}_1-\mathbf{x}_2|\geq a'} d^D\mathbf{x}_1\, d^D\mathbf{x}_2\, \delta^d[\vec{\mathbf{r}}(\mathbf{x}_1)-\vec{\mathbf{r}}(\mathbf{x}_2)] \ . \quad (2.3)$$

The rescaled effective interaction parameter is given by $u_1 \equiv u l^{2D-d\nu}$ and is usually written as

$$u_1 = u l^{\epsilon/2} ,$$

where

$$\epsilon = 4D - 2d\nu \ . \quad (2.4)$$

If we require that the Gaussian and the interaction terms scale in the same way with l, namely,

$$l^{D-2+2\nu} \sim l^{2D-d\nu} ,$$

we must have

$$D - 2 + 2\nu = 2D - d\nu ,$$

and, thus,

$$\nu = \frac{D+2}{d+2} \ . \quad (2.5)$$

This expression is the same as what one would obtain by generalizing the Flory theory for polymers to a D-dimensional manifold. Hence, it is often called the generalized Flory theory. It should not be surprising that we arrived at the same expression for ν in both approaches, since dimensional analysis is essentially the same as the mean-field theory presented in Chapter 1.

The Flory prediction of the fractal dimension of the network is

$$D_{\mathrm{f}} \equiv \frac{D}{\nu} = \frac{d+2}{D+2} D \ . \quad (2.6)$$

In particular, $\nu = 4/5$ and $D_f = 5/2$ for a tethered membrane in three dimensional embedding space. Note that it predicts a crumpled phase for two-dimensional networks, an unavoidable consequence of our isotropic rescaling of the variable $\vec{\mathbf{r}}$.

For a manifold of dimension D in an embedding space of dimension d, if $2D - d\nu > 0$, the rescaled effective interaction parameter u_1 approaches infinity in the $l \to \infty$ limit, and self-avoidance is relevant; while, for $2D - d\nu < 0$, $u_1 \to 0$ when l increases, yielding an effective ideal Gaussian manifold at large distances. The dimension of the embedding space in which $2D - d\nu = 0$ (or equivalently, $\epsilon = 0$) is defined as the (upper) critical dimension of the embedding space, d_c,

$$d_c = \frac{2D}{\nu} .$$

The exponent ν should be that of a Gaussian manifold, $\nu_0 = \frac{2-D}{2}$, at the critical dimension and beyond, since self-avoidance is irrelevant in these dimensions. Hence,

$$d_c = \frac{4D}{2 - D} . \tag{2.7}$$

Note that $l^{D-2+2\nu}$ in the first term of (2.3) becomes constant for $d \geq d_c$. The Gaussian term is invariant under the rescaling process when $d \geq d_c$, and $\nu_0 = \frac{2-D}{2}$ is a fixed point of the rescaling transformation. Note also that the upper-critical dimension for membranes is $d_c = \infty$. Excluded-volume effects of self-avoiding membranes, according to this theory, are relevant in an embedding space of any dimension, unlike the case of polymers, whose upper-critical dimension is $d_c = 4$.

The quantity ϵ, defined in (2.4), can be expressed, using (2.7), as

$$\epsilon = (2 - D)(d_c - d) . \tag{2.8}$$

One can similarly define a critical (internal) dimension of a manifold in a d-dimensional embedding space, D_c, at which ϵ in (2.4) vanishes. This yields

$$D_c = \frac{2d}{d + 4} , \tag{2.9}$$

and ϵ can be expressed in terms of D and D_c as

$$\epsilon = 4(D - D_c) \; . \tag{2.10}$$

D_c serves as the lower-critical dimension for a manifold and is usually not an integer. For instance, D_c is equal to $6/7$ in three-dimensional space according to (2.9), and, thus, self-avoidance is relevant for both membranes ($D = 2$) and polymers ($D = 1$) in three-dimensional space. Rewriting ϵ in terms of D and D_c is technically convenient for discussing membranes, since d_c diverges for membranes while D_c remains finite for any d. A perturbation analysis (see Section 2.2) should be carried out about a finite critical dimension. While traditionally one expands about $d_c = 4$ for polymers, we have to expand about $D_c = 6/7$ for membranes. For $D \neq 2$, expansions can be carried out about either of the critical dimensions.

Dimensional analysis predicts an infinite upper-critical dimension and a crumpled phase for self-avoiding membranes, while computer simulations produced very different results. Our earlier studies [23] showed the existence of a flat phase for a tethered membrane in 3-, 4-, and 5-dimensional embedding spaces. Recently Grest [25] suggested that the upper-critical dimension might be $d_c = 5$. It is argued that the effective excluded-volume effects in the computer simulations may not simply be represented by a two-body interaction term, and it is the higher-order interactions which generate an effective bending rigidity responsible for the existence of the flat phase [25].

It is interesting to consider n-body interaction terms, which are generically described by

$$\frac{u_n}{n!} \int \prod_{i=1}^{n} d^D \mathbf{x}_i \prod_{i=1}^{n-1} \delta^d(\vec{\mathbf{r}}(\mathbf{x}_i) - \vec{\mathbf{r}}(\mathbf{x}_{i+1})) \; . \tag{2.11}$$

Performing rescaling as before, we obtain the rescaling relations for u_n,

$$\begin{aligned} u_n(l) &= u_n l^{nD-(n-1)d\nu} \\ &= u_n l^{\epsilon(n)/2} \; , \end{aligned} \tag{2.12}$$

where

$$\epsilon(n) = 2nD - 2(n-1)d\nu. \tag{2.13}$$

At the Gaussian fixed point ($\nu = \nu_0 = \frac{2-D}{2}$), the importance of the n-body interaction is determined by $\epsilon^{\mathrm{G}}(n) = 2nD - (n-1)(2-D)d$, where the superscript G is used to indicate that $\epsilon(n)$ is evaluated at the Gaussian fixed point. The upper-critical dimensions, $d_c^{\mathrm{G}}(n)$, for n-body interactions are derived from the condition that $\epsilon^{\mathrm{G}}(n) = 0$ at $d_c^{\mathrm{G}}(n)$, leading to

$$d_c^{\mathrm{G}}(n) = \frac{2nD}{(n-1)(2-D)} . \tag{2.14}$$

One can easily see that $d_c^{\mathrm{G}}(n) = \infty$ for $D = 2$ meaning that all high-order interactions are relevant for self-avoiding membranes.

This does not help, of course, to explain the simulational results found by Grest [25], that self-avoiding tethered membranes may crumple for $d_c \geq 5$. He suggested looking at the scaling behavior of the high-order interaction terms at the Flory point, at which the Gaussian term and the 2-body term scale similarly. This leads to a set of upper-critical dimensions, $d_c^{\mathrm{F}}(n)$, for n-body interactions,

$$d_c^{\mathrm{F}}(n) = \frac{2nD}{2n-2-D} , \tag{2.15}$$

where the superscript F indicates that the Flory exponent (2.5) is used in the derivation.

For membranes, the above expression yields $d_c^{\mathrm{F}}(n=2) = \infty$, $d_c^{\mathrm{F}}(n=3) = 6$, and $d_c^{\mathrm{F}}(n=4) = 4$, *etc.*. The 2-body interaction is relevant in all dimensions, while the 3- and 4-body interactions cease to be relevant above 6 and 4 dimensions, respectively. When we apply this theory to the simulational results, it appears that 4- or more-body interactions should be responsible for the flat phase of a self-avoiding membrane. This theory does not explain why the upper-critical dimension is 5 in the simulation rather than 4 which is the critical dimension for the 4-body interaction.

Our discussion of critical dimensions is illustrated in Fig. 2.1.

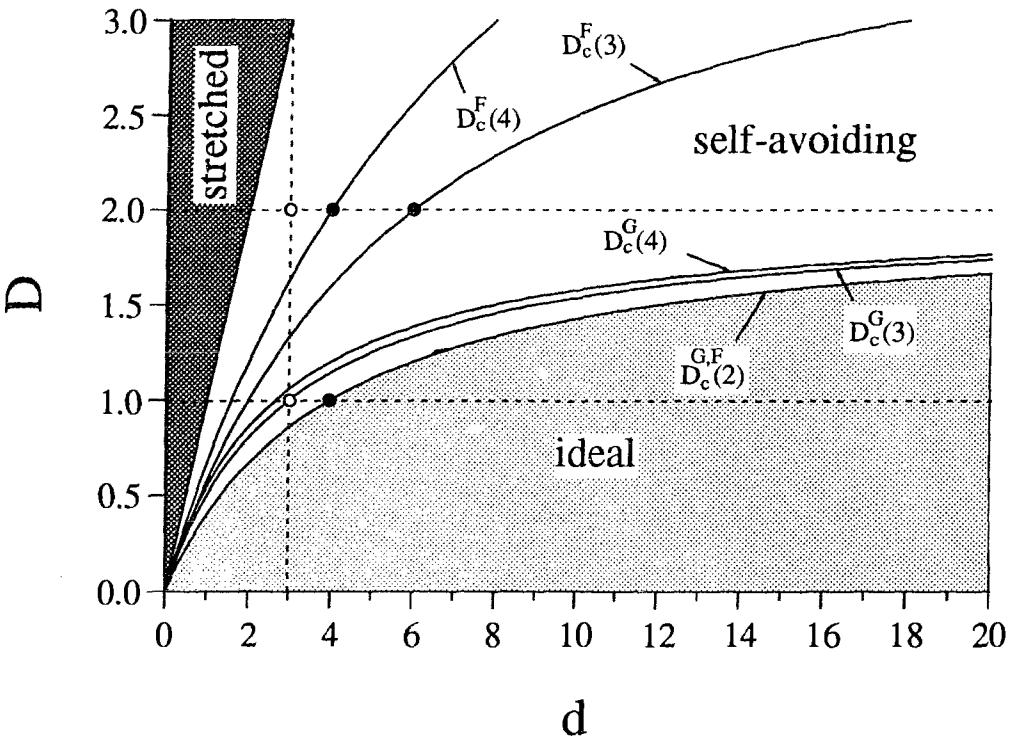

Figure 2.1: Phase diagram for D-dimensional manifolds in d dimensions. The phases of manifolds are divided by the critical (internal) dimensions, $D_c^{G,F}(n)$, below which the n-body interactions cease to be relevant at the Gaussian fixed point and the Flory point, respectively. Above the $D = d$ line, the manifolds are stretched. Below the two-body curve $D_c^{G,F}(2)$, all interactions are irrelevant and the manifolds behave ideally as Gaussian manifolds. In the region between the stretched and the ideal phases, self-avoidance is relevant. All interactions are relevant for membranes ($D = 2$) at the Gaussian fixed point in any dimensions. At the Flory point, however, all but the 2-body interactions are irrelevant in dimensions higher than 6.

2.2 Perturbative renormalization-group analysis

As we showed in the last section, self-avoidance is irrelevant above the upper-critical dimension. Thus, if we perform a RG transformation for a network in $d(> d_c)$-dimensional space, the excluded-volume interaction will be renormalized to zero as the

degrees of freedom are being thinned out. The RG transformation has the Gaussian fixed point ($R_g \sim N^{\nu}$ and $\nu = \nu_0$). In dimensions $d < d_c$, self-avoidance is relevant and a new fixed point may arise as a result of the increasingly important excluded-volume effects as d is lowered below d_c. In this section, I shall treat the excluded-volume effects as a perturbation to a Gaussian network and calculate the corrections to the exponent ν_0 of the unperturbed ideal membrane network. However, I shall mostly outline the perturbative renormalization-group approach rather than present detailed calculations [16, 35].

2.2.1 Simple renormalization-group ideas

The Hamiltonian of a D-dimensional manifold embedded in d-dimensional space is given by (1.25),

$$\mathcal{H} = \frac{1}{2}\kappa \int d^D\mathbf{x}\,(\nabla\vec{\mathbf{r}})^2 + \frac{1}{2}v \iint_{|\mathbf{x}_1-\mathbf{x}_2|\geq a} d^D\mathbf{x}_1\, d^D\mathbf{x}_2\, \delta^d\left[\vec{\mathbf{r}}(\mathbf{x}_1) - \vec{\mathbf{r}}(\mathbf{x}_2)\right] .$$

$\mathcal{H}$ is a function of κ, v, and implicitly of a.

The most intuitively appealing RG approach is to rescale the short-distance cutoff a —a Kadanoff block-spin concept. Consider the case of polymers again for simplicity [12]. We begin the Kadanoff procedure by grouping l successive monomers into subunits (see Fig. 1.2). We define a new chain of N/l units, each having l monomers. We then ask how such a transformation affects the interaction between subunits and, thus, how the Hamiltonian transforms, i.e., we hope to find relations between renormalized parameters $\tilde{\kappa}$, $\tilde{v}$, and the original κ, v. Fixed points can be found from these recursion relations, and exponents characterizing the fixed points, such as ν, may be obtained.

Imagine computing the size of a block subunit a_1 and the excluded-volume interaction parameter u_1 for the subunits. The procedure is the same as in Kadanoff spin-block procedures: integrate out degrees of freedom inside each block. If we were

dealing with ideal polymer chains, we would simply have $a_1 = l^{1/2}a$, as demonstrated previously. However, the effects of self-avoidance swell the subunits. Let us write a_1 as

$$a_1 = l^{1/2}a\,[1 + \mathrm{h}(l,u)] \ , \tag{2.16}$$

and the new interaction parameter as

$$u_1 = ul^{\epsilon/2}\,[1 - \mathrm{k}(l,u)] \ . \tag{2.17}$$

where $\mathrm{h}(l,u)$ and $\mathrm{k}(l,u)$ are some functions. The function $\mathrm{h}(l,u)$ may modify the scaling exponent of the radius of gyration, ν, from its Gaussian value of $1/2$ to possibly some other value. The $\epsilon/2$ exponent in (2.17) is expected on the basis of the previous dimensional analysis. The variable u_1 should be smaller than $ul^{\epsilon/2}$— the renormalized value of u_1 for a non-self-avoiding manifold, since the number of interacting pairs is smaller than l^2 due to self-avoidance.

The essential idea of the renormalization-group analysis is to repeat the operation and generate a sequence

$$\begin{array}{ccccccc} a_1 & & a_2 & & & & a_m \\ & \rightarrow & & \rightarrow \cdots \rightarrow & & & \rightarrow \cdots \ . \\ u_1 & & u_2 & & & & u_m \end{array}$$

Any pair (a_m, u_m) in this sequence represents one possible realization of the single-chain problem. The sequence of interaction parameter $\{u_m\}$ approaches a fixed point u^*, as $m \rightarrow \infty$, at which the relationship between a_m and a_{m-1} $(m \rightarrow \infty)$ becomes a simple geometric series,

$$a_m = a_{m-1}l^{1/2}\,[1 + \mathrm{h}(u^*,l)] = \mathrm{A}(l)\,a_{m-1} \ .$$

The radius of gyration of the manifold is invariant under the rescaling operation and, thus, if we write it as $R_g = a\,\mathrm{f}(N,u)$, where $\mathrm{f}(N,u)$ is a function, the invariance is expressed as

$$R_g = a_m\,\mathrm{f}\left(\frac{N}{l^m}, u_m\right) = a_{m-1}\,\mathrm{f}\left(\frac{N}{l^{m-1}}, u_{m-1}\right) \ .$$

At the fixed point $u_m = u_{m-1} = u^*$, we have

$$\frac{\mathrm{f}\left(\frac{N}{l^m}\right)}{\mathrm{f}\left(\frac{N}{l^{m-1}}\right)} = \frac{a_{m-1}}{a_m} = \text{const.} .$$

This relation implies that $\mathrm{f}(x) \sim x^\nu$ and, thus,

$$R_g \cong N^\nu a ,$$

or

$$a_1 = l^\nu a ,$$

where $\nu = \ln(a_m/a_{m-1})/\ln(l)$.

The above illustrates how important information, such as the value of ν, is obtained from the renormalization-group methods.

2.2.2 Perturbation expansions

Exact solutions for $\mathrm{h}(l,u)$ and $\mathrm{f}(l,u)$ formulated above are very difficult to obtain in practice. Approximations, such as expansions, have to be made in analytical calculations. In this section, I shall discuss the perturbation-expansion theory for membranes from the recent literature [16, 35].

A Gaussian manifold is the unperturbed state of the expansion theory. As we know, a self-avoiding manifold behaves like an ideal Gaussian manifold above the upper-critical dimension. Thus, there are two perturbation expansions which we can make: one about the interaction parameter $u = 0$, and one about the upper-critical dimension d_c, or, in the case of membranes, about the lower-critical internal dimension D_c. The expansion parameters are ϵ in (2.4) and u. We are interested in the behavior of self-avoiding membranes and, therefore, ϵ and u are taken to be positive.

Let's look again, say, at the function $\mathrm{k}(l,u)$ introduced in the last section to see that it is also a function of ϵ. When $\epsilon < 0$, it is evident from (2.17) that $u^* = 0$ and

the behavior of a_1 should be Gaussian-like, i.e., $a_1 = l^{1/2} a_0$. Thus, when ϵ is positive but small (d slightly below d_c), we can compute $\mathrm{k}(l, u^*)$ (and $\mathrm{h}(l, u^*)$ similarly) by expanding in ϵ,

$$u^* = u^* l^{\epsilon/2} [1 - \mathrm{k}(l, u^*)] \,,$$

therefore,

$$1 - \mathrm{k}(l, u^*) = l^{-\epsilon/2} = 1 - \epsilon/2 \ln(l) \,.$$

We see that $\mathrm{k}(l) = \frac{\epsilon}{2} \ln(l)$, having the same order as ϵ.

We now proceed with the expansions. The Edwards Hamiltonian (1.25) can be written in the following form,

$$\mathcal{H} = \mathcal{H}_0 + \mathcal{H}_1 \,, \tag{2.18}$$

where

$$\mathcal{H}_0 = \frac{1}{2} \kappa \int d^D \mathbf{x} \, (\nabla \vec{\mathbf{r}})^2 \tag{2.19}$$

is simply the Hamiltonian for a Gaussian network, and

$$\mathcal{H}_1 = \frac{1}{2} v \iint_{|\mathbf{x}_1 - \mathbf{x}_2| \geq a} d^D \mathbf{x}_1 \, d^D \mathbf{x}_2 \, \delta^d \left[\vec{\mathbf{r}}(\mathbf{x}_1) - \vec{\mathbf{r}}(\mathbf{x}_2) \right] \tag{2.20}$$

is the interaction term.

The partition function of a manifold is given by

$$\mathcal{Z} = \int \mathcal{D}\vec{\mathbf{r}} \, \exp\left(-\mathcal{H}\right) = \int \mathcal{D}\vec{\mathbf{r}} \, \exp\left[-(\mathcal{H}_0 + \mathcal{H}_1)\right] \tag{2.21}$$

and the expectation value of any quantity A is

$$\langle A \rangle = \frac{1}{\mathcal{Z}} \int \mathcal{D}\vec{\mathbf{r}} \, A \, \mathrm{e}^{-(\mathcal{H}_0 + \mathcal{H}_1)} \,. \tag{2.22}$$

To first order in $\mathcal{H}_1$ (thus, in v),

$$\langle A \rangle = \langle A \rangle_0 - \langle A \mathcal{H}_1 \rangle_0 + \langle A \rangle_0 \langle \mathcal{H}_1 \rangle_0 \,, \tag{2.23}$$

all the terms on the right-hand side of the equation are evaluated for a Gaussian network.

As for the Gaussian manifold, we calculate the generating function $\Phi(\vec{\mathbf{k}}, \mathbf{x}_1, \mathbf{x}_2)$ and, using (2.23) and (1.20), we obtain

$$\begin{aligned}\left\langle |\vec{\mathbf{r}}(\mathbf{x}_1) - \vec{\mathbf{r}}(\mathbf{x}_2)|^2 \right\rangle &= \left\langle |\vec{\mathbf{r}}(\mathbf{x}_1) - \vec{\mathbf{r}}(\mathbf{x}_2)|^2 \right\rangle_0 \left[1 + \frac{v\kappa^{d/2}}{2^{d+2}\pi^{d/2}} \frac{(2-D)^{1+d/2} S_D^{2+d/2}}{D} \frac{L^{\epsilon/2} - a^{\epsilon/2}}{\epsilon/2} \right] \\ &= \frac{2dG_D(\mathbf{x}_1 - \mathbf{x}_2)}{\kappa} \left(1 + uB \frac{L^{\epsilon/2} - a^{\epsilon/2}}{\epsilon/2} \right) , \end{aligned} \tag{2.24}$$

where

$$B \equiv \frac{1}{2^{d+2}\pi^{d/2}} \frac{(2-D)^{1+d/2} S_D^{2+d/2}}{D}$$

is a constant, $u = v\kappa^{d/2}$, and a is the lower cutoff limit, for which there is no unique choice.

Suppose now that we started to describe the very same system on a somewhat larger microscopic scale, $a \to a(1+\Delta)$. The Hamiltonian would have been given by

$$\mathcal{H}' \mid_{a(1+\Delta)} = \frac{1}{2}\kappa' \int d^D\mathbf{x} (\nabla \vec{\mathbf{r}})^2 + \frac{1}{2} v' \iint_{|\mathbf{x}_1 - \mathbf{x}_2| \geq a(1+\Delta)} d^D\mathbf{x}_1 d^D\mathbf{x}_2 \delta^d[\vec{\mathbf{r}}(\mathbf{x}_1) - \vec{\mathbf{r}}(\mathbf{x}_2)] . \tag{2.25}$$

The radius of gyration, or $\langle |\vec{\mathbf{r}}(\mathbf{x}_1) - \vec{\mathbf{r}}(\mathbf{x}_2)|^2 \rangle \mid_{\mathcal{H}'}$, should be given by (2.24) after we replace κ, u, and a by κ', u', and $a(1+\Delta)$. However, $\langle |\vec{\mathbf{r}}(\mathbf{x}_1) - \vec{\mathbf{r}}(\mathbf{x}_2)|^2 \rangle$ is a measurable quantity and is invariant for Hamiltonians on different microscopic scales, i.e.

$$\left\langle |\vec{\mathbf{r}}(\mathbf{x}_1) - \vec{\mathbf{r}}(\mathbf{x}_2)|^2 \right\rangle \mid_{\mathcal{H}} = \left\langle |\vec{\mathbf{r}}(\mathbf{x}_1) - \vec{\mathbf{r}}(\mathbf{x}_2)|^2 \right\rangle \mid_{\mathcal{H}'} . \tag{2.26}$$

By using this identity and (2.24), we now relate κ', u' to κ, u.

$$\begin{aligned}\left\langle |\vec{\mathbf{r}}(\mathbf{x}_1) - \vec{\mathbf{r}}(\mathbf{x}_2)|^2 \right\rangle \mid_{\mathcal{H}'} &= \frac{2dG_D(\mathbf{x}_1 - \mathbf{x}_2)}{\kappa'} \left[1 + u'B \frac{L^{\epsilon/2} - a^{\epsilon/2}(1+\Delta)^{\epsilon/2}}{\epsilon/2} \right] \\ &\approx \frac{2dG_D(\mathbf{x}_1 - \mathbf{x}_2)}{\kappa'} \left(1 + u'B \frac{L^{\epsilon/2} - a^{\epsilon/2}}{\epsilon/2} - u'a^{\epsilon/2}B\Delta \right) \\ &\approx \frac{2dG_D(\mathbf{x}_1 - \mathbf{x}_2)}{\kappa'} \left(1 + u'B \frac{L^{\epsilon/2} - a^{\epsilon/2}}{\epsilon/2} \right) (1 - u'a^{\epsilon/2}B\Delta) \\ &\approx \frac{2dG_D(\mathbf{x}_1 - \mathbf{x}_2)}{\kappa'(1 + u'a^{\epsilon/2}B\Delta)} \left(1 + u'B \frac{L^{\epsilon/2} - a^{\epsilon/2}}{\epsilon/2} \right) \end{aligned}$$

Clearly, (2.26) holds if κ' is taken to be, to first order in u,

$$\kappa' = \kappa \left(1 - u a^{\epsilon/2} B \Delta\right) ,$$

and

$$u' = u[1 - \mathrm{k}(\Delta, u)] .$$

The function $\mathrm{k}(\Delta, u)$ cannot be found from this, since we are only collecting terms linear in u.

We have just coarse-grained the manifold (and its Hamiltonian) and found the relationship between a manifold with cutoff length a and one with cutoff length $a(1+\Delta)$. The Hamiltonians $\mathcal{H}'$ and $\mathcal{H}$ are descriptions of a manifold on different scales, and we may rescale, say $\mathcal{H}'$, to match with $\mathcal{H}$ on the same scale. Let $l = 1 + \Delta$ and $\mathbf{x}' = \mathbf{x}/l$. Naturally, the scale of the embedding space needs to be changed as well under this transformation. We let $\vec{\mathbf{r}}' = \vec{\mathbf{r}}/l^{\nu}$, where ν is the exponent governing the scaling behavior of the embedding space and is to be determined from the fixed-point calculation presented later. We now can write a renormalized Hamiltonian $\tilde{\mathcal{H}}$ in a form identical to that of original Hamiltonian,

$$\tilde{\mathcal{H}} = \frac{1}{2}\tilde{\kappa} \int d^D\mathbf{x} \, (\nabla \vec{\mathbf{r}})^2 + \frac{1}{2}\tilde{v} \iint_{|\mathbf{x}_1 - \mathbf{x}_2| \geq a} d^D\mathbf{x}_1 \, d^D\mathbf{x}_2 \, \delta^d[\vec{\mathbf{r}}(\mathbf{x}_1) - \vec{\mathbf{r}}(\mathbf{x}_2)] \tag{2.27}$$

with

$$\begin{aligned} \tilde{\kappa} &= \kappa \left(1 - u a^{\epsilon/2} B \Delta\right) l^{D-2+2\nu} \\ &= \kappa l^{D-2+2\nu-u a^{\epsilon/2} B} , \end{aligned} \tag{2.28}$$

and

$$\tilde{u} = u[1 - \mathrm{k}(l, u)] l^{2D - d\nu} . \tag{2.29}$$

The renormalization of u must involve at least expansion to second-order in u. One cannot obtain the function $\mathrm{k}(l, u)$ from the calculation of the two-point distance

at first order in u. The recursion relation for u can be obtained from the partition function $\mathcal{Z}$, normalized by $\mathcal{Z}_0(\equiv \mathcal{Z}|_{v=0})$,

$$\begin{aligned}\frac{\mathcal{Z}}{\mathcal{Z}_0} &= 1 - \frac{v}{2}\int d^D\mathbf{x}\, d^D\mathbf{x}' \left\langle \delta^d(\vec{\mathbf{r}}(\mathbf{x}) - \vec{\mathbf{r}}(\mathbf{x}'))\right\rangle_0 \\ &\quad + \frac{v^2}{8}\int d^D\mathbf{x}\, d^D\mathbf{x}'\, d^D\mathbf{y}\, d^D\mathbf{y}' \left\langle \delta^d(\vec{\mathbf{r}}(\mathbf{x}) - \vec{\mathbf{r}}(\mathbf{x}')) \cdot \delta^d(\vec{\mathbf{r}}(\mathbf{y}) - \vec{\mathbf{r}}(\mathbf{y}'))\right\rangle_0 \\ &\quad + \cdots \\ &= 1 + z_1 + z_2 + \cdots . \end{aligned} \tag{2.30}$$

The next step, as before, is to eliminate configurations that have pairs of points whose separation is smaller than the new cutoff parameter $a(1+\Delta)$. Carrying out this task is tedious, and I will not present the calculations in detail. Instead I shall discuss, with the help of figures, what we may expect from coarse-graining the 2-body, 4-body, and higher-order terms in (2.30) [15].

Fig. 2.2 shows a chain (for ease of drawing, we consider a polymer chain again) interacting with itself via 2-body interaction. A coarse-graining will change the strength of the interaction but not its 2-body interaction nature. On the other hand, 2-, 3-, and 4-body interactions may emerge from an original 4-body interaction under coarse-graining. This is demonstrated in Fig. 2.3.

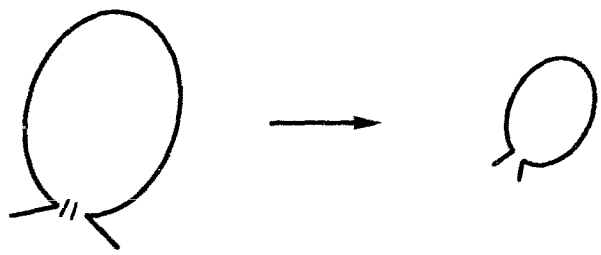

Figure 2.2: Coarse-graining a two-body interaction makes another effective two-body interaction.

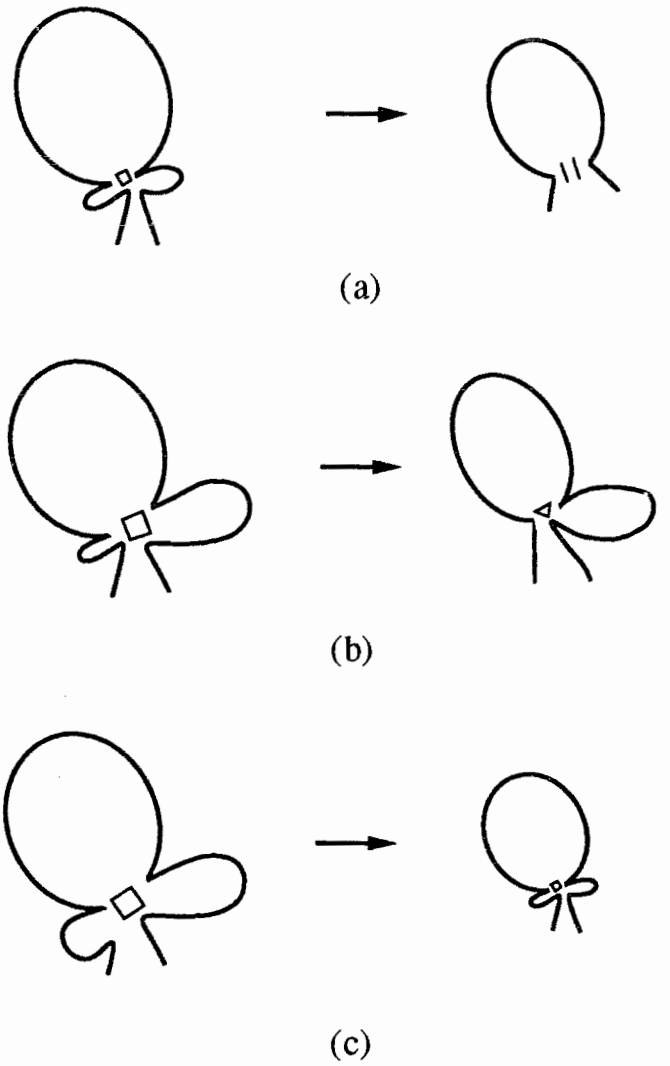

Figure 2.3: Four-body interaction under coarse-graining. Depending on the conformation of the chain and the resolution of coarse-graining, a coarse-graining can make a 4-body interaction an effective 2-, 3-, and 4-body interaction. The symbols "||", "$\triangle$", and "$\square$" denote 2-, 3-, and 4-body interactions, respectively.

In our case, we would like to get a contribution from z_2, by integrating over the range $[a, a(1+\Delta)]$, proportional to $\left\langle \delta^d(\vec{\mathbf{r}}(\mathbf{x}) - \vec{\mathbf{r}}(\mathbf{x}')) \right\rangle_0 \Delta$, thus extracting a renormalized interaction parameter u.

Omitting derivations, we write down the expression for the renormalized and rescaled interaction parameter,

$$\begin{aligned} \tilde{u} &= u\left(1 - ua^{\epsilon/2}C\Delta\right) l^{2D-d\nu} \\ &= u l^{2D-d\nu-ua^{\epsilon/2}C} , \end{aligned} \tag{2.31}$$

where the constant C is

$$C \equiv \frac{(2-D)^{2/d} S_D^{2+d/2}}{(4\pi)^{d/2}} \mathrm{J}(d, D) , \tag{2.32}$$

and

$$\mathrm{J}(d, D) = \int_1^\infty dx \, \frac{x^{D-1}}{(1+x^{2-D})^{d/2}} . \tag{2.33}$$

We have obtained the renormalized Hamiltonian to the lowest order in u with

$$\begin{cases} \tilde{\kappa} &= \kappa l^{D-2+2\nu-ua^{\epsilon/2}B} \\ \tilde{u} &= u l^{2D-d\nu-ua^{\epsilon/2}C} . \end{cases} \tag{2.34-1,2}$$

Using the following definition of $\bar{u}$ to simplify (2.34-1) and (2.34-2),

$$\bar{u} = \frac{S_D^2}{D}\left[\frac{S_D(2-D)}{4\pi}\right]^{d/2} a^{\epsilon/2} u , \tag{2.35}$$

and applying the rescaling operator $l\frac{\partial}{\partial l}$ to these equations, we obtain the renormalization-flow equations,

$$\begin{cases} l\frac{\partial \tilde{\kappa}}{\partial l} &= \tilde{\kappa}\left(2\nu + D - 2 - \frac{2-D}{4}\bar{u}\right) \\ l\frac{\partial \tilde{\bar{u}}}{\partial l} &= \tilde{\bar{u}}\left[2D - d\nu - D\bar{u}\mathrm{J}(d, D)\right] . \end{cases} \tag{2.36-1,2}$$

These equations are easily solved for the fixed point $\bar{u}^*$ at which the derivatives vanish. We obtain

$$\bar{u}^* = \frac{\epsilon}{\frac{d(2-D)}{4} + 2D\mathrm{J}} , \tag{2.37}$$

where $\epsilon = 4D - (2-D)d$. Using this, we finally obtain from (2.36-1) the expression for the exponent ν at the self-avoiding fixed point $\bar{u}^*$

$$\nu = \frac{2-D}{2} + P\epsilon\,, \tag{2.38}$$

where

$$P = \frac{2-D}{2d(2-D) + 16D\,\mathrm{J}}\,.$$

The correction to the Gaussian exponent, $\nu_0 = \frac{2-D}{2}$, is of first order in ϵ and is valid when ϵ is small. The coefficient of ϵ, P, in (2.38) should, of course, be evaluated at $\epsilon = 0$. We recall that $\epsilon = 0$ corresponds to the critical-dimension line, $D_c^G(2)$, in Fig. 2.1. Any point on this line can be chosen as a point about which the expansion is carried out. On the critical-dimension line the function $\mathrm{J}(d, D)$ has a simpler form

$$\mathrm{J}(d^*, D^*) = \frac{2^{1-d^*/2}\pi^{1/2}\Gamma(2+\frac{d^*}{4})}{d^*\Gamma(\frac{1}{2}+\frac{d^*}{4})}\,. \tag{2.39}$$

The correction to the Gaussian exponent, $P\epsilon$, can easily be calculated and is given in Table 2.1.

			polymer		membrane	
d	$D^* = \frac{2d}{4+d}$	P	ϵ	$P\epsilon$	ϵ	$P\epsilon$
1	2/5	0.089	3	0.267	8	0.712
2	2/3	0.075	2	0.150	8	0.600
3	6/7	0.067	1	0.067	8	0.536
4	1	0.063	0	0.000	8	0.504
5	10/9				8	0.472
⋮	⋮				8	⋮

Table 2.1: Correction to the Gaussian exponent for various combinations of d and D that satisfy the condition $\epsilon = 0$.

When comparing against the known case of polymers and a limiting case for membranes (i.e., a membrane embedded in a 2-dimensional space) we immediately

see that this theory does not produce quantitatively correct results. It does not agree with the Flory prediction for membranes, either. There is no reason to believe that this theory should work for membranes at this order of the expansion. The value of ϵ for the physical situations that we are interested in is too large ($\epsilon = 8$ for membranes) for the expansion theory to be valid. And, as we discussed in the first section of this chapter, a 2-body interaction description of a self-avoiding membrane may not be adequate to begin with.

2.3 Summary

An exact solution of the statistical mechanics of self-avoiding membranes is so far non-existent. I have, in this chapter, carried out dimensional analysis and outlined the perturbative expansion theory of self-avoiding membranes. A generalized Flory theory is developed for the membranes and the expansion calculations are carried out to obtain the scaling exponent ν analytically. Both theories predict a crumpled phase for self-avoiding membranes. Although neither theory is known to be correct quantitatively in general, they do provide us with some insights and, therefore, with guidance into this not-so-well-understood problem. The renormalization-group approach used in this chapter will be utilized in my numerical studies of self-avoiding membranes to be presented in Chapter 4.

Chapter 3

Numerical Simulations

3.1 Introduction

Numerical studies of tethered membranes have produced important qualitative and quantitative results. Some of these results are unexpectedly different from analytical analyses such as those presented in Chapter 2. In this chapter, I shall present the Monte Carlo procedure that I have used in the thesis research. I shall report my contribution to the numerical studies of self-avoiding membranes in the two following chapters.

Much of the theoretical work on polymerized membranes has been based on the tethered membrane model introduced by Kantor, Kardar, and Nelson [33], on which my work is also based. In this model, particles are connected to each other in a fixed D-dimensional network (normally $D = 2$ and the network is chosen to be triangular). A model hexagonal tethered membrane of linear size La, where L is the number of particles on the longest diagonal, is shown in Fig. 3.1 for the fully stretched configuration. We shall conventionally refer to L as the linear size of the membrane.

Kantor *et al.* [19] first studied a 'phantom' membrane with bending rigidity in which the excluded-volume effect is neglected except for nearest neighbors. In their

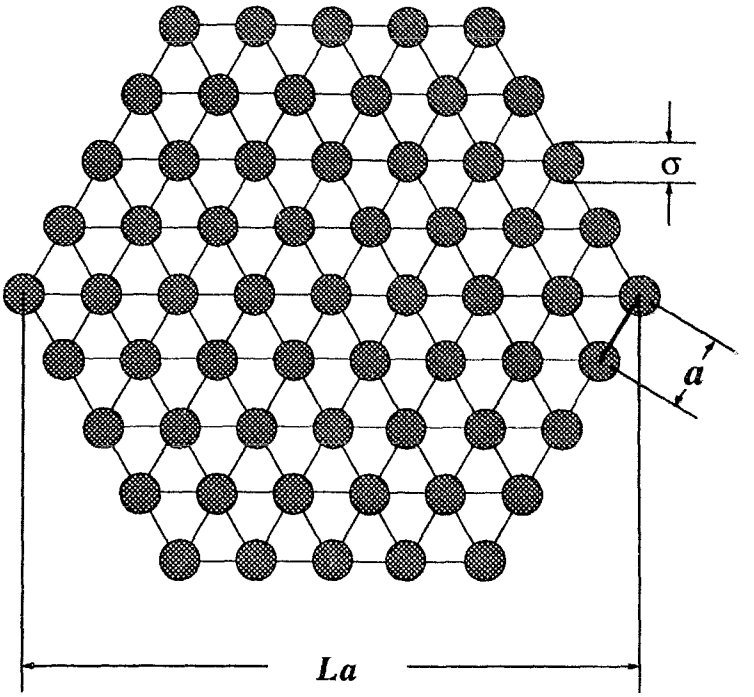

Figure 3.1: The tethered membrane model. A model hexagonal tethered membrane, when fully stretched, is shown. L is conventionally referred to as the (internal) linear size of the membrane. Tethers of length a connect particles of diameter σ to form the network.

simulation the bending rigidity is given by $\kappa(1 - \hat{\mathbf{n}}_i \cdot \hat{\mathbf{n}}_j)$, where $\hat{\mathbf{n}}$ is the normal to an elementary triangle in the network (see Fig. 3.1). i and j are indices of neighboring triangles. The nearest-neighbor particles interact via an infinite potential well the width of which corresponds to the maximum tether length. They found, among other characteristics, that this model exhibits a sharp transition at $k_B T_c \approx \kappa/0.33$ from a low-temperature flat phase to a high-temperature crumpled phase characterized by a scaling law $R_g \sim \sqrt{\ln L}$, consistent with that of the ideal Gaussian network. Ambjorn *et al.* [36] later confirmed this result.

Such studies were quickly extended to more realistic self-avoiding tethered membranes. Plischke and Boal [20] first studied a truly self-avoiding tethered membrane network. The excluded-volume interaction is still the short-range hard-core potential

but any two particles interact if they come too close to each other. Moreover, the ratio of the diameter of the particles on the network to the maximum length of the tethers was set at $1/\sqrt{3}$ to ensure that no self-penetration of the membrane could occur in the simulation. Unlike what happens for linear polymers immersed in good solvents, a flat phase was always observed for the strongly self-avoiding membrane even in the absence of bending rigidity [20, 21, 22, 23, 24]. It is believed that the effective bending rigidity generated by the excluded-volume interaction between particles is responsible for the existence of the flat phase [43].

Clearly, the effective bending rigidity depends on the radius of the hard-core particles. One would naturally raise the question of whether decreasing the diameter of the particles sufficiently reduces the effective bending rigidity to such a point that the crumpled phase may be recovered or, equivalently, how the effective bending rigidity depends on the excluded-volume interaction. My first project was to study numerically a tethered-membrane network of particles of variable diameters. I will present the details of this study in Chapter 4.

Inspired by this work, we studied the same model with an added attractive interaction among particles on the network. In the presence of an attractive interaction, it is conceivable that the effective bending rigidity generated by self-avoidance may be overcome at sufficiently low temperature and that the membrane will no longer be flat. The results of this study will be reported in Chapter 5. They will also be compared with the simulational results of Abraham and Kardar on a similar model [28], and with recent light-scattering experiments on graphite-oxide membranes [30, 31].

In the remainder of this chapter, I shall present in more detail the model and the Monte Carlo procedure used in our simulations. A few quantities which characterize the shape of a membrane will be introduced and discussed. This part is relevant to both Chapter 4 and Chapter 5.

3.2 The model and Monte Carlo procedure

The model which I study consists of hard spheres connected by non-interacting flexible strings as shown in Fig. 3.1 for the fully stretched configuration. The particles are connected in a triangular network and a finite membrane consists of a hexagonal cluster of linear dimension L. In such a cluster there are $N = (3L^2 + 1)/4$ particles of diameter σ and we take the maximum distance between nearest neighbors (measured from the center of the particles) to be $\sqrt{3}$. Nearest neighbors on the lattice interact with each other through an infinite square-well potential. Basically, the major difference between the models that I use in Chapters 4 and 5 is in the interaction potential between non-nearest neighbors.

This square-well potential for nearest neighbors prevents two particles from overlapping and restricts the maximum separation of nearest-neighbor particles. The tethers are not allowed to break and, thus, the connectivity is preserved at all times.

The Monte Carlo simulation procedure which I use is the standard Metropolis method. Except for the central particle, which is held fixed to prevent drifting of the surface, each particle on the network is consecutively displaced by a trial move of length s in a random direction, starting from some initial membrane configuration. A trial move, provided that it does not violate the hard core or the maximum tether length, yields a new configuration of the membrane, which is to be accepted or rejected according to the conventional procedure of comparing $\exp(-\beta\Delta E)$ with a random number in the range $[0, 1]$, where $\Delta E = E_{\text{after}} - E_{\text{before}}$ is the energy difference between this new configuration and the initial starting one. A new configuration of lower energy is always accepted. For a configuration with higher energy to be accepted, the random number selected must be smaller than $\exp(-\beta\Delta E)$. Since successive states differ by the displacement of only one particle, they are strongly correlated and I do not collect data after every move but only after a large number of trial moves.

A convenient time unit to use is a Monte Carlo (MC) step defined as an attempt to move all N particles in the network once. I collect data after every $\tau_R = L^2/s^2$ MC steps—the Rouse time [37]. For the largest membrane that I have been able to simulate, this means that successive samples are separated by $33^2/0.2^2 = 27225$ MC steps, or a τ_R. However, there is no reason to believe that the successive samples are uncorrelated. This issue can only be settled after one has studied the relaxation time of the membrane into its equilibrium states. I will discuss it later in this chapter.

The choice of the trial displacement affects the relaxation time as well as the acceptance rate of the simulation. If s is too small, the membrane will take too long a time to relax into the equilibrium states, although the Monte Carlo acceptance rate will be high; whereas, if s is too large, a particle will likely bump into others in the attempt to move or the tethers involved will likely go beyond the maximum length, so the acceptance rate will be too low. In either case, more computing time will be needed in order to acquire statistically independent data samples. I have varied the magnitude of s to suit each case which I simulated and obtained a reasonable acceptance rate of about 30–50%. For most cases, a choice of $s \approx 0.2$ is appropriate.

Long-range self-avoidance is computationally demanding compared with a 'phantom' case. The most obvious and least efficient way to implement self-avoidance is to check for overlap of hard cores among all N particles on the network for every attempted movement of a particle. This would require evaluation of distances between $N(N-1)/2 \sim N^2$ pairs of particles. A MC step would then involve $N \times N^2 \sim N^3 \sim L^6$ such calculations. This is, of course, prohibitively high for large systems. One must devise a more efficient method to do the task in order to be able to simulate tethered membrane of any reasonably large size at all.

We use the following scheme in our simulation: Note that all particles are confined to a cube of linear size of $\sqrt{3}L$, the maximum linear length of the network when it is fully stretched, centered at the central particle of the membrane. We then divide this

large cube into cells of size of $\sigma + s$ (diameter + trial displacement) and the center of each particle belongs uniquely to a cell. For this choice of size of the cells, only particles in neighboring cells can possibly overlap as the result of a trial move. This drastically cuts down the number of particles that have to be monitored during the calculation. The price to pay is that a dictionary of the occupancy of the cells must be kept and updated after every successful move. This, however, is much less work since the number of evaluations involved is now proportional to $N \sim L^2$. In any case, maintaining self-avoidance is time consuming, and we always first check, after a trial move, whether the tethering constraints and nearest-neighbor hard-core exclusion have been violated. If a trial move is rejected by these constraints, which are quick to check, further checking of long distance self-avoidance becomes unnecessary.

3.3 Relaxation studies

We begin the simulation from some initial configuration (usually a completely flat configuration). The membrane fluctuates freely in three-dimensional space and eventually settles into equilibrium, where our study is carried out.

We are concerned with a few important aspects of the Monte Carlo simulation related to the relaxation characteristics of the membrane:

- the samples that we collect should be equilibrium states;
- the samples should be uncorrelated with each other, i.e., they should be separated in time by a characteristic relaxation time τ_0;
- a large region of the phase space should be sampled.

It is possible to derive analytically the normal modes for ideal polymers [12] and phantom membranes [17]. These normal modes have a correlation function that

decays exponentially as function of time. The relaxation time of the slowest mode is characterized by the Rouse time τ_R, which I have mentioned before. A self-avoiding tethered membrane, however, relaxes much more slowly towards equilibrium than a phantom membrane, as demonstrated by previous studies [17, 23]. Nelson *et al.* [17] suggested that for self-avoiding membranes the relevant time unit scales like $L^{3.6}/s^2$ rather than L^2/s^2. To study and confirm the relaxation behavior of a tethered membrane quantitatively, we calculate the autocorrelation function of a measurable quantity O such as the radius of gyration. The autocorrelation function, $C(\tau)$, is defined as

$$C(\tau) = \frac{\langle [O(t+\tau) - \langle O \rangle]\,[O(t) - \langle O \rangle] \rangle}{\left\langle [O(t) - \langle O \rangle]^2 \right\rangle} \tag{3.1}$$

where the angular brackets denote an average over samples labeled by the time variable t. We begin averaging only after equilibrium has been reached. This starting time can be determined from the behavior of $\langle O(t) \rangle$. The relaxation time which comes out of the study of the relaxation function will confirm whether or not this judgement is correct.

In Fig. 3.2, the square of the radius of gyration of a membrane, R_g^2, is displayed as a function of the time t measured in units of the Rouse times τ_R. It is clear that the initial transient region is rather small in this case, and it is reasonable to assume that equilibrium has been achieved after, say, the first 500 Rouse times. R_g^2 fluctuates about its average value according to a Gaussian distribution.

We have calculated autocorrelation functions of the quantities of physical interest, fitted them to exponential functions for short times, and, thus, determined relaxation times for each size of the membranes at which simulations were carried out. In particular, we are interested in the three eigenvalues of the inertia tensor λ_1, λ_2 and λ_3 (see the next section for definitions) and the radius of gyration, whose square is the sum of these three eigenvalues. These eigenvalues have different relaxation times, and that of the radius of gyration is dominated by the largest of the three relaxation

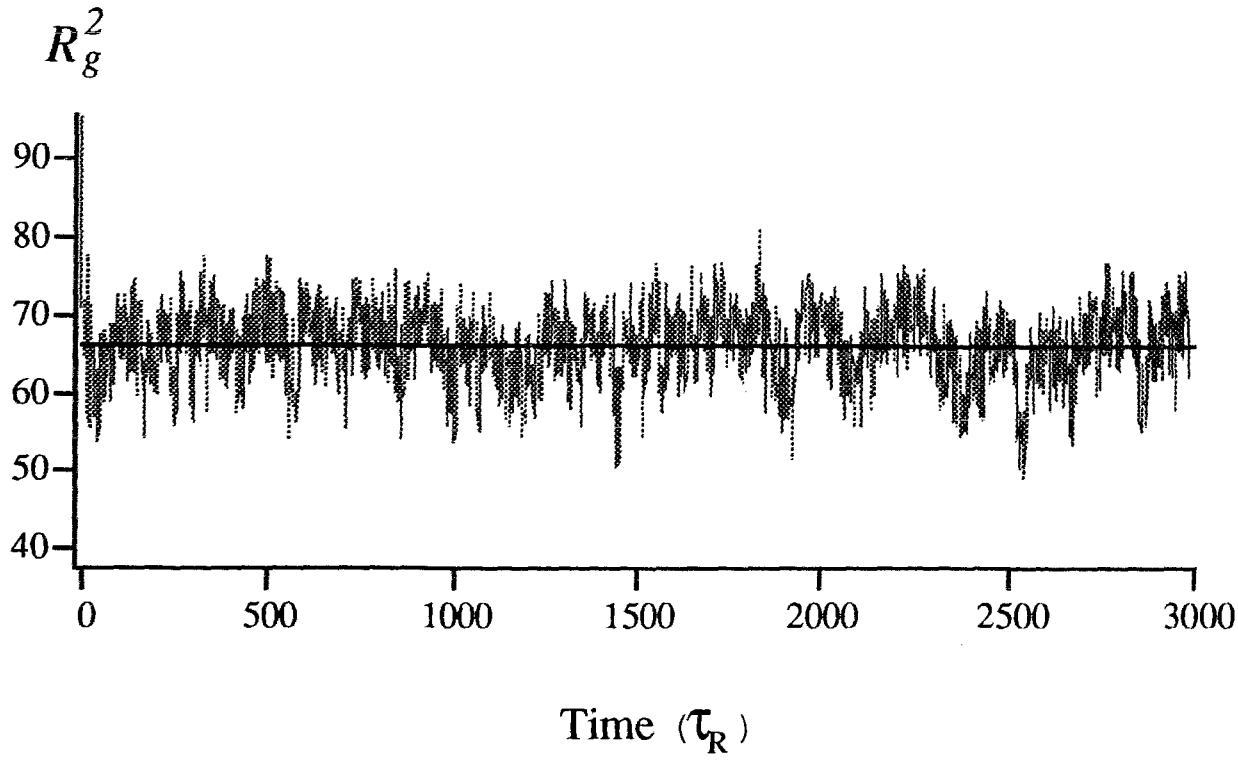

Figure 3.2: The square of the radius of gyration, R_g^2, for a membrane of size $L = 25$ as function of simulation time whose unit is the Rouse time τ_R. In this case, the diameter of the particles is taken to be 1 and the maximum tether length is $\sqrt{3}$. It appears that the initial transient region is rather small. The solid line represents the average value of R_g^2 calculated beginning at $t = 500\tau_R$.

times. We found that the relaxation time is usually longer when excluded-volume effects are stronger. For strongly self-avoiding membranes, the relaxation time τ_0 scales with the membrane size L according to L^x, where $3 < x < 4$, consistent with [17]. Despite the fact that this exponent is much larger than the exponent $x = 2$ of the Rouse time, we have found that the longest relaxation time for our samples ($L \leq 25$) is of the order of a few dozen Rouse times. Fig. 3.3 shows typical results for the autocorrelation function of the eigenvalues of the inertia tensor.

To check whether the fact that we usually start simulation from a flat membrane configuration confines the membrane to a region in phase space such that other parts

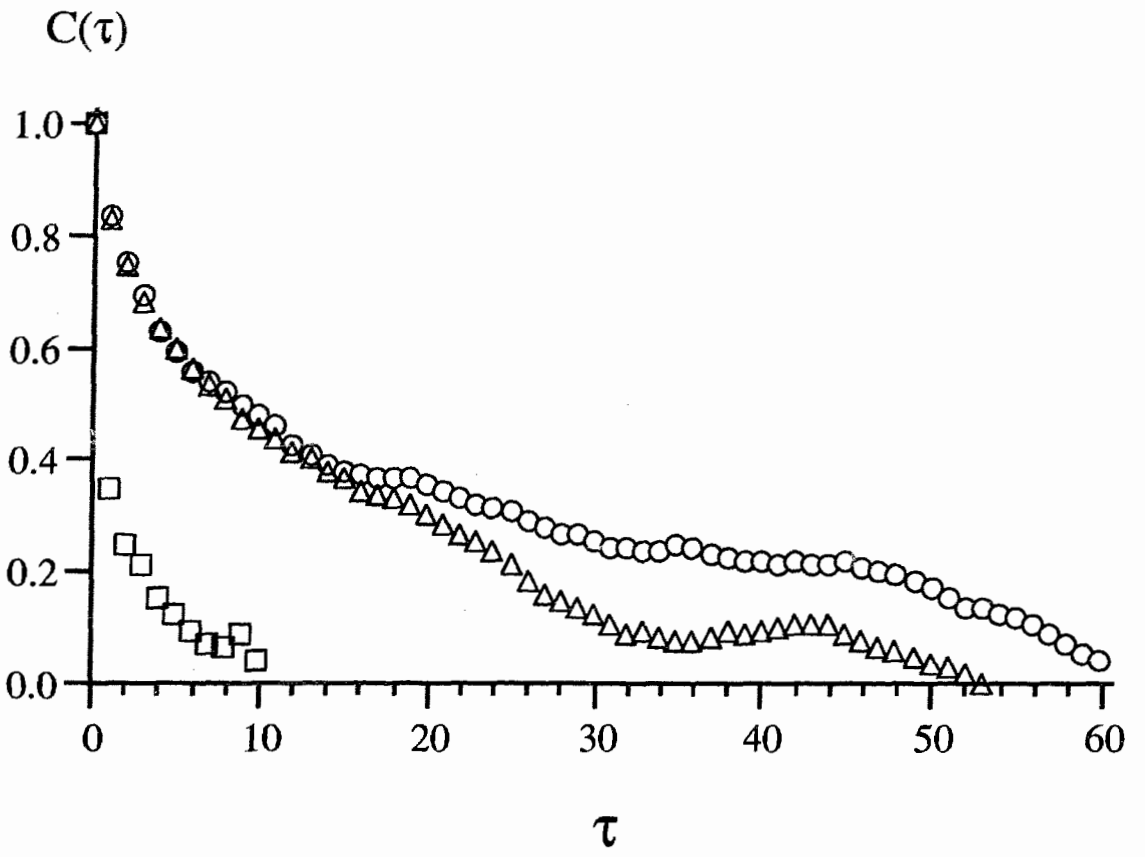

Figure 3.3: The autocorrelation function $C(\tau)$ for λ_1, λ_2, and λ_3, for the same simulation described in Fig. 3.2. The symbols "o", "$\triangle$", and "$\square$" correspond to λ_1, λ_2, and λ_3, respectively.

of the phase space can not be sampled, we have also started simulations from purposely generated crumpled, collapsed, and folded initial configurations. We found that the system always eventually reaches the same equilibrium state for the simulations reported in both Chapter 4 and Chapter 5.

3.4 Characterization of membrane shapes

The focus of our study is on thermodynamic properties, such as the phases and phase transitions of a self-avoiding tethered membrane network. We have found that the

functions which characterize the shape of the membrane are the best indicators of a phase transition. We primarily use the eigenvalues, λ_1, λ_2, and λ_3, of the inertia tensor, which is defined as

$$I_{\alpha\beta} = \frac{1}{2N^2} \sum_{i,j} (r_{i\alpha} r_{j\beta} - \bar{r}_\alpha \bar{r}_\beta) \,, \qquad (\alpha = x, y, z) \tag{3.2}$$

where $r_{i\alpha}$ is the α-component of the position of particle i in the embedding space. The sum is taken for a given configuration over all particles, and $\bar{r}_\alpha$ is the average over i of $r_{i\alpha}$ in that configuration. The three eigenvalues are ordered according to magnitude $\lambda_1 \leq \lambda_2 \leq \lambda_3$. The directions of the principal axes are given by the eigenvectors $\hat{\mathbf{e}}_1$, $\hat{\mathbf{e}}_2$ and $\hat{\mathbf{e}}_3$ corresponding to λ_1, λ_2 and λ_3, respectively. The geometrical meaning of the eigenvectors and the eigenvalues is schematically shown in Fig. 3.4. For the flat initial

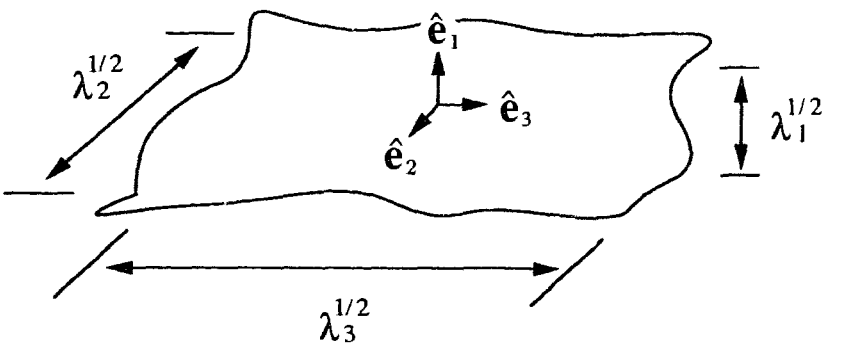

Figure 3.4: Illustration of the geometrical meaning of the eigenvectors and the eigenvalues of the inertia tensor. The eigenvalues λ_j correspond to the principal directions, $\hat{\mathbf{e}}_j$, j=1,2,3, respectively.

configuration that we use in the simulations, $\hat{\mathbf{e}}_1$ is perpendicular to the plane of the membrane, while $\hat{\mathbf{e}}_2$ and $\hat{\mathbf{e}}_3$ lie in the plane. Thermal fluctuations deform a perfectly flat plane. But, if a configuration of the membrane maintains the overall shape of a smooth plane, this picture is still applicable. For a more isotropic conformation of the membrane, the distinction between the principal directions becomes less clear.

In any case, $\sqrt{\lambda_1}$, $\sqrt{\lambda_2}$, and $\sqrt{\lambda_3}$ are the length scales that characterize the extent of the membrane in the three directions. In the flat phase these eigenvalues should scale with the linear dimension L of the membrane according to $\lambda_1 \sim L^{2\nu_1}$, and $\lambda_2 \sim \lambda_3 \sim L^{2\nu_3}$, where $\nu_3 = 1$ and where the 'thickness' exponent ν_1 is smaller than ν_3. In the crumpled phase, however, we expect that the three eigenvalues scale with the membrane size with the same exponent, $\nu_1 = \nu_2 = \nu_3 = \nu$, which, according to the generalized Flory theory, takes on the value of 4/5. In a collapsed phase, the membrane is still expected to be isotropic but the exponents should be given by the 'close packing' value $\nu = 2/3$.

In addition to studying the scaling properties of the three eigenvalues of the inertia tensor, we use the shape factor as an indicator of a phase transition. The shape factor, A, is defined to be

$$A = \langle \lambda_1 / \lambda_3 \rangle \ , \tag{3.3}$$

namely, the smallest eigenvalue divided by the largest. As L becomes large, A approaches zero in the thermodynamic limit for the flat phase due to strong anisotropy, whereas it becomes a non-zero constant for the crumpled phase and the collapsed phase.

We also study the structure factor of a membrane, $S(\vec{k})$, defined by

$$S(\vec{k}) = \frac{1}{N^2} \left\langle \sum_{l,m} \exp\left[i\vec{k} \cdot (\vec{r}_l - \vec{r}_m) \right] \right\rangle \ , \tag{3.4}$$

where l, m are the indices of the particles on the network of the membrane and $\vec{r}_l$ is the position of particle l in the embedding space. The angular brackets indicate averaging over equilibrated samples. The quantity $S(\vec{k})$[1] is experimentally accessible through light-scattering experiments [30, 31] and is, therefore, of practical interest. If one fixes $\vec{k}$ in a certain direction in space, the structure factor will be spherically symmetric regardless of the true shape of the membrane due to its overall rotation

[1] More precisely, its spherically averaged version $S(|\vec{k}|)$.

in the embedding space. In order to remove the effect of this rotation, we elect to evaluate $S(\vec{k})$ for $\vec{k} = |\vec{k}|\hat{e}_j = k\hat{e}_j$, $j = 1,2,3$, where $\hat{e}_j$ are the directions of the principal axes, calculated for each sample configuration. The average $\langle\ \rangle$ is therefore taken with respect to a reference frame rotating with the membrane rather than with respect to the laboratory frame.

Let's examine the structure factor $S(\vec{k})$ more closely. We use a continuum membrane for convenience and assume that the membrane has the shape of a D-dimensional disc of diameter L when fully stretched. For the radius of gyration of such a membrane to scale as $R_g \sim L^\nu$, the two-point averaged distance should scale as

$$\left\langle [\vec{r}(\mathbf{x}) - \vec{r}(\mathbf{x}')]^2 \right\rangle \sim |\mathbf{x} - \mathbf{x}'|^{2\nu} \ .$$

In turn, we must have for the generating function $\Phi(\vec{k}, \mathbf{x}, \mathbf{x}')$ defined by (1.13),

$$\Phi(\vec{k}, \mathbf{x}, \mathbf{x}') = \left\langle \exp\left\{ i\vec{k} \cdot [\vec{r}(\mathbf{x}) - \vec{r}(\mathbf{x}')] \right\} \right\rangle = \mathrm{F}(k\,|\mathbf{x} - \mathbf{x}'|^\nu),$$

where $\mathrm{F}(x)$ is a dimensionless generating function.

The structure factor $S(\vec{k})$ can be easily shown to have the form of a scaling function:

$$\begin{aligned}
\mathrm{S}(\vec{k}) &= \frac{1}{L^{2D}} \int\int d\mathbf{x}\, d\mathbf{x}'\, \Phi(\vec{k}, \mathbf{x}, \mathbf{x}') \\
&= \frac{1}{L^{2D}} \int\int d\mathbf{x}\, d\mathbf{x}'\, \mathrm{F}(k\,|\mathbf{x} - \mathbf{x}'|^\nu) \\
&= \frac{1}{L^D} \int d\mathbf{x}\, \mathrm{F}(k\,|\mathbf{x}|^\nu) \\
&= (kL^\nu)^{-D_f}\, \mathrm{G}(kL^\nu) \qquad (3.5) \\
&= \Psi(kL^\nu) \qquad (3.6)
\end{aligned}$$

where $D_f = D/\nu$ is the conventional fractal dimension, and G and Ψ are unknown functions.

The structure factor, therefore, is expected to have a scaling form as shown above. As well, the function $G(x)$ must reflect the properties of the structure factor due to the finite-size cutoff and a small-length-scale limit due to the diameter σ of the particles on the network. The wavelength of the incident beam ($\sim k^{-1}$) must be within the regime $\sigma < k^{-1} < R_g \sim L^\nu$ in order that the structural information be obtained from the scattering experiments. In the region $k^{-1} \gg R_g$, the membrane appears as a point compared to the wavelength of the incident beam and the structure factor has a common parabolic behavior $S(\vec{\mathbf{k}}) = 1 - \frac{1}{3}(kR_g)^2 + \cdots = 1 - \text{const.} \times (kL^\nu)^2 + \cdots$. For $k^{-1} \sim \sigma$, we should see the atomic oscillations typical of a hard-sphere gas. On the scale much smaller than σ, the cross terms in $\left\langle \sum_{l,m} \exp\left\{ i\vec{\mathbf{k}} \cdot [\vec{\mathbf{r}}(\mathbf{x}) - \vec{\mathbf{r}}(\mathbf{x}')] \right\} \right\rangle$ vanish and the oscillations disappear. The structure factor then becomes a constant: $S(\vec{\mathbf{k}}) = 1/N$.

Having broken down $S(\vec{\mathbf{k}})$ for various regions in k, we put them back together to make a sketch of $S(\vec{\mathbf{k}})$ as function of kL^ν in Fig. 3.5. This sketch is valid for isotropic phase(s) as well as for the anisotropic flat phase, as long as it is understood that all scaling exponents ν_j, $j = 1, 2, 3$, are not equal, and one should treat ν as ν_j and substitute $\sqrt{\lambda_j}$ for R_g in the above arguments. The structure factor can be used to study the scaling behavior of the eigenvalues and, hence, that of the radius of gyration. As well, it can be used to distinguish between isotropic and anisotropic phases. One expects, in the flat phase, that $S(k\hat{\mathbf{e}}_j) = \Psi_j(kL^{\nu_j})$ in the scaling regime, where the ν_j's determine the scaling behavior of the moments of inertia. Conversely, in an isotropically crumpled or collapsed phase one expects that $S(k\hat{\mathbf{e}}_j) = \Psi_j(kL^\nu)$ with a single exponent ν for all j.

It should be mentioned that although $S(\vec{\mathbf{k}})$ is easily obtained from numerical calculations, it may be difficult to measure experimentally because the sample membranes are usually suspended in solutions with no preferred orientation. One must, in this

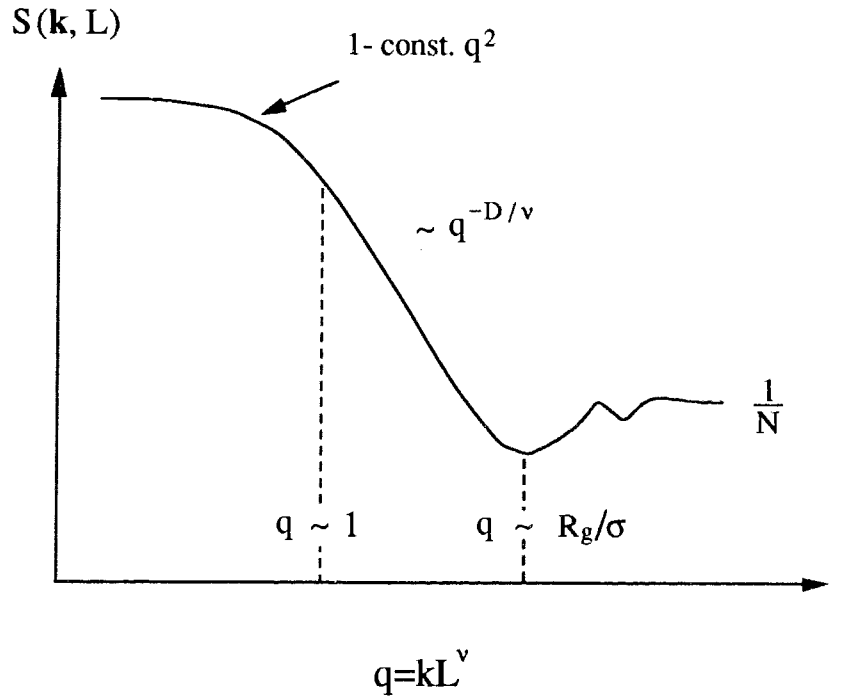

Figure 3.5: Schematic sketch of the structure factor $S(\vec{k}, L)$ as function of the scaled variable kL^{ν}.

situation, study the spherically-averaged version of $S(\vec{k})$ [38],

$$\begin{aligned} S(k) &= \int \frac{d\Omega}{4\pi} S(\vec{k}) \\ &= \frac{1}{N} + \frac{2}{N^2} \sum_{i>j} \left\langle \frac{\sin(k|\vec{r}_i - \vec{r}_j|)}{k|\vec{r}_i - \vec{r}_j|} \right\rangle . \end{aligned} \tag{3.7}$$

While the behavior of $S(k)$ is expected to be the same as that of $S(\vec{k})$ for the isotropic phase(s), the previous sketch must be modified for the flat phase to accommodate the fact that there are different scaling regimes. In the region $w < k^{-1} < R_g$ where w is the thickness of the membrane, one sees a flat, smooth membrane and $S(k) \sim k^{-2}$. In the region $\sigma < k^{-1} < w \sim L^{\nu_1}$, the structure of the membrane in the out-of-plane direction can be probed and the exponent ν_1 extracted from the scal-

ing behavior of S(k) at this length scale. As pointed out recently by Abraham and Goulian [49], the structure factor S(k) may yield the same scaling behavior for a flat membrane as for a crumpled membrane, unless the membrane under consideration is very large, so S(k) should be used with caution. I shall not report on S(k) in this thesis.

Further information about isotropic and anisotropic phases and transition points can be obtained by studying the behavior of the normal vectors of elementary triangles formed by nearest neighbors on the network. We define $M_j(\alpha)$ to be the projection of the normal of triangle α along the eigenvector $\hat{\mathbf{e}}_j$ and calculate

$$M_j = \sum_\alpha M_j(\alpha)/N_\Delta \,, \qquad (j = 1,2,3) \tag{3.8}$$

where N_Δ is the number of elementary triangles. All normal vectors in the formula are consistently taken from one side of the membrane surface. In the flat phase, we expect the expectation value of M_1, or equivalently M_1^2, to be non-zero whereas $\langle M_2^2 \rangle$ and $\langle M_3^2 \rangle$ will be zero in the thermodynamic limit. In a crumpled or collapsed phase, we expect $\left\langle M_j^2 \right\rangle = 0$ for all j. The quantity $\langle M_1^2 \rangle$ can be used as an order parameter for the flat phase of a membrane.

We may calculate yet another set of quantities $\left\langle P_j^2 \right\rangle$ where

$$P_j^2 = \sum_\alpha M_j^2(\alpha)/N_\Delta \qquad (j = 1,2,3)\,. \tag{3.9}$$

In the flat phase $\langle P_1^2 \rangle$ should be greater than $\langle P_2^2 \rangle$ and $\langle P_3^2 \rangle$ since $M_j(\alpha)$ are mostly aligned along the short direction, and all three of them should approach 1/3 in the isotropic phases. While it is obvious that they can not be used to distinguish the crumpled phase and the collapsed phase, these quantities may be useful in providing information about whether folding transitions occur. For instance, one would expect a membrane with a single fold to have a vanishing $\langle M_1^2 \rangle$, whereas $\langle P_1^2 \rangle$ should be appreciably greater than 1/3.

Thermodynamic functions can also be calculated in the simulation. In particular, the specific heat is used to investigate phase transitions and the order of transitions. The specific heat, C, is given by

$$\begin{aligned} C &= \frac{\partial \langle E \rangle}{\partial T} \\ &= \frac{1}{k_B T^2} \left(\left\langle E^2 \right\rangle - \langle E \rangle^2 \right). \end{aligned} \tag{3.10}$$

In the studies of a phantom membrane with bending rigidity, the specific heat provided the best evidence for the presence of the second-order phase transition from the crumpled phase to the flat phase [19]. This phase transition is characterized by a strong peak in the specific heat. At low temperature the specific heat of the phantom membrane with bending rigidity approaches $\frac{1}{2}k_B$ per particle, indicating that the transverse oscillations are essentially uncoupled in the flat phase.

Chapter 4

Tethered Membranes of Variable-size Hard-core Particles

4.1 The Hamiltonian

When a membrane is immersed in a solvent, as it usually is in the laboratory, the effective interaction between monomers at the scale of inter-molecular spacing depends on the properties of the solvent and the membrane monomers. In a 'good' solvent, in the terminology of polymer physics, the effective interaction is repulsive. In this chapter, we will consider the model tethered membrane described in the previous chapter with particles on the network interacting through hard-core interactions.

The interaction potential between nearest-neighbor particles is taken to be an infinite square-well potential,

$$U_{NN}(r) = \begin{cases} \infty & r < \sigma \\ 0 & \sigma \leq r \leq \sqrt{3} \\ \infty & \sqrt{3} < r \end{cases} , \tag{4.1}$$

where we set the maximum distance between nearest neighbors (measured from the center of the particles, see Fig. 3.1) to be $\sqrt{3}$. Among non-nearest-neighbor particles,

the interaction potential is given by

$$\mathrm{U(r)} = \begin{cases} \infty & r < \sigma \\ 0 & \sigma \leq r \end{cases} . \tag{4.2}$$

The potentials above simply prevent two particles from overlapping with each other and control the maximum length of the tethers.

It is evident that the potential energy of our model membrane is a constant (conveniently chosen to be zero here). Temperature is therefore an irrelevant parameter and the thermodynamics of the membrane is purely entropy-driven.

All conformations of the membrane have the same energy and, thus, have equal statistical weight in the Monte Carlo simulation. The simulational procedure in this case is particularly simple, since neither the energy difference nor the Boltzmann factor need be computed in the simulation. For all of our simulations, we have at least 100 and in most cases 300 or more samples separated in time by relaxation times described in Chapter 3.

4.2 Strong self-avoidance and the flat phase

I first studied the case of a strongly self-avoiding membrane in which l/σ is taken to be $\sqrt{3}$. Although this case had been studied previously by Plischke and Boal [20], I nevertheless carried this study to a larger membrane size ($L = 25$ as opposed to the largest size $L = 19$ previously) to confirm their findings. The results are presented here to demonstrate the behavior of the quantities that I have discussed in Chapter 3.

First of all, we display in Fig. 4.1 the shape factor, A, the expectation value of the smallest eigenvalue of the inertia tensor divided by the largest, as a function of the size of the system. Note that the shape factor is small and decreases as L becomes large. This indicates an anisotropic shape of the membrane in the thermodynamic

limit.

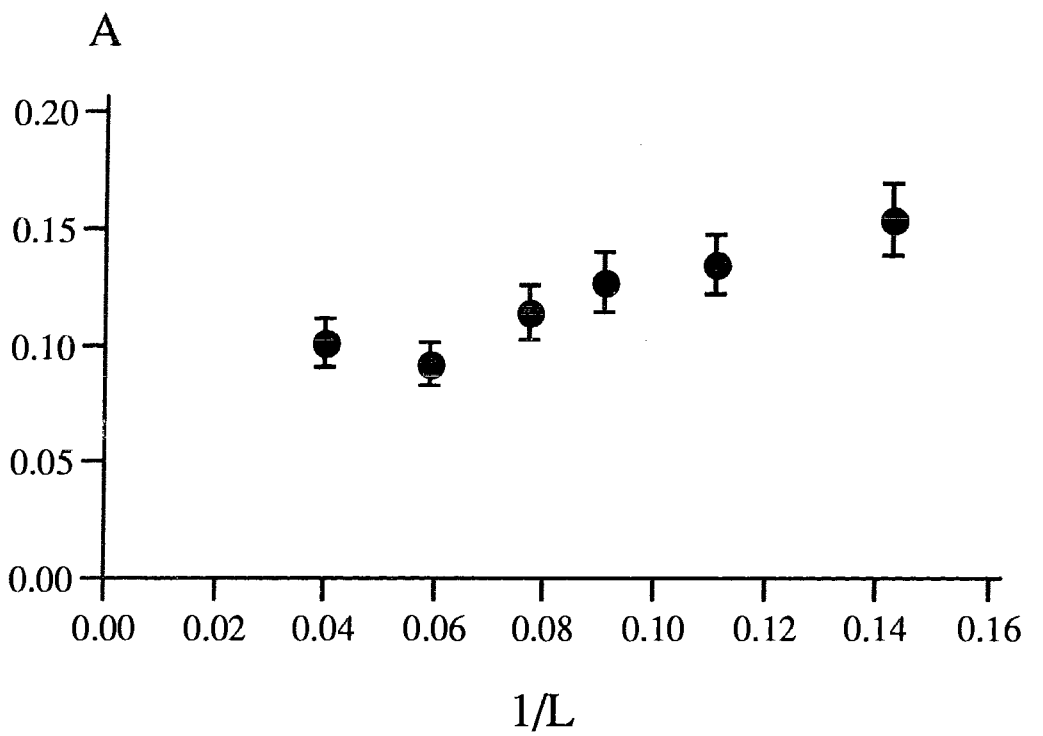

Figure 4.1: The shape factor, $A \equiv \langle \lambda_1/\lambda_3 \rangle$, as function of the inverse linear size of the tethered membranes.

We first determine the exponent ν_3 by fitting the eigenvalue λ_3 to a functional form $\lambda_3 = aL^{2\nu_3}$ for L=7–25 using the least-squares fit. A log–log plot of λ_3 as a function of L, along with the fitting curve, is presented in Fig. 4.2. The exponent ν_3 is found to be 0.95 ± 0.05, with the error bar estimated using standard error analysis. The exponent ν_2 is similarly determined to be 0.95. The error bar for λ_2 is greater than that of λ_3, since, according to the relaxation study we performed, we have fewer independent samples for λ_2 than for λ_3 due to a longer relaxation time for λ_2. Even with such error bars, the exponents ν_2 and ν_3 are unambiguously larger than the Flory prediction of 4/5. The statistics for λ_1 are poorer than for the other two eigenvalues, because this quantity has the longest relaxation time. The 'thickness' exponent ν_1 is clearly less than ν_3, but, its value is not known accurately. Early estimates [20, 21, 23]

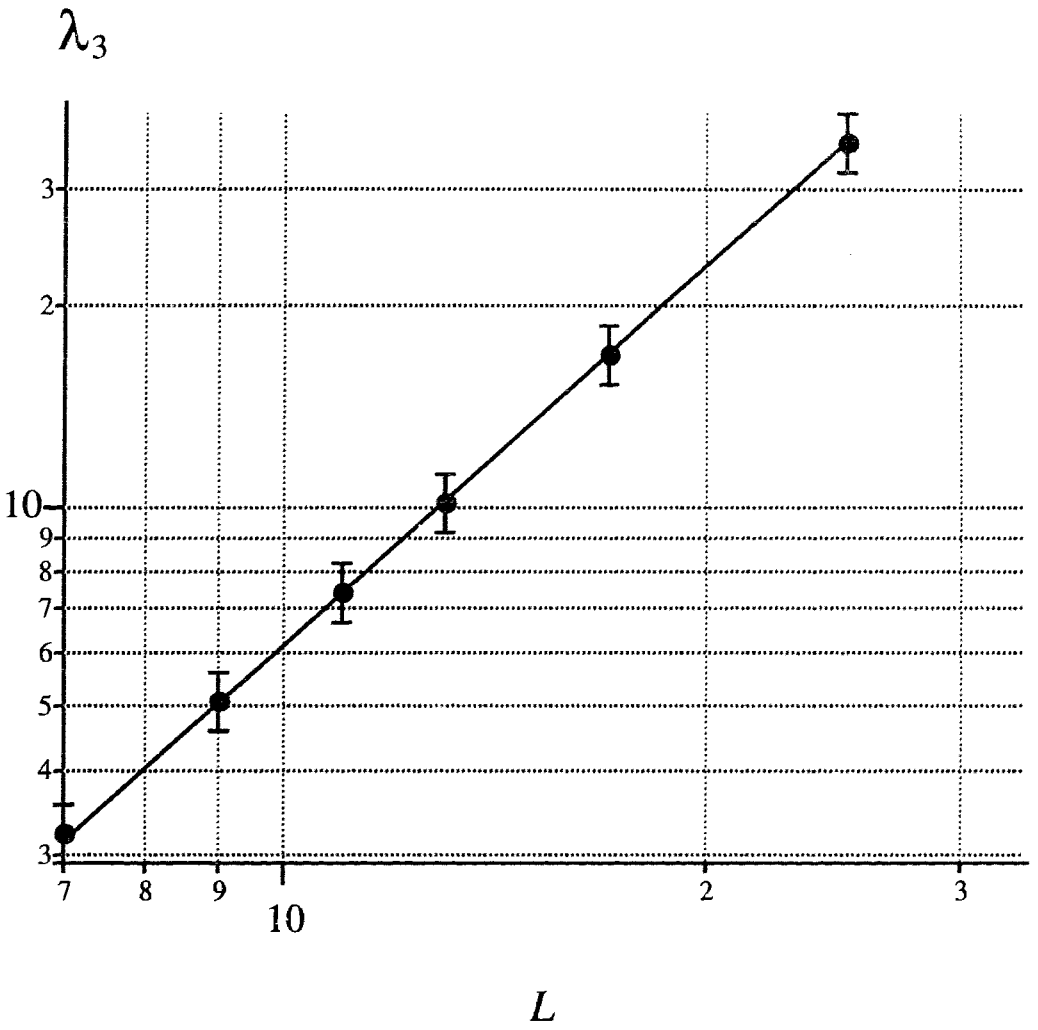

Figure 4.2: Scaling behavior of the largest eigenvalue, λ_3, of the inertia tensor. The data points, represented by "•", have an error bar of $\pm 10\%$. The solid line is the fitting power-law curve which gives $\nu_3 = 0.95$.

including ours yielded $\nu_1 \approx 2/3$ but Lipowsky and Girardet [39] have later suggested that $\nu_1 = 1/2$. Abraham [40], using periodic boundary conditions in order to suppress the effects of boundary fluctuations, has obtained $\nu_1 \approx 0.53$. Joining the continuing debate, Gompper and Kroll [41] found $\nu_1 \approx 0.70$ on the basis of both Monte Carlo simulations and scaling arguments. Schmidt *et al.* recently [42] performed small angle X-ray and light-scattering experiments on closed red blood cell membrane skeletons and found that $\nu_1 \approx 0.65$.[1] The question of the value of ν_1 is far from settled at this time.

We also study the structure factor in order to determine the scaling exponents. In Figs. 4.3, 4.4, and 4.5 the structure factors $S(k\hat{\mathbf{e}}_j)$, $j = 1, 2, 3$, are plotted as a function of the variable kL^{ν_j}. The data collapse onto a single curve rather well in each of the three cases, judged by visual inspection, for a single choice of ν_1, ν_2, and ν_3. The plots shown are for $\nu_1 = 0.70$, $\nu_2 = 1.00$, and $\nu_1 = 1.00$, respectively. They confirm the scaling behavior of the eigenvalues of the inertia tensor and provide us with scaling exponents consistent with those obtained from fitting the principal moments by a power law.

In summary, we conclude that a strongly self-avoiding tethered membrane is highly anisotropic, even in the absence of an explicit bending rigidity. The widths of the two independent in-plane directions are proportional to the linear size, L, of the membrane, while the fluctuating thickness perpendicular to the plane scales as a power law of L with a power of roughly 0.70. The overall shape of the membrane is, hence, considered flat and rough, since λ_1 diverges as $L \to \infty$. A picture of a flat membrane generated in my simulation is shown in Fig. 4.6.

[1] It is not clear at this point what the effects of the closed geometry of the skeletons are on this exponent and whether a direct comparison may be made.

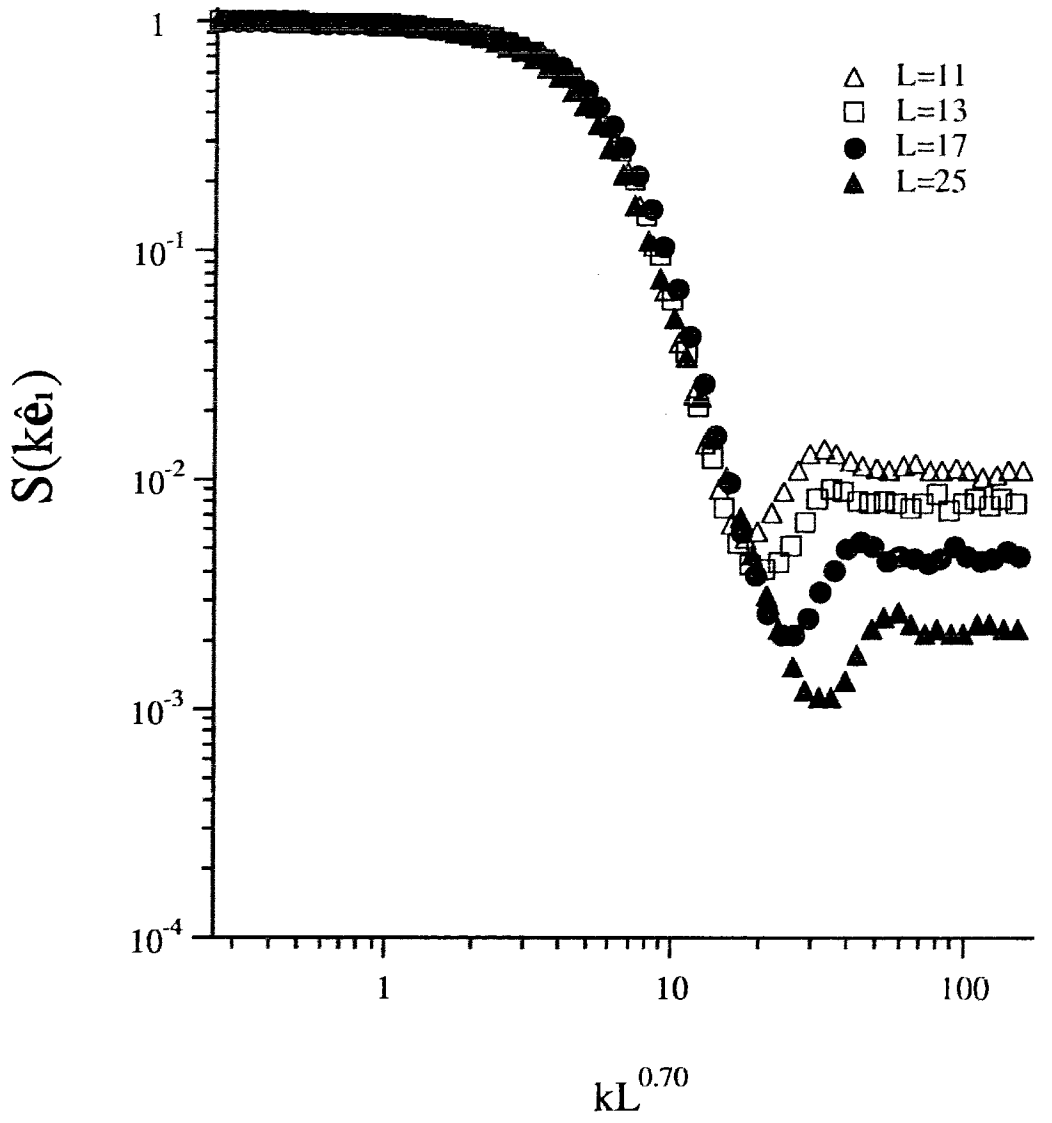

Figure 4.3: Structure factor $S(k\hat{\mathbf{e}}_1)$ plotted as a function of $kL^{0.70}$ for L=11, 13, 17, 25.

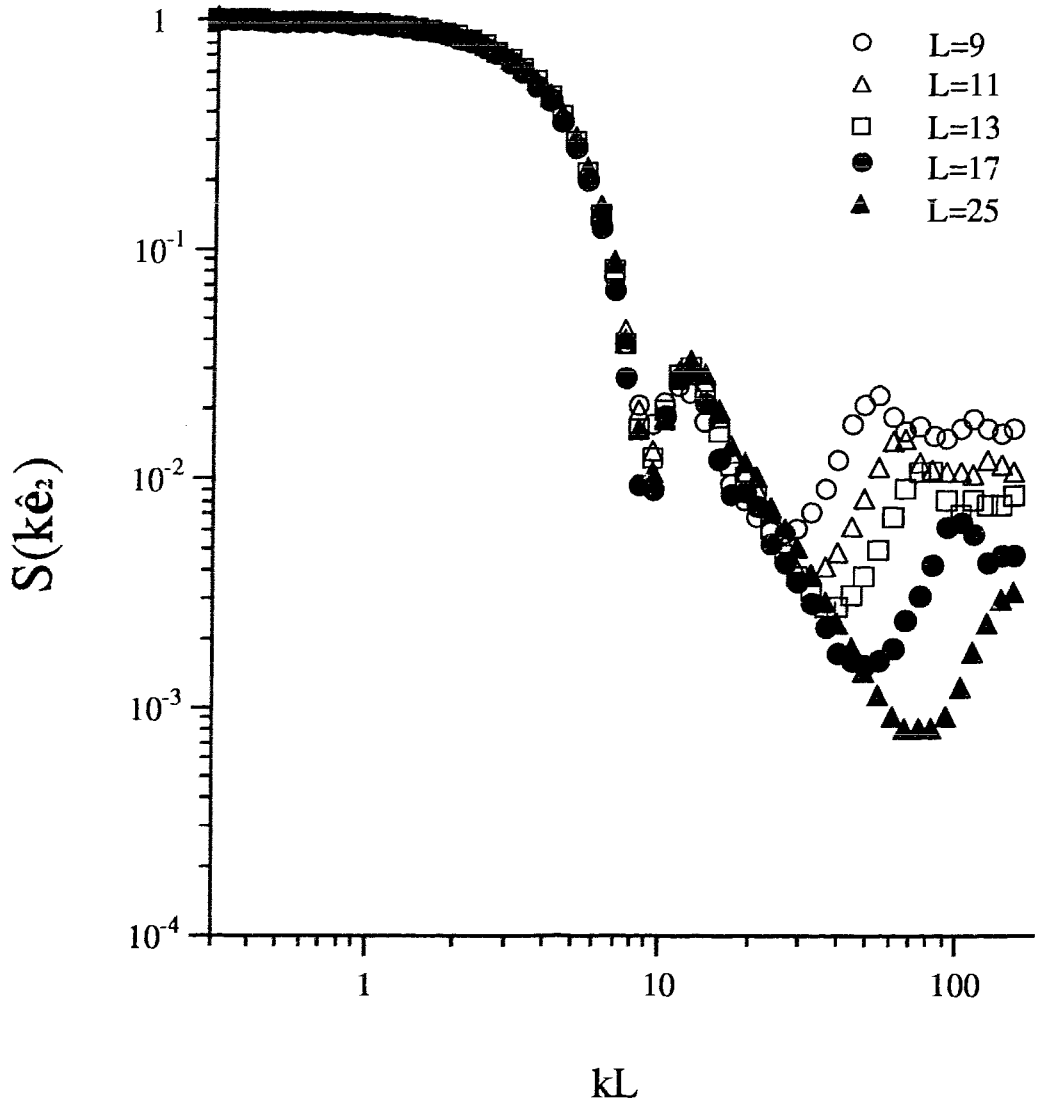

Figure 4.4: Structure factor $S(k\hat{\mathbf{e}}_2)$ plotted as a function of kL for L=9, 11, 13, 17, 25.

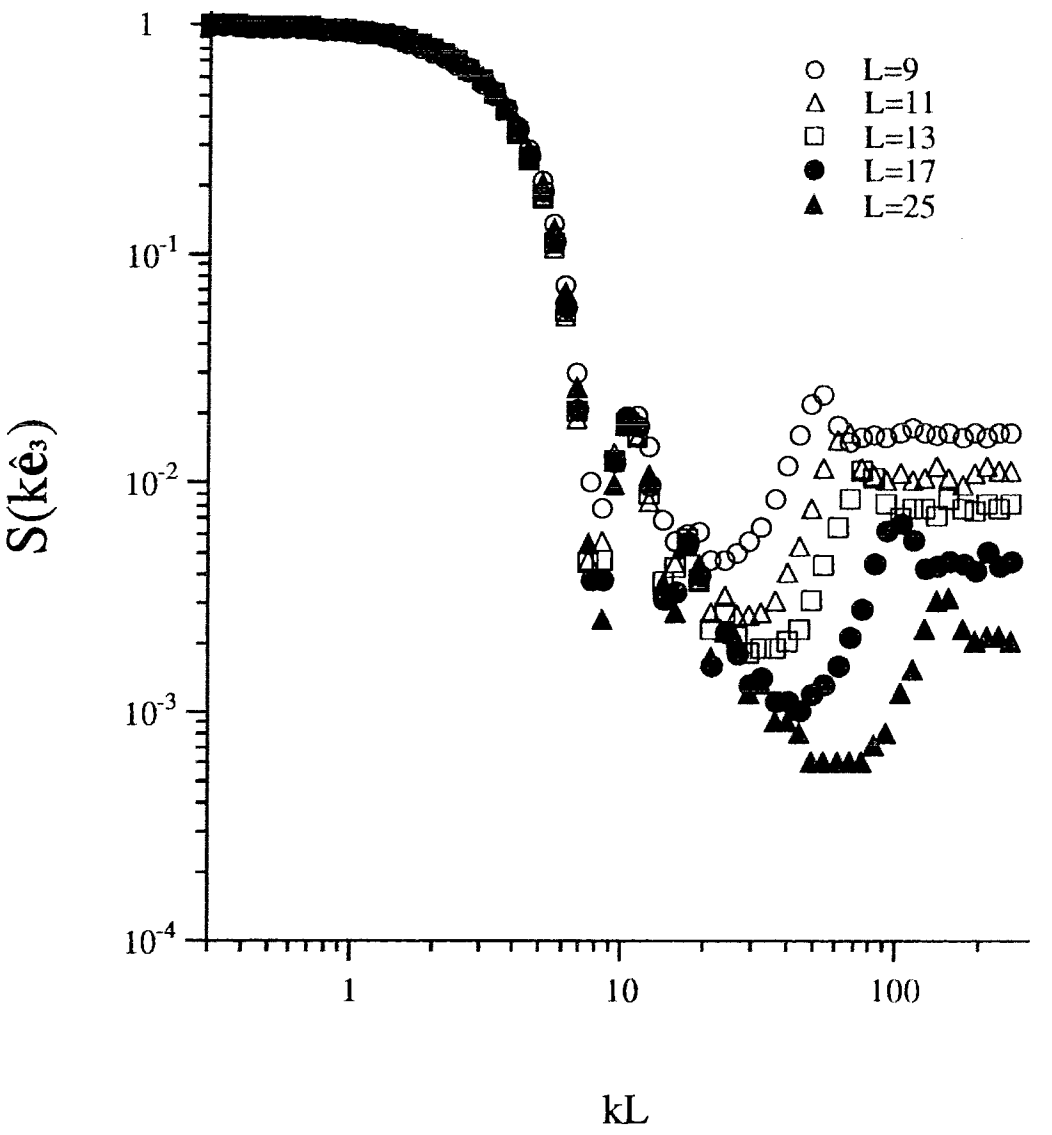

Figure 4.5: Structure factor $S(k\hat{e}_3)$ plotted as a function of kL for L=9, 11, 13, 17, 25.

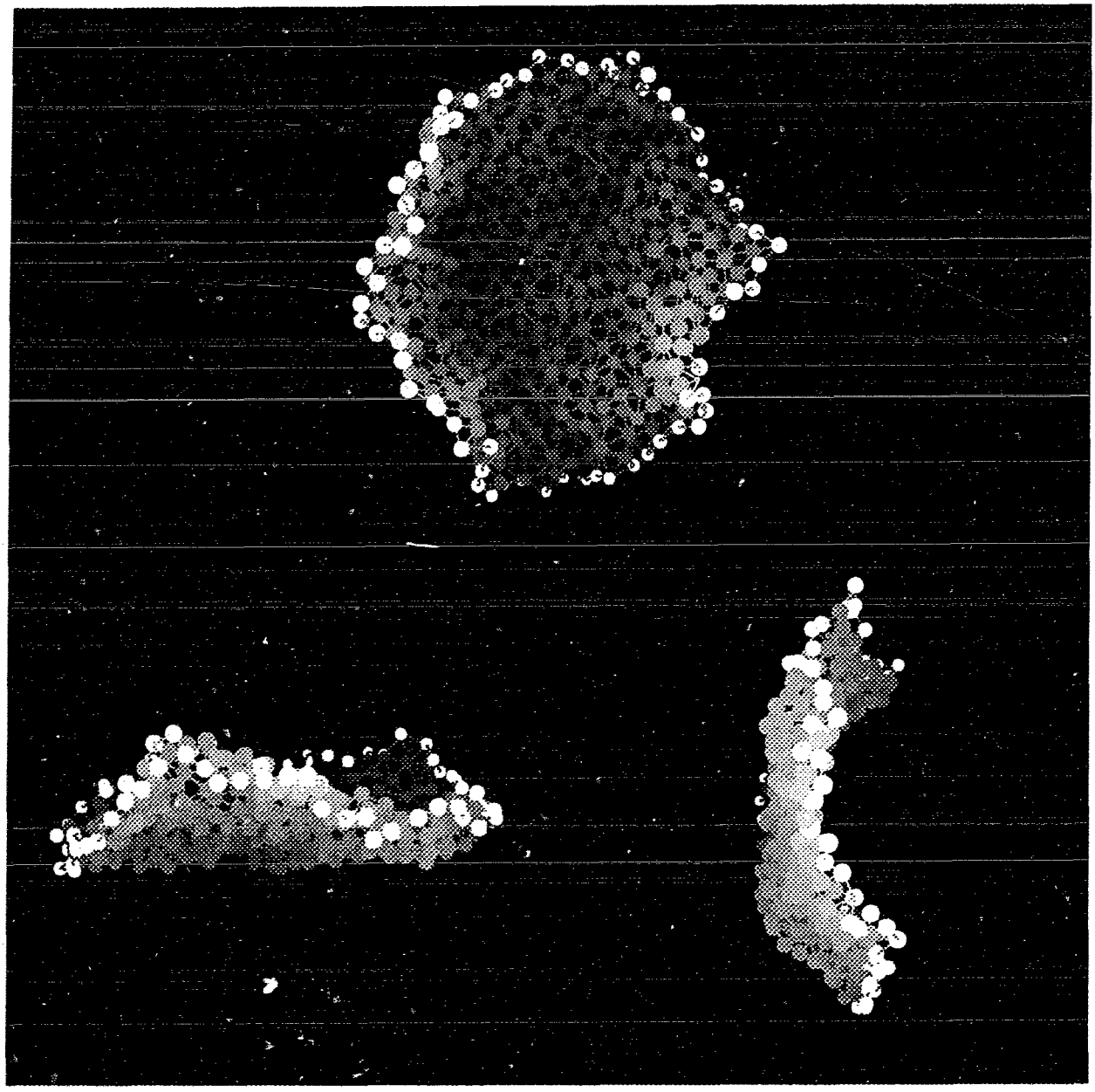

Figure 4.6: A configuration of a flat membrane of size $L = 25$. The unshaded particles are on the perimeter of the membrane. Top: viewed from the short direction, $\hat{\mathbf{e}}_1$, of the principal axes; Bottom left: viewed from one of the two long directions; Bottom right: viewed from the other long direction.

4.3 Weak self-avoidance and numerical RG study

We have demonstrated that a strongly self-avoiding tethered membrane is always flat. It seems that the effective bending rigidity generated by the excluded-volume effect is sufficiently strong to make the membrane flat. This can be qualitatively explained [43] by the following simple argument. Consider the four particles of diameter σ connected by tethers of length l in Fig. 4.7.

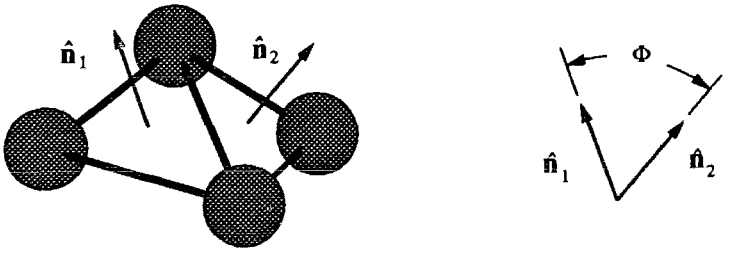

Figure 4.7: A four-particle tethered network with $\hat{\mathbf{n}}_1$ and $\hat{\mathbf{n}}_2$ as the normals of the two triangles spanned by the particles.

The average value of $\hat{\mathbf{n}}_1 \cdot \hat{\mathbf{n}}_2$ is, assuming equal weight for all Φ,

$$\langle \hat{\mathbf{n}}_1 \cdot \hat{\mathbf{n}}_2 \rangle = \frac{1}{\Phi_0} \int_0^{\Phi_0} \cos\Phi d\Phi = \frac{\sin\Phi_0}{\Phi_0} , \tag{4.3}$$

where Φ_0 is the maximum angle allowed by the constraints between $\hat{\mathbf{n}}_1$ and $\hat{\mathbf{n}}_2$, given by

$$\Phi_0 = \pi - 2\arcsin\left(\frac{\sigma}{\sqrt{3}l}\right) .$$

For $\sigma/l = 1/\sqrt{3}$, $\langle \hat{\mathbf{n}}_1 \cdot \hat{\mathbf{n}}_2 \rangle = 0.25$. Imagine now that this four-particle network is a phantom network with bending energy $\kappa(1 - \hat{\mathbf{n}}_1 \cdot \hat{\mathbf{n}}_2)$. A simple calculation shows that in order that $\langle \hat{\mathbf{n}}_1 \cdot \hat{\mathbf{n}}_2 \rangle$ for this phantom membrane match 0.25, the temperature T must be well below the critical temperature T_c at which the phantom membrane undergoes a transition to the low-temperature flat phase (see page 36). It appears, therefore, that self-avoidance produces an effective bending rigidity that is large enough

to keep a membrane flat. Simple as it is, the qualitative picture presented above provides us with some idea about excluded-volume effects in a membrane network, and is basically correct. It has also been shown numerically that the introduction of self-avoidance among merely first- and second-nearest neighbors in an otherwise phantom membrane makes the membrane flat if the ratio of particle diameter to the tether length is sufficiently large [43].

The above argument also predicts a crumpled phase. If we follow the same matching scheme used above, we find that the transition happens when σ/l is decreased below 0.39, or σ below 0.68 for a fixed $l = \sqrt{3}$. Intuitively this is reasonable, since, the smaller the diameter is, the weaker the excluded-volume effects are. There may exist a non-zero size of particles at which the excluded-volume effects are sufficiently weak so that the tethered membrane becomes crumpled. It is worth pointing out that if such a crumpled phase does exist, the exponent governing this phase will be bounded by the physical limits (see Section 1.2.2). This phase will be different from that of a phantom membrane ($\sigma = 0$) for any self-avoiding membrane.

I have studied the thermodynamic behavior of weakly self-avoiding tethered membrane at infinite temperature by varying the size of the hard-core particles, namely σ in (4.1) and (4.2), in the range $0 < \sigma < 1$. The computational procedure is the same as for the strong-self-avoidance case, except that the time required to check for overlap of spheres increases dramatically as the diameter is decreased. We simulated membranes ranging in size from $L = 5$ to only $L = 13$, limited by the computing power that we had. For all sizes, we have at least 1500 configurations separated by one Rouse time and in some cases, many more.

The shape factor A for various sizes of the model membrane is shown in Fig. 4.8 as a function of the hard-sphere diameter σ. We note that A increases as a function of L for small σ and decreases for large σ, consistently with the picture which we have already formed: In the thermodynamic limit, a phantom membrane is isotropic while

a strongly self-avoiding one is highly anisotropic. If there exists a critical diameter σ_c^*, one would expect that for sufficiently large L the curves $A(\sigma, L)$ would intersect close to σ_c^*. The intersection points of the curves drawn through the data points in Fig. 4.8 thus provide a sequence of estimates of this critical diameter. Denote the intersection point of the curves for L_1 and L_2 by $\sigma_c(L_1, L_2)$. The critical diameter in the thermodynamic limit is given by $\sigma_c^* = \sigma_c(L_1 \to \infty, L_2 \to \infty)$. By examining Fig. 4.8 we find $\sigma_c(5,7) \approx 0.36$, $\sigma_c(7,9) \approx 0.20$, $\sigma_c(9,11) \approx 0.18$, $\sigma_c(9,13) \approx 0.14$, and $\sigma_c(11,13) \approx 0.09$. We conjecture that the rapid decrease of $\sigma_c(L_1, L_2)$ as L_1 and L_2 become large means that any $\sigma > 0$ is sufficient to make a tethered membrane flat in the thermodynamic limit. The ideal Gaussian fixed point (for $\sigma = 0$ phantom membrane) is unstable against any increase in diameter or, in other words, self-avoidance is relevant for tethered membranes in three dimensions, however weak it may be.

We next examine the shape factor from a different point of view. In Fig. 4.9 we plot A for various σ as a function of L. The large L limit is, of course, the most interesting. For $\sigma \geq 0.15$, the shape factor decreases, presumably to zero, as L becomes large. For $\sigma = 0.10$, membranes larger than $L = 11$, as seen from the figure, begin to demonstrate this behavior. The shape factor for $\sigma = 0.05$ is indistinguishable from that of a phantom membrane, and for the largest model system which we were able to simulate it shows no sign of decreasing. However, this is a *very* small diameter compared with the strong self-avoidance case. This plot indicates that self-avoiding tethered membranes are asymptotically flat at least for $\sigma \geq 0.1$, consistent with the analysis presented above.

For very small σ, it is difficult to determine whether a membrane is crumpled or flat due to the limited size of the membrane. In general, such cross-over effects can be studied by finite-size analysis and by renormalization-group methods. These again require simulation of model systems of reasonably large sizes.

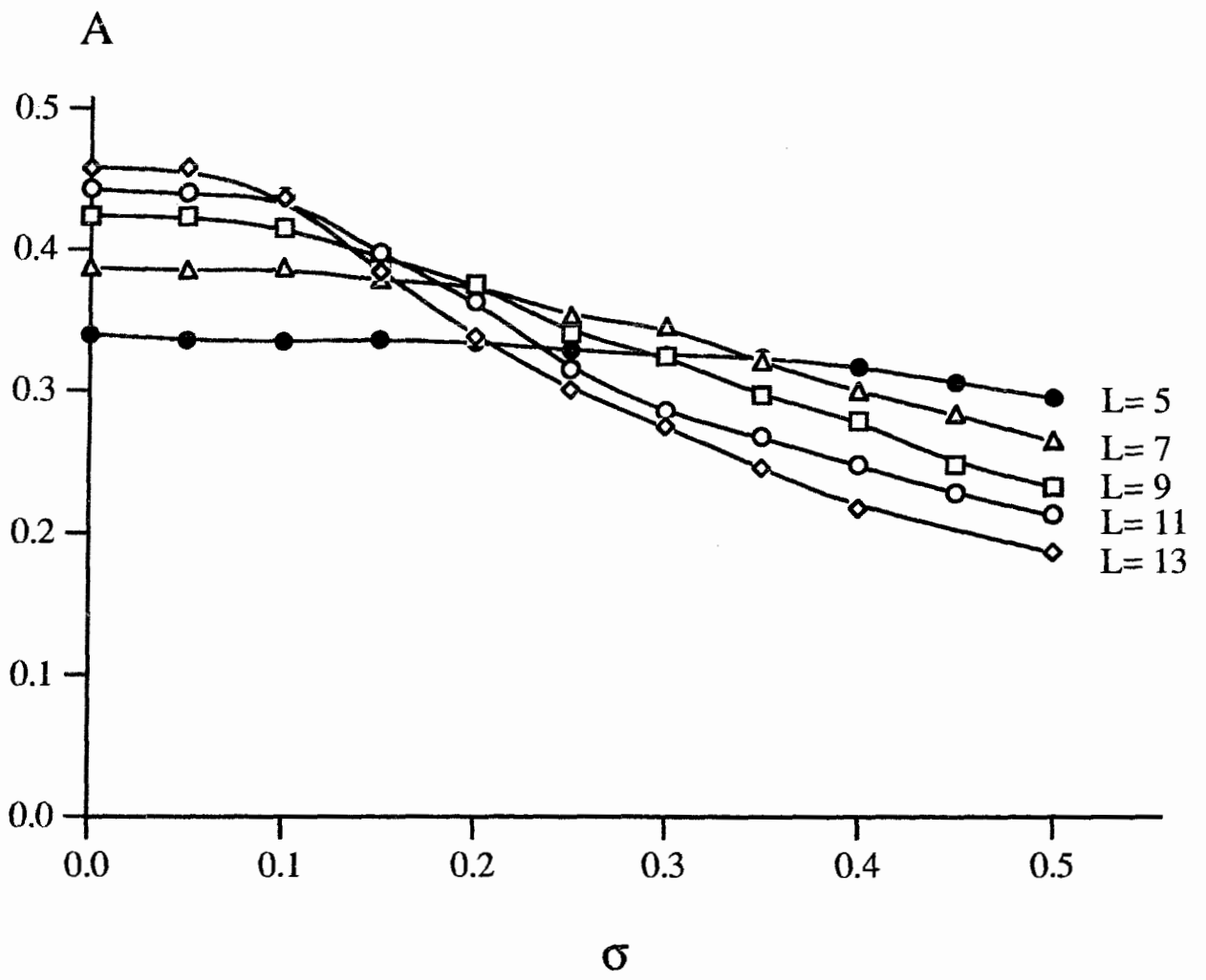

Figure 4.8: The shape factor, $A \equiv \langle \lambda_1/\lambda_3 \rangle$, as a function of diameter σ for various values of L.

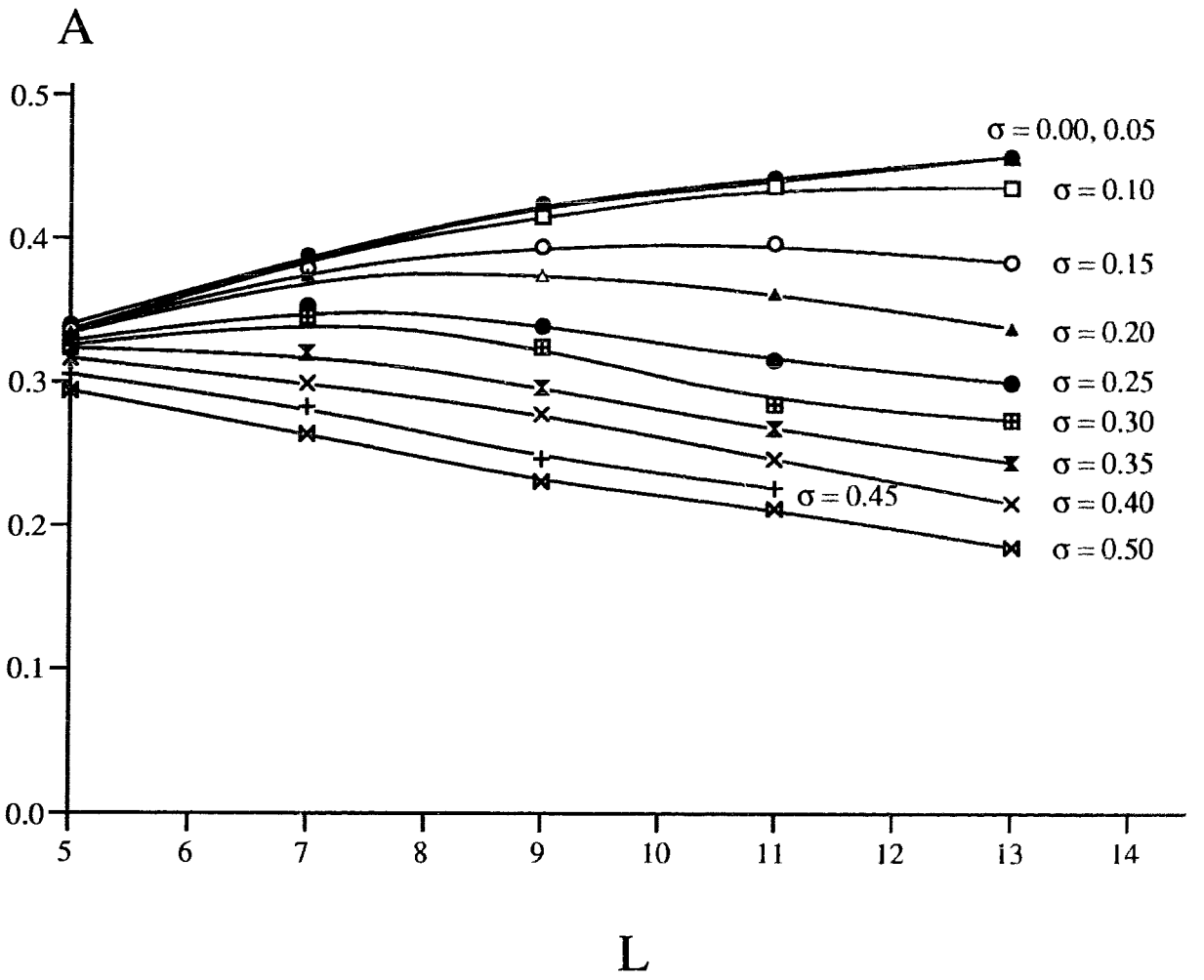

Figure 4.9: The shape factor, $A \equiv \langle \lambda_1/\lambda_3 \rangle$, as a function of membrane size L for various σ. This figure suggests that for any finite σ, self-avoiding membranes are flat in the thermodynamic limit.

I have attempted a numerical renormalization-group (RG) study of the present model.[2] The basic idea of the RG analysis has been introduced in Chapter 2. Fig. 4.10 displays the RG transformation used in this calculation. According to the scheme, a membrane of size L_1 may be mapped onto a membrane of size L_2 by a 'decimation' transformation. Some possible sequences are: $\cdots \to L = 25 \to L = 13 \to L = 7$; $\cdots \to L = 17 \to L = 9 \to L = 5 \to L = 3$. Physical quantities, such as the radius of the gyration and the shape factor, should be invariant under the transformation. For instance,

$$R_g(L_1, \sigma_1, a_1) = R_g(L_2, \sigma_2, a_2) \, ,$$

where a is the average tether length. Recall that L is taken to be an integer and is dimensionless. The quantity a_2 can be calculated from the original network as the average distance between nearest shaded monomers in diagram (a) in Fig. 4.10 and σ_2 is to be calculated. When this transformation is repeated, one obtains the flow of the dimensionless quantity σ/a which measures the strength of the excluded-volume effects,

$$\frac{\sigma_1}{a_1} \to \frac{\sigma_2}{a_2} \to \cdots \, .$$

We have applied this method to various membranes. Since the results are generally consistent with the analysis presented above, we merely illustrate the procedure for a single set of parameters. For example, beginning with a membrane of size $L_1 = 17$ and $\sigma_1 = 0.1$ we found $a_1 = 1.101$ and $a_2 = 1.303$ for this membrane. The newly formed membrane is of size $L_2 = 9$ with a_2 as the inter-monomer distance. We now rescale this membrane to match one of the membranes of size L_2 which we have simulated for various σ, according to the following rescaling property

$$\frac{R_g(L_2, \sigma_2, a_2)}{a_2} = \frac{R_g(L_2, \sigma, a)}{a} = \text{dimensionless} \, .$$

Once σ and a are found, we take

$$\frac{\sigma_2}{a_2} = \frac{\sigma}{a} \, .$$

[2]Reference: c.f. [44] for polymer chains.

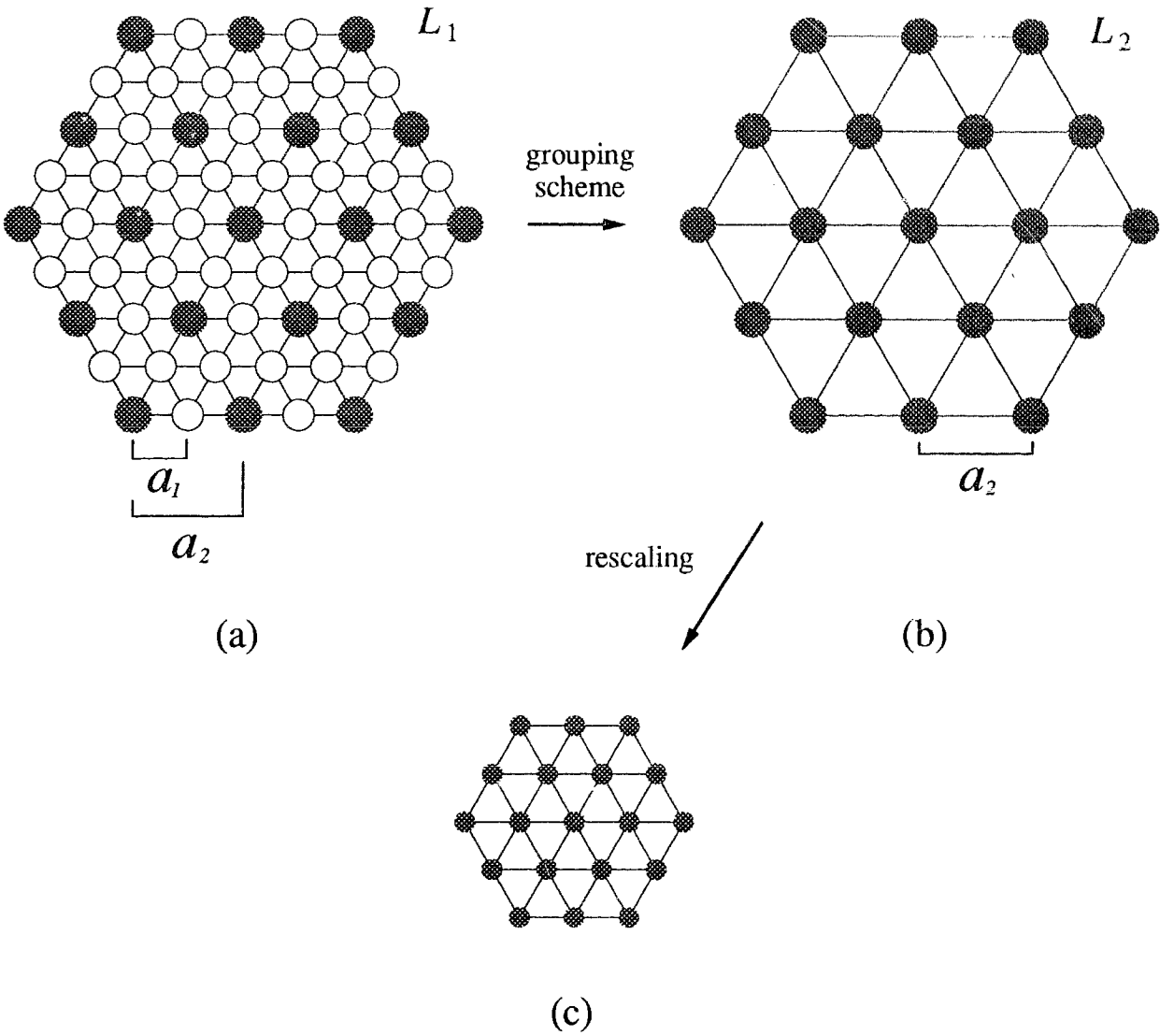

Figure 4.10: Renormalization-group transformation scheme. The shaded particles in the membrane of size L_1 are the analog of block spins in a renormalization transformation for a spin system.

For the RG procedure performed on the membrane described above, we found $\frac{\sigma}{a} = \frac{0.12}{1.110} = 0.11$. Comparing with $\frac{\sigma_1}{a_1} = \frac{0.10}{1.101} = 0.09$, we see that the RG flow goes in the opposite direction of the ideal Gaussian fixed point ($\sigma/a = 0$) indicating that for small diameter (as small as 0.10 at least) the membrane approaches the self-avoidance limit under the RG procedure.

Because of the limited size of our systems, we could carry out the RG procedure only once or at most twice. The change in σ/a in the flow is small, so that the direction of the flow is not unambiguously determined. Nevertheless, the flow direction obtained from the radius of the gyration is the same as that obtained from the shape factor, and is consistent with the conclusions that we drew about the properties of the membranes with $\sigma \geq 0.10$. The RG approach could be very useful if it were possible to simulate larger systems.

As I have demonstrated previously, excluded-volume effects generate effective bending rigidity on intermediate length scales, although no explicit bending rigidity is present in our model. A RG analysis should include the bending rigidity as a parameter as well. I have attempted to calculate the renormalization flow in the two-parameter (κ, σ)-plane where κ is the spring constant of a repulsive spring potential which we implemented between second-nearest-neighbor particles in place of the bending rigidity in Ref. [19]. Due to lack of extensive data, the results will not be reported in this thesis.

4.4 Conclusions

We have studied the behavior of strongly self-avoiding tethered membranes as well as weakly self-avoiding membranes at infinite temperature. For the strongly self-avoiding membranes, we find a flat but rough phase: $\sqrt{\lambda_2} \sim \sqrt{\lambda_3} \sim L$, and $\sqrt{\lambda_1} \sim L^{0.70}$. There is no evidence for the existence of a crumpled phase. For the weakly self-

avoiding membrane, we find that, when the diameter of the monomers is decreased, the membrane remains in the flat phase in the thermodynamic limit. The situation is not unambiguously clear for the case of very small diameter. However, we suggest that for any finite σ, self-avoiding membranes are flat in a three-dimensional embedding space in the thermodynamic limit.

Chapter 5

Self-avoiding Membranes With Attractive Potentials

5.1 Introduction

We concluded at the end of Chapter 4 that a self-avoiding tethered membrane is flat when the only interaction between the particles is the hard-core potential. However, physical membranes or solid sheets cannot be described only in terms of connectivity and hard-core interactions. For instance, particles in a membrane in a poor solvent tend to attract each other due to effective van der Waals and screened Coulomb interactions between solvent particles and membrane particles. These attractive interactions, at sufficiently low temperatures, may overcome the effective bending rigidity due to the hard cores and lead to a collapsed or crumpled phase.

In Chapter 1 we introduced, in the light of mean-field theory [13], the concept of the θ-temperature, at which the effective pair interaction between particles of a self-avoiding polymer vanishes. One can see easily that the Flory scheme for a polymer chain in a good solvent discussed in Chapter 1 will not work without modification below the θ-point. In fact, since the pair interaction vanishes at the θ-point, higher-order interactions, such as the three-body interaction, come into play. While a three-body interaction does not change the behavior of a chain at the θ-point (quasi-ideal)

very much from that of an ideal chain, it gives rise to a more compact structure than the spatial structure of an ideal chain when the temperature is below the θ-point. The size of this collapsed structure is found [45, 46, 47] to scale with the number of particles of the chain with an exponent of 1/3—the close-packing exponent for polymers. Depending on its properties and that of the solvent, at a certain temperature a single polymer may find itself in a swollen (but crumpled) phase, in an ideal (crumpled) phase , or in a collapsed phase [12].

A natural question for one to ask is how tethered membranes behave at low temperatures when the effective interaction between membrane particles vanishes or becomes attractive. The flat phase for tethered membranes in a good solvent, which is non-existent for polymers, has been found both by theory and experiment [42][1]. The behavior of tethered membranes in a poor solvent has been the subject of interest of a few research groups [28, 29, 30, 31, 32, 48].

For tethered membranes, there have been a few recent experiments, which discovered a crumpled phase [30, 31, 32, 48] and a collapsed phase [31], although the interpretation of these experiments has recently been questioned [49]. From the theory side, Abraham and Kardar have studied tethered membranes with attractive interactions [28]. I shall describe the results of some of these studies in the following, since they are closely related to my work which is to be reported in this chapter.

[1]Recently Schmidt *et al.* reported light-scattering studies of the spectrin network of red blood cells. Although this network is in the shape of a vesicle, these authors concluded that the structure factor indicated a 'flat' phase rather than a crumpled one.

Molecular Dynamics Simulation

Abraham and Kardar [28] studied self-avoiding tethered membranes with an attractive potential,

$$U_{NN}(r) = \begin{cases} 4\varepsilon\left[\left(\frac{1}{r}\right)^{12} - \left(\frac{1}{r}\right)^{6} + \frac{1}{4}\right] & r < 2^{1/6} \\ 0 & 2^{1/6} \leq r \leq 2^{1/6} + l \\ 4\varepsilon\left[\left(\frac{1}{r'}\right)^{12} - \left(\frac{1}{r'}\right)^{6} + \frac{1}{4}\right] & r > 2^{1/6} + l \end{cases} , \quad (5.1)$$

for nearest-neighbor particles and a truncated Lennard-Jones potential for non-nearest-neighbor particles,

$$U(r) = \begin{cases} 4\varepsilon\left[\left(\frac{1}{r}\right)^{12} - \left(\frac{1}{r}\right)^{6}\right] & r < 2.5 \\ 0 & \text{otherwise} \end{cases} , \quad (5.2)$$

where $r' = 2(2^{1/6}) + l - r$ and l is taken to be 0.5. A plot of $U(r)$ can be found in Fig. 5.1.

The geometry of Abraham and Kardar's model membrane is identical to the one shown in Fig. 3.1, and these authors were able to simulate membranes as large as $L = 75$ by molecular dynamics simulations.

At high temperatures the attractive potential is not important and the membrane is found to be flat, reaffirming the previous findings. As the temperature is decreased the attractive potential begins to dominate and a collapsed phase is achieved at sufficiently low temperature. What is most interesting is the behavior of the membrane at intermediate temperatures. These authors found that a single-fold configuration is first formed at a certain temperature ($k_B T_{c1} = 3.15\varepsilon$ for $L = 75$) with the crease neatly dividing the membrane in half. At a lower temperature ($k_B T_{c2} = 2.75\varepsilon$ for $L = 75$) the membrane is folded one more time, to make four roughly equal parts folded together. At still lower temperatures, more distinct foldings are hard to identify but eventually a collapsed phase is clearly identified. They concluded that the

collapsed and the flat phases are separated by a folded phase. In this work only one size of membrane was studied, and it is unclear whether or not the sequence of folding transitions becomes a single crumpling or collapse transition in the thermodynamic limit.

Light-Scattering Experiments

There have been few experimental studies of tethered membranes. One major difficulty is the preparation of thin membrane samples which will equilibrate in experimentally feasible times. Recently, Hwa *et al.* [30] and Wen *et al.* [31] succeeded in synthesizing thin membranes of graphite oxide (GO) by exfoliating sheets of graphite oxide. These solid thin membranes have a thickness of less than 100Å and possess a six-fold symmetry to some extent. A large film has a linear size of a few microns and the interatomic spacing is estimated to be roughly 2.5Å. These workers performed light-scattering experiments on the films in solution. In these experiments, sheets of GO were suspended in aqueous solutions at different pH and the structure factor was obtained by light-scattering measurements. Remarkably, a crumpled phase was observed and the exponent ν remained constant at roughly the Flory value ($\nu = 4/5$) for a considerable range of pH. A collapsed phase with fractal dimension $D_f = 2/\nu = 3$ was also found by these workers when the sheets were suspended in an acetone solution, in which the effective intrasheet interaction was presumably stronger.

In the next two sections, I present our extensive Monte Carlo simulation study of a model in which the particles on the network interact through a potential which is hard-core repulsive and square-well attractive. Although similar to the model studied in Ref. [28], this model exhibits different behavior at intermediate temperatures and seems to be consistent with the experiments.

5.2 The model with attractive potential

The model which we use is identical to the one studied in Chapter 4 except that an additional attractive two-body interaction is introduced between particles on the tethered membrane network. The diameter of the particles is fixed at $\sigma = 1$ in the simulation, so this is a strong-self-avoidance model. The two-body nearest-neighbor interaction potential is given by

$$U_{NN}(r) = \begin{cases} \infty & r < 1 \\ -\varepsilon & 1 \le r \le \sqrt{3} \\ \infty & \sqrt{3} < r \end{cases} . \tag{5.3}$$

Non-nearest-neighbor particles interact through the attractive interaction potential,

$$U(r) = \begin{cases} \infty & r < 1 \\ -\varepsilon & 1 \le r \le \sqrt{3} \\ 0 & \sqrt{3} < r \end{cases} . \tag{5.4}$$

It is, therefore, energetically favorable for non-nearest-neighbor particles to come close to each other to take advantage of the attractive potential. The attractive potential creates the possibility of new phases for the membranes. Our binding potential between nearest-neighbor particles, $U_{NN}(r)$, is essentially identical to the potential used in the simulation in Ref. [28]. The interaction potential $U(r)$ between non-nearest-neighbor particles is displayed in Fig. 5.1, along with the potential used in Ref. [28] for the purpose of comparison.

The range of the attractive potential is chosen purely for computational efficiency: Nearest neighbors on the network are constrained by the tethers to be always inside the well and, therefor, contribute only a constant to the internal energy. This constant can be ignored in the calculation of the energy difference generated by a trial step in the Monte Carlo simulation. The equilibrium state of the system is controlled by

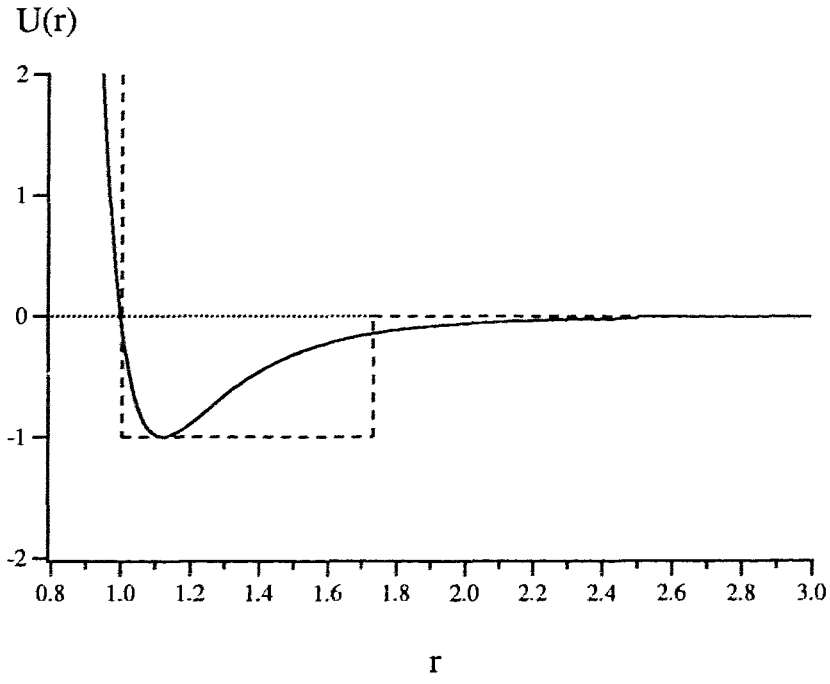

Figure 5.1: Interaction potentials between non-nearest-neighbor particles. The potential drawn in dashed lines is used in our simulations. The solid curve is used in Ref. [28] and has a minimum at $r = 2^{1/6}$. The parameter ε in both models is taken to be the same in this figure.

the product of ε and β, where $\beta = (k_B T)^{-1}$ and T is the temperature. We shall use $\tilde{\beta} = \varepsilon\beta$ to denote this control parameter. At $\tilde{\beta} = 0$ this system is equivalent to the strongly self-avoiding membrane studied in Chapter 4.

We used the standard Metropolis Monte Carlo procedure to simulate membranes ranging in size from $L = 7$ to 25 at all temperatures investigated. For a few temperatures, we have also simulated clusters of size $L = 33$ ($N = 817$). We have started simulations from flat, purposely generated crumpled, collapsed, and folded initial configurations, and we found that the system eventually reaches the same equilibrium state. According to the relaxation studies which we performed on all the simulations, we have in most cases 300 samples separated by a relaxation time. These calculations were carried out on Silicon Graphics 240D workstations and consumed several

processor-years.

5.3 Thermodynamic behavior and phase transitions

The Principal Moments

We first study the properties of the principal moments, as they are good indicators of the membrane shape. Fig. 5.2 shows the eigenvalues λ_j as function of $\tilde{\beta}$ for a membrane of size $L = 25$.

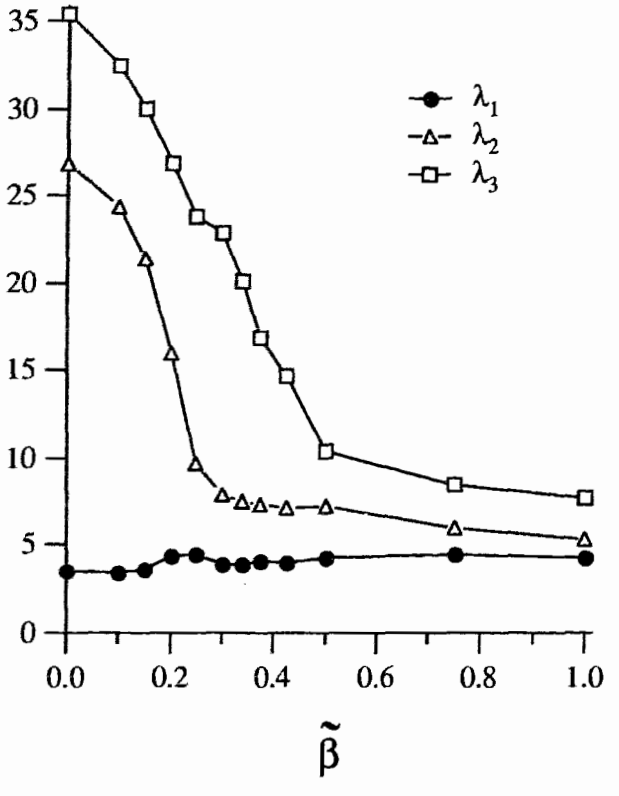

Figure 5.2: Eigenvalues λ_1, λ_2, and λ_3 for L=25 displayed as function of the control parameter.

Both λ_2 and λ_3 decrease sharply for $\tilde{\beta} > 0.2$ and saturate at a low-temperature

value for $\tilde{\beta} > 0.5$. The behavior of these eigenvalues is the same for all values of L but the decrease becomes sharper and shifts to lower values of $\tilde{\beta}$ as L is increased. We determine the exponent ν_3 by fitting the eigenvalue λ_3 to the functional form $\lambda_3 = aL^{2\nu_3}$ for $7 \leq L \leq 33$. The results of that fit are shown in Table 5.1. We have also studied λ_3 by neglecting the smaller system sizes one by one in the fitting process, and obtained a sequence of best-fit exponents. These exponents are found to scatter about the values quoted in Table 5.1 and show no systematic trend of either increase or decrease. The average value of λ_3 at $\tilde{\beta} = 0.25$ is plotted as a function of L in Fig. 5.3.

$\tilde{\beta}$	ν_3
0.00	[a]0.95 ± 0.05
0.10	[a]0.93 ± 0.05
0.15	0.91 ± 0.04
0.20	0.83 ± 0.04
0.25	0.81 ± 0.04
0.30	0.80 ± 0.04
1.00	[a][b]0.63 ± 0.05

[a]Data for $7 \leq L \leq 25$.

[b]Obtained by fitting the radius of gyration.

Table 5.1: The exponent ν_3 obtained from fitting λ_3 to the formula $\lambda_3 = aL^{2\nu_3}$ for $7 \leq L \leq 33$.

It is clear that, in the range $0.2 < \tilde{\beta} < 0.25$, this exponent crosses over from the flat-phase value of 1.0 to a value close to 0.80. Clearly, the exponent ν_2 must be less than or equal to ν_3 and the corresponding analysis for λ_2 indicates that $\nu_2 = \nu_3$ to within numerical uncertainty. Table 5.1 also shows that ν_3 is essentially constant for $0.2 \leq \tilde{\beta} \leq 0.3$. This exponent reaches a value of 0.67 at $\tilde{\beta} = 1.0$ indicating that the membrane is in the collapsed phase at this low temperature.

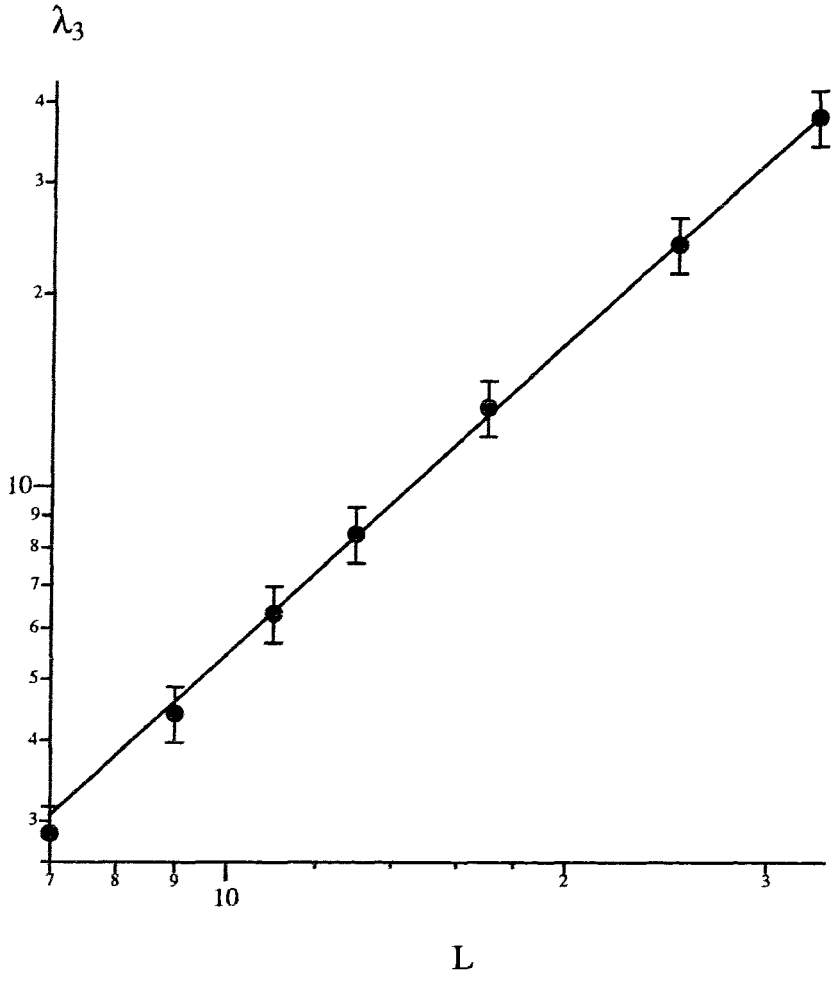

Figure 5.3: The average value of λ_3 at $\tilde{\beta} = 0.25$ as function of L. The data points are marked by "•". The fitting function has the form $\lambda_3 = aL^{2\nu_3}$ and is plotted as the solid line with $\nu_3 = 0.81$.

The behavior of the principal moments shown in Fig. 5.2 is similar to that seen by Abraham and Kardar [28]. These authors observed a sharp decrease in λ_2 followed by a sharp drop in λ_3 at a lower temperature and interpreted this as successive transitions from a flat phase to a phase with a single fold followed by a transition to a phase with a double fold. We have checked in our simulation the density of states as a function of the principal moments and analyzed the shape of the membrane in various ranges of λ_1, λ_2, and λ_3. Although we have seen isolated configurations with folds present, we do not believe that in our case the equilibrium states are characterized by the number of folds. Instead we believe that for a range of temperatures ($0.2 < \tilde{\beta} < 0.5$) the equilibrium state is isotropically crumpled with $\nu \approx 0.80 \pm 0.05$. Our data in the range $0.3 < \tilde{\beta} < 1.0$ are not extensive enough to permit a reliable determination of the exponent ν and, therefore, we do not know the extent of the crumpled phase.

The Shape Factors

In addition to the shape factor A [(3.3)], one may study other quantities that characterize the shape of a membrane. For example, $\langle \lambda_2/\lambda_{20} \rangle$ and $\langle \lambda_3/\lambda_{30} \rangle$ can be used where the subscript 0 indicates that the eigenvalues are calculated when the membrane is in its initial flat conformation and, thus, $\lambda_{20} \sim \lambda_{30} \sim L$. The quantities $\langle \lambda_2/\lambda_{20} \rangle$ and $\langle \lambda_3/\lambda_{30} \rangle$ are not essentially different from the principal moments $\langle \lambda_2 \rangle$ and $\langle \lambda_3 \rangle$ but are more informative, since they approach zero in the isotropic phases and become constant in the flat phase, rather than diverging as λ_2 and λ_3 do in all phases, in the large-L limit. We plot $\langle \lambda_2/\lambda_{20} \rangle$ and $\langle \lambda_3/\lambda_{30} \rangle$ as function of $\tilde{\beta}$ in Fig. 5.4 for $L = 17, 25$, and 33. The transition from the flat phase to the crumpled phase for both sets of curves becomes sharper as L increases.

Further information about the high- and low-temperature phases and the transition point can be obtained by studying the behavior of the normal vectors of elemen-

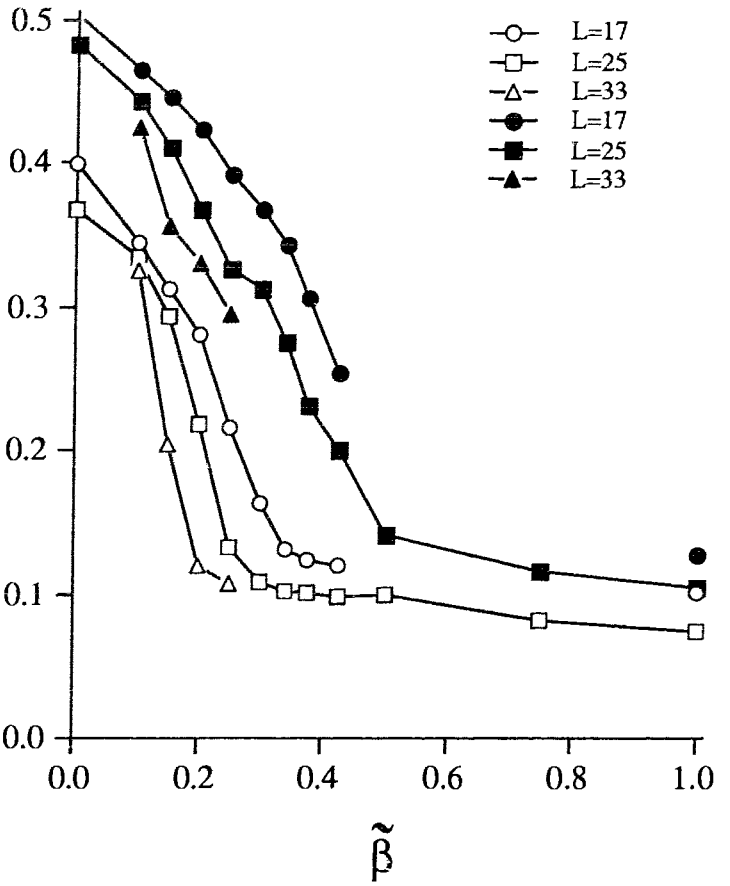

Figure 5.4: $A_{20} \equiv \langle \lambda_2/\lambda_{20} \rangle$ (open symbols) and $A_{30} \equiv \langle \lambda_3/\lambda_{30} \rangle$ (full symbols) as function of $\tilde{\beta}$.

tary triangles formed by nearest neighbors on the network. In Fig. 5.5 we display the quantities $\langle M_j^2 \rangle$ [(3.8)] and $\langle P_j^2 \rangle$ [(3.9)] as function of $\tilde{\beta}$ for a membrane of size $L = 25$. For all temperatures, $\langle M_2^2 \rangle$ and $\langle M_3^2 \rangle$ are zero to within numerical accuracy whereas $\langle M_1^2 \rangle$ drops sharply to zero in the same temperature range in which the exponent ν_3 crosses over to the value 0.80. The behavior of $\langle P_j^2 \rangle$ is consistent with that of $\langle M_j^2 \rangle$ in that the quantities $\langle P_j^2 \rangle$ reach their $\frac{1}{3}$-limit in the same temperature range in which the $\langle M_j^2 \rangle$ drop to zero, as expected for isotropic phases. The behavior of $\langle P_1^2 \rangle$ produced no evidence of a folding transition.

It is also interesting to study $\langle \hat{\mathbf{n}}(\mathbf{0}) \cdot \hat{\mathbf{n}}(\mathbf{x}) \rangle$ where $\hat{\mathbf{n}}(\mathbf{0})$ is the average normal of

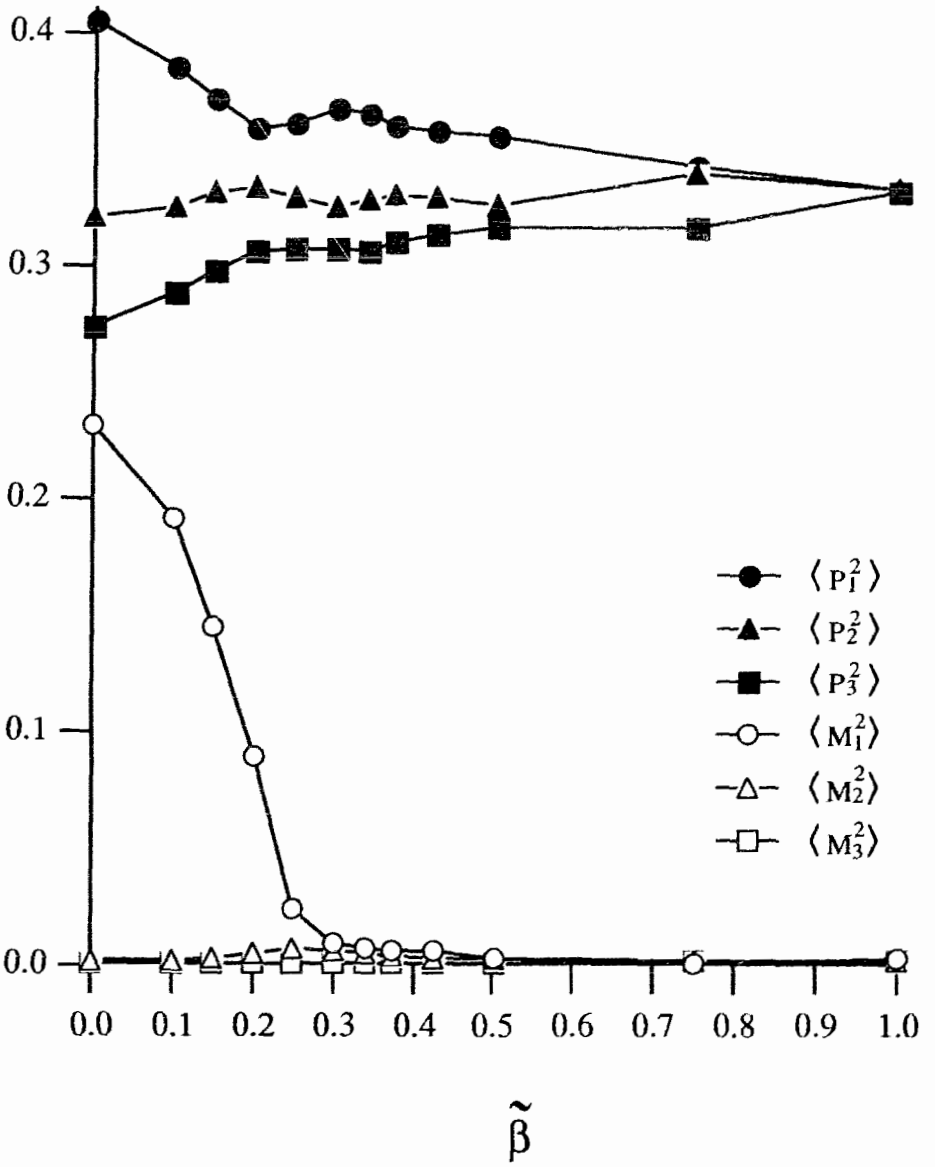

Figure 5.5: $\left\langle M_j^2 \right\rangle$ and $\left\langle P_j^2 \right\rangle$ as function of $\tilde{\beta}$ for a membrane of size $L = 25$.

the innermost ring composed of elementary triangles at the center of the membrane, and $\hat{\mathbf{n}}(\mathbf{x})$ is the average normal of the ring indexed by the distance $\mathbf{x}$ from the center. The quantity $\langle \hat{\mathbf{n}}(\mathbf{0}) \cdot \hat{\mathbf{n}}(\mathbf{x}) \rangle$ is essentially the normal-normal correlation. For the flat phase, $\langle \hat{\mathbf{n}}(\mathbf{0}) \cdot \hat{\mathbf{n}}(\mathbf{x}) \rangle$ decreases slowly from the center to the perimeter and remains finite for all rings, while for $\tilde{\beta} \geq 0.2$ it drops quickly to approach zero beyond roughly 3–5 rings towards the edge of the membrane.

The Structure Factor

In Figs. 5.6, 5.7, and 5.8 we show the structure factors $S(k\hat{\mathbf{e}}_1)$, $S(k\hat{\mathbf{e}}_2)$ and $S(k\hat{\mathbf{e}}_3)$ as function of the variable $kL^{0.80}$ at $\tilde{\beta} = 0.25$ for the larger membranes that we have simulated. The excellent collapse of the data to a single curve in each of the three cases indicates that the membranes are isotropic and that $\nu \approx 0.80$, consistently with the scaling behavior of the principal moments. An equally good collapse of the data is found for $\tilde{\beta} = 0.2$ and $\tilde{\beta} = 0.3$ with the same exponent, $\nu = 0.80$.

For the low temperature, $\tilde{\beta} = 1.0$, we plot $S(k\hat{\mathbf{e}}_j)$, j=1, 2, 3, as functions of the scaled variable $kL^{0.67}$ in Figs. 5.9, 5.10, and 5.11. The data collapse to single curves remarkably well even for rather small membranes, indicating that this temperature lies well below the transition to the collapsed phase.

Other Thermodynamic Quantities

In our simulations we have also obtained other thermodynamic functions, such as the internal energy and specific heat. We have calculated the internal energy $\langle E \rangle$ for each membrane size at all the temperatures investigated and have performed extrapolation to obtain $\langle E \rangle$ in the thermodynamic limit. The behavior of $\langle E \rangle$ is essentially the same as $\langle E \rangle_{L=25}$ and, since we have more data for $L = 25$ at low temperatures, we show $\langle E \rangle_{L=25}$ in Fig. 5.12.

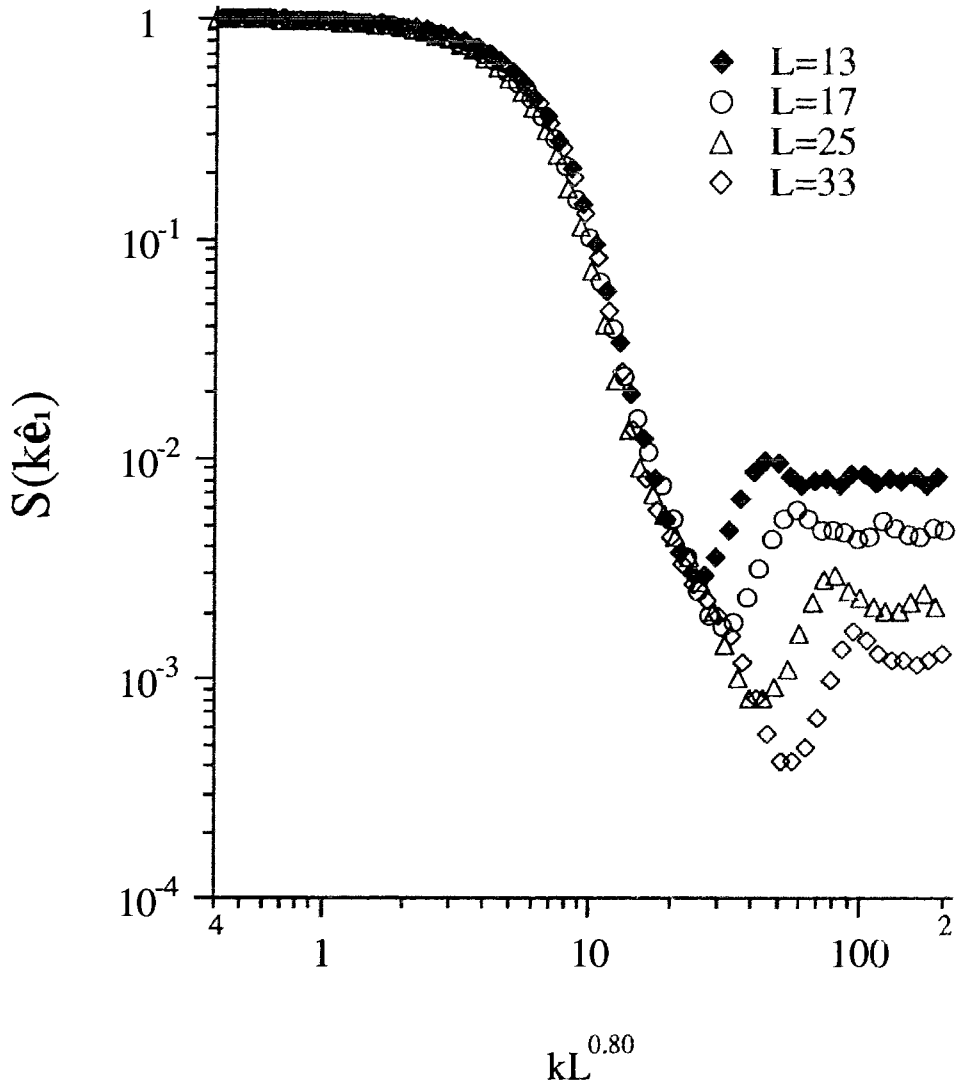

Figure 5.6: Structure factor $S(k\hat{\mathbf{e}}_1)$ plotted as function of $kL^{0.80}$ for L= 13, 17, 25, 33 at $\tilde{\beta} = 0.25$.

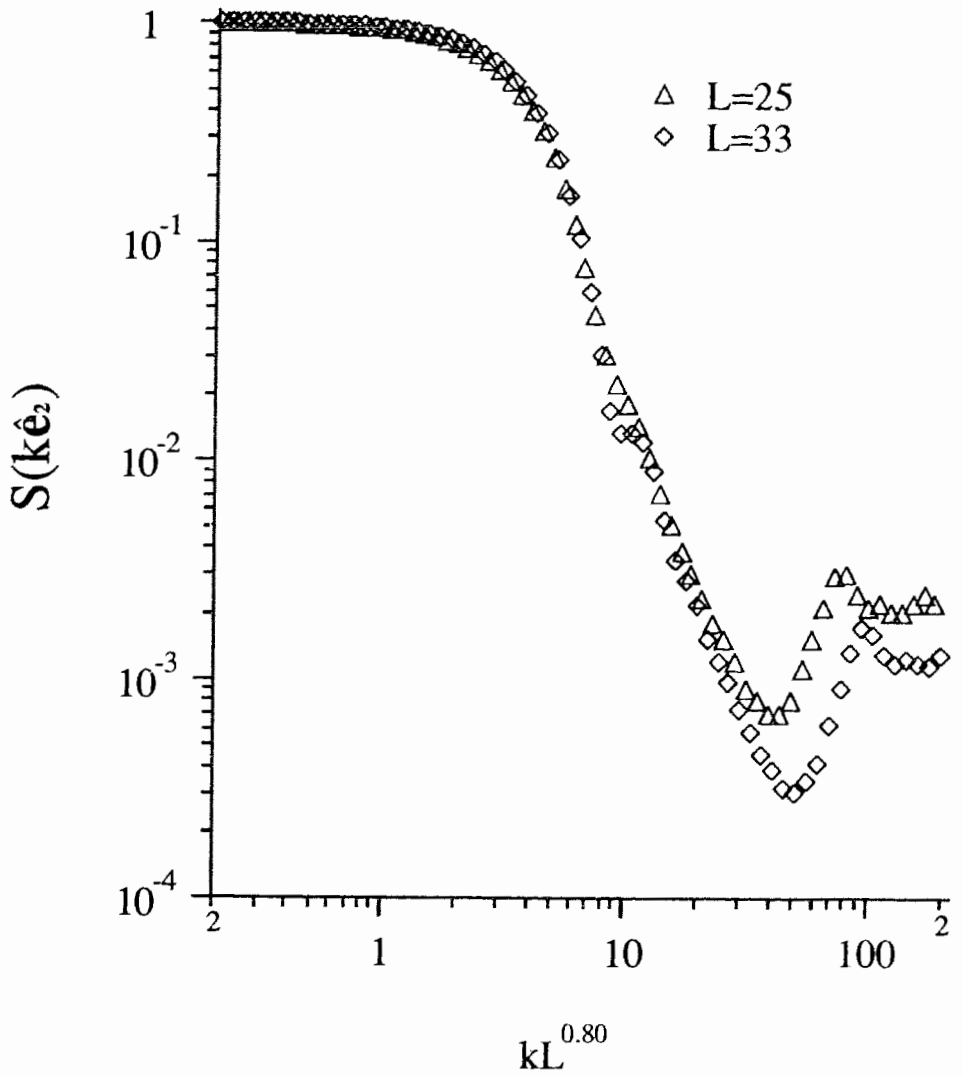

Figure 5.7: Structure factor $S(k\hat{\mathbf{e}}_2)$ plotted as function of $kL^{0.80}$ for $L = 25$, 33 at $\tilde{\beta} = 0.25$.

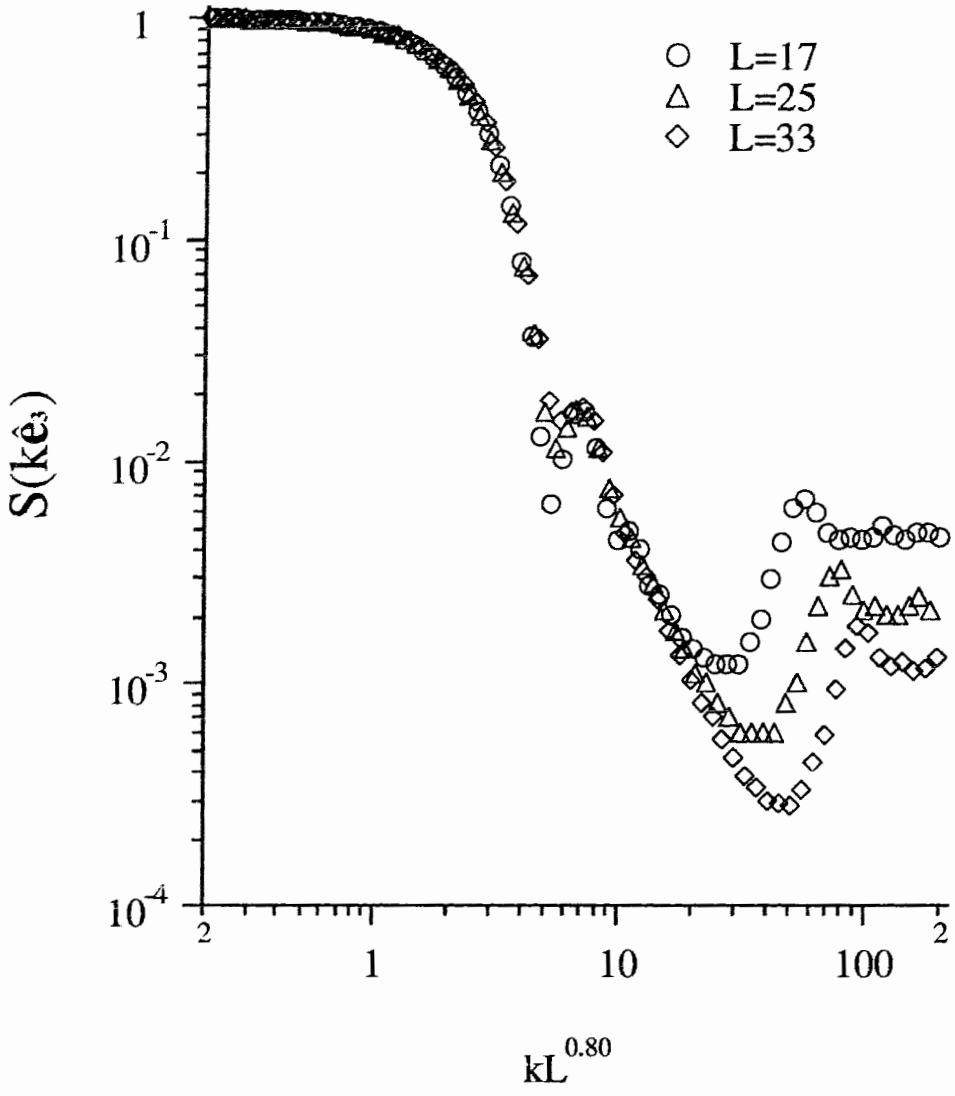

Figure 5.8: Structure factor $S(k\hat{\mathbf{e}}_3)$ plotted as function of $kL^{0.80}$ for $L = 17$, 25, 33 at $\tilde{\beta} = 0.25$.

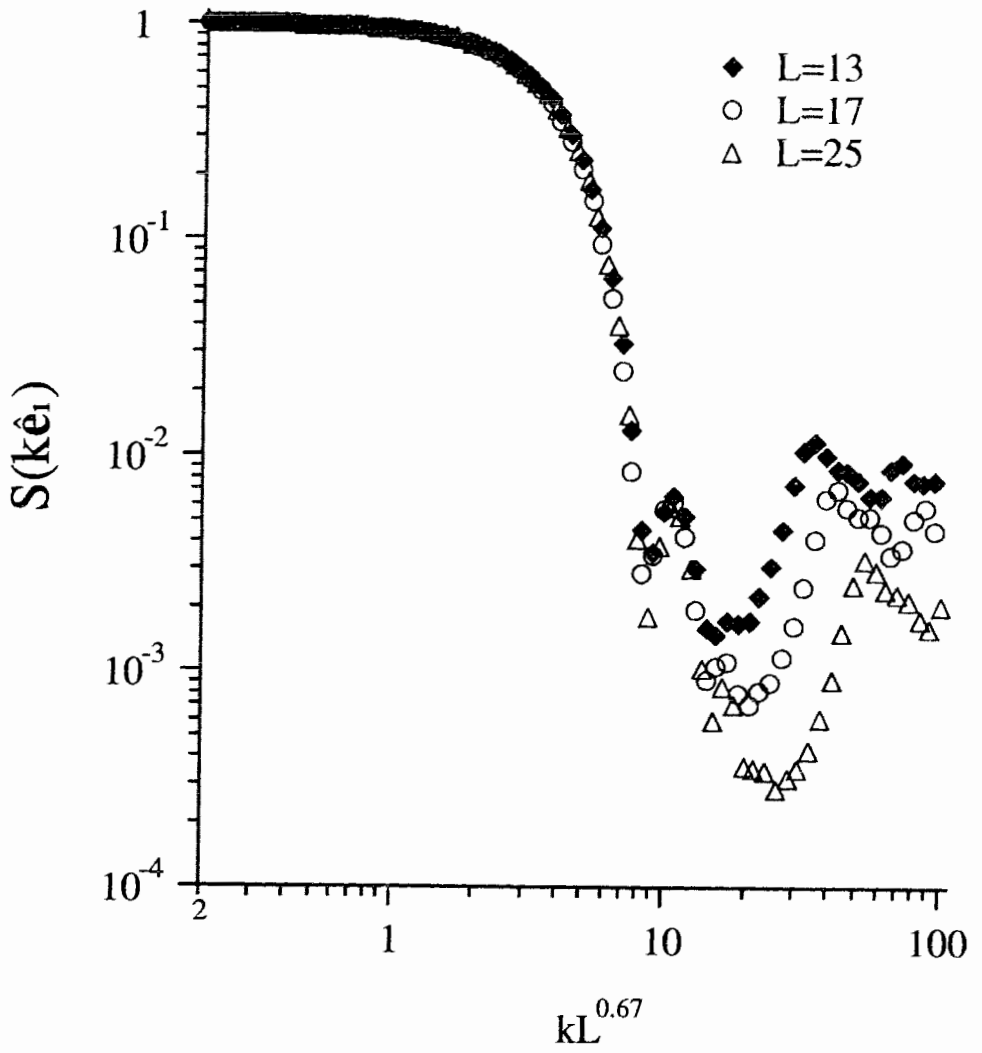

Figure 5.9: Structure factor $S(k\hat{\mathbf{e}}_1)$ plotted as function of $kL^{0.67}$ for $L = 13, 17, 25$ at $\tilde{\beta} = 1.00$.

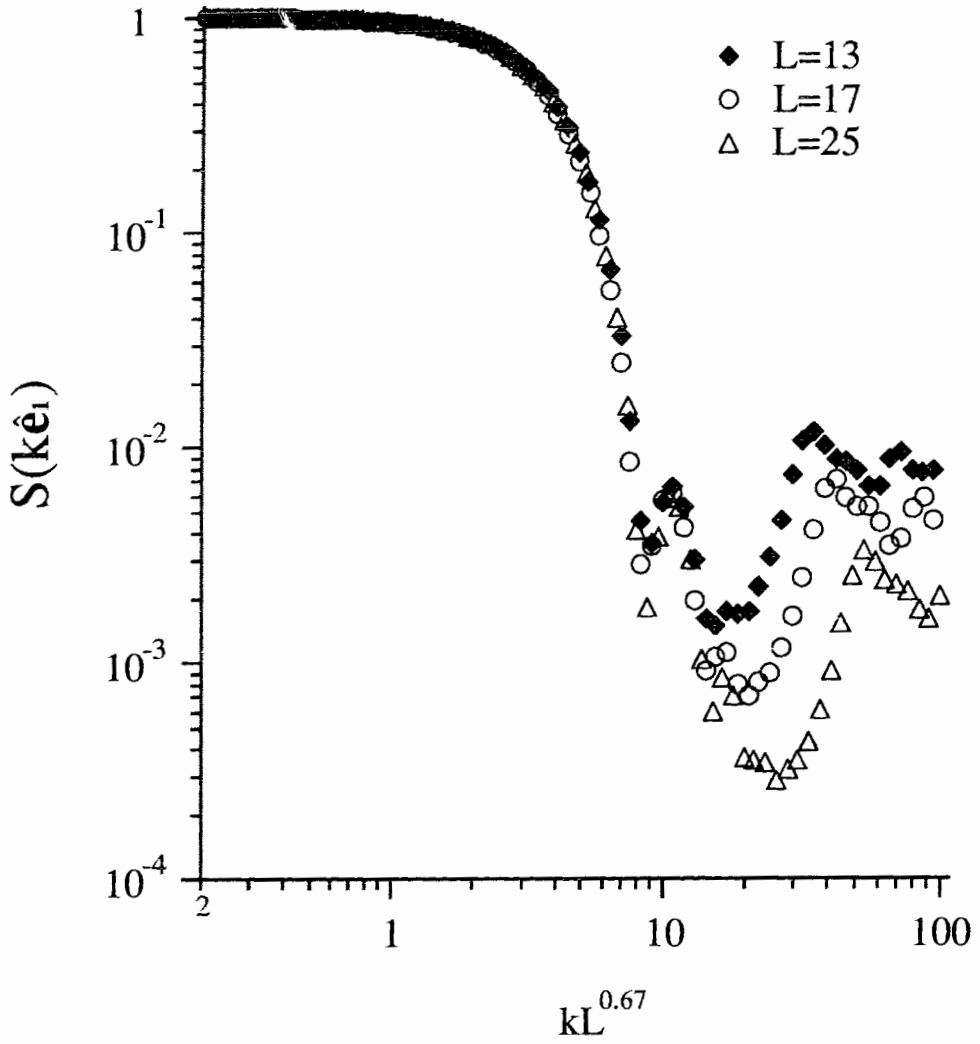

Figure 5.10: Structure factor $S(k\hat{\mathbf{e}}_2)$ plotted as function of $kL^{0.67}$ for $L = 13, 17, 25$ at $\beta = 1.00$.

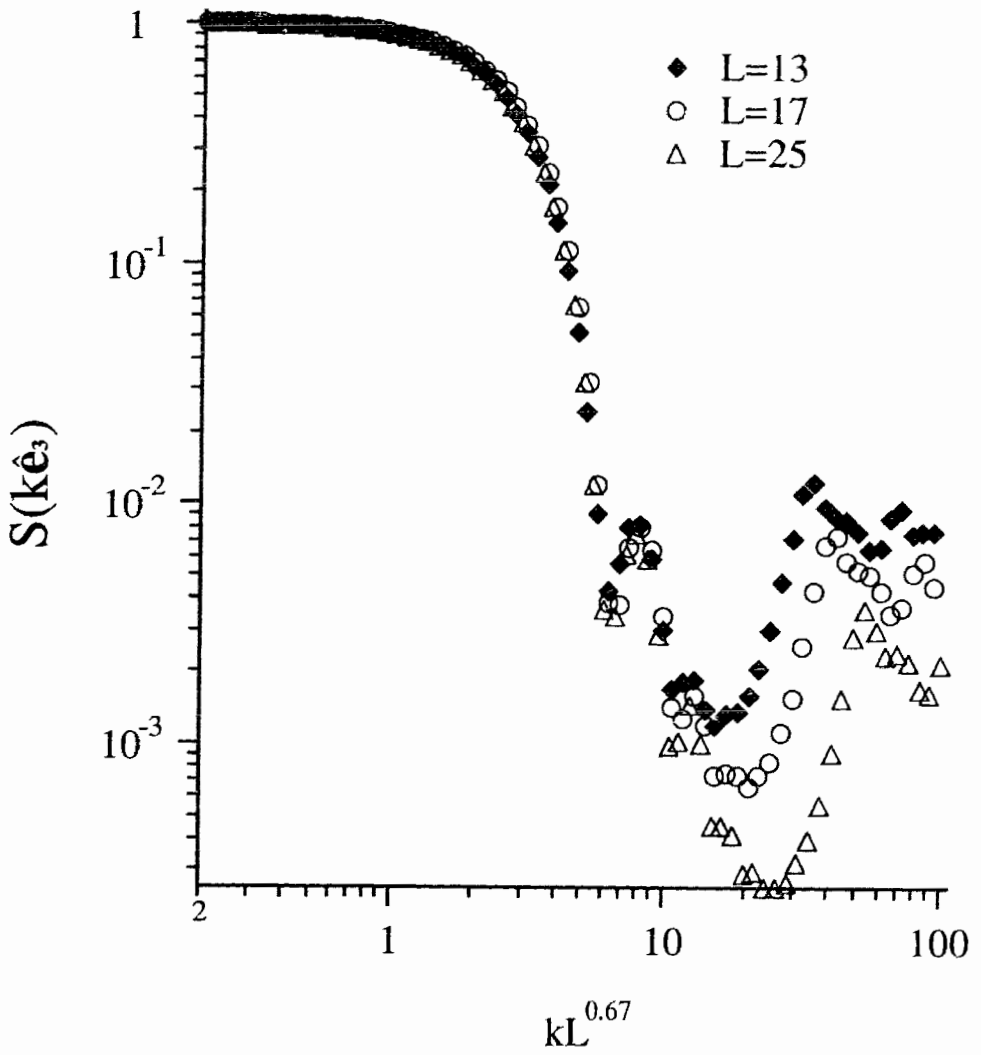

Figure 5.11: Structure factor $S(k\hat{\mathbf{e}}_3)$ plotted as function of $kL^{0.67}$ for $L = 13, 17, 25$ at $\tilde{\beta} = 1.00$.

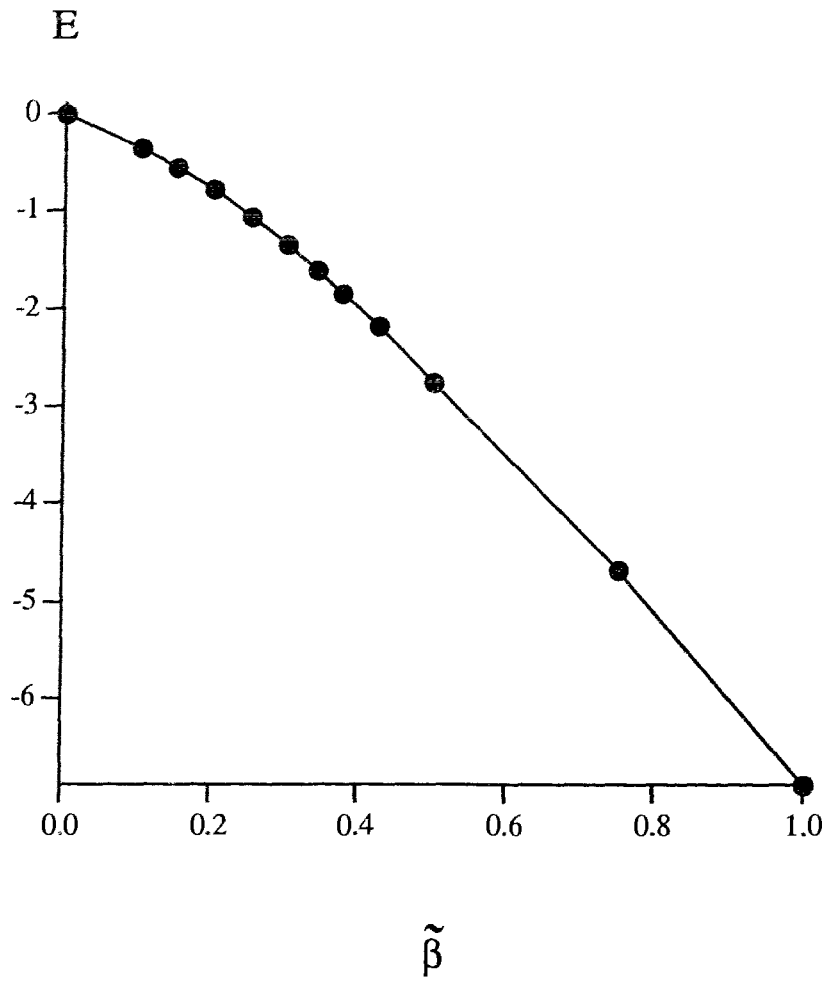

Figure 5.12: Energy $\langle E \rangle$ as function of $\tilde{\beta}$ for a membrane of size $L = 25$.

The specific heat, C, is given by (3.10). In contrast to the situation of a phantom membrane with curvature energy [19], where the transition from the flat phase to the crumpled phase is characterized by a strong peak in the specific heat, we find no indication whatsoever of a singularity in either the internal energy or the specific heat. This is similar to the behavior for the specific heat observed for polymer chains with attractive interactions in Monte Carlo simulations [50]: The specific-heat peak for a polymer chain of length, N, occurs at temperatures distinctly below the θ-point for the chain lengths simulated, and C is monotonously decreasing at temperatures near θ.

The position of the peak, $\theta_c(N)$, approaches the θ-point according to $(\theta - \theta_c) \propto N^{-1/2}$. I believe that this is also the case for tethered membranes. The membrane sizes which we have been able to simulate are small and the peak of the specific heat is far away from the transition point, $\tilde{\beta} \approx 0.2$, such that no peak was observed in the temperature range in which simulations were carried out.

We have also visually examined a large number of configurations, so as to develop some intuition about the behavior of this system. In Fig. 5.13 we display a typical configuration for a membrane at temperature $\tilde{\beta} = 0.25$. The quantitative results which we have obtained are calculated by averaging over a large number of sample configurations like this.

5.4 Discussion and summary

Lately, Baumgärtner and W. Renz [51, 52] studied a model membrane composed of impenetrable flexible plaquettes. They claimed that the intrinsic bending rigidity is absent since the hard cores have a zero size in their model, and their Monte Carlo studies revealed a crumpled phase, characterized by the scaling exponent $\nu = 0.81$. It seems to us that the effective bending rigidity is present, due to the geometrical constraints and impenetrability of the surface explicitly implemented in the model. Therefore, their conjecture [51, 52] that this model belongs to a different universality class than that of a strongly self-avoiding membrane is unclear and puzzling. In any case, the mechanisms which lead to a crumpled phase for this model and for ours are different.

The nature of the phases of equilibrium tethered membranes is determined by the free energy. For membranes with attractive interaction, it is energetically favorable to have folded and accordion-like conformations, whereas at the same time the increase in free energy due to creation of edges [28, 41], the loss of entropy at the edges and

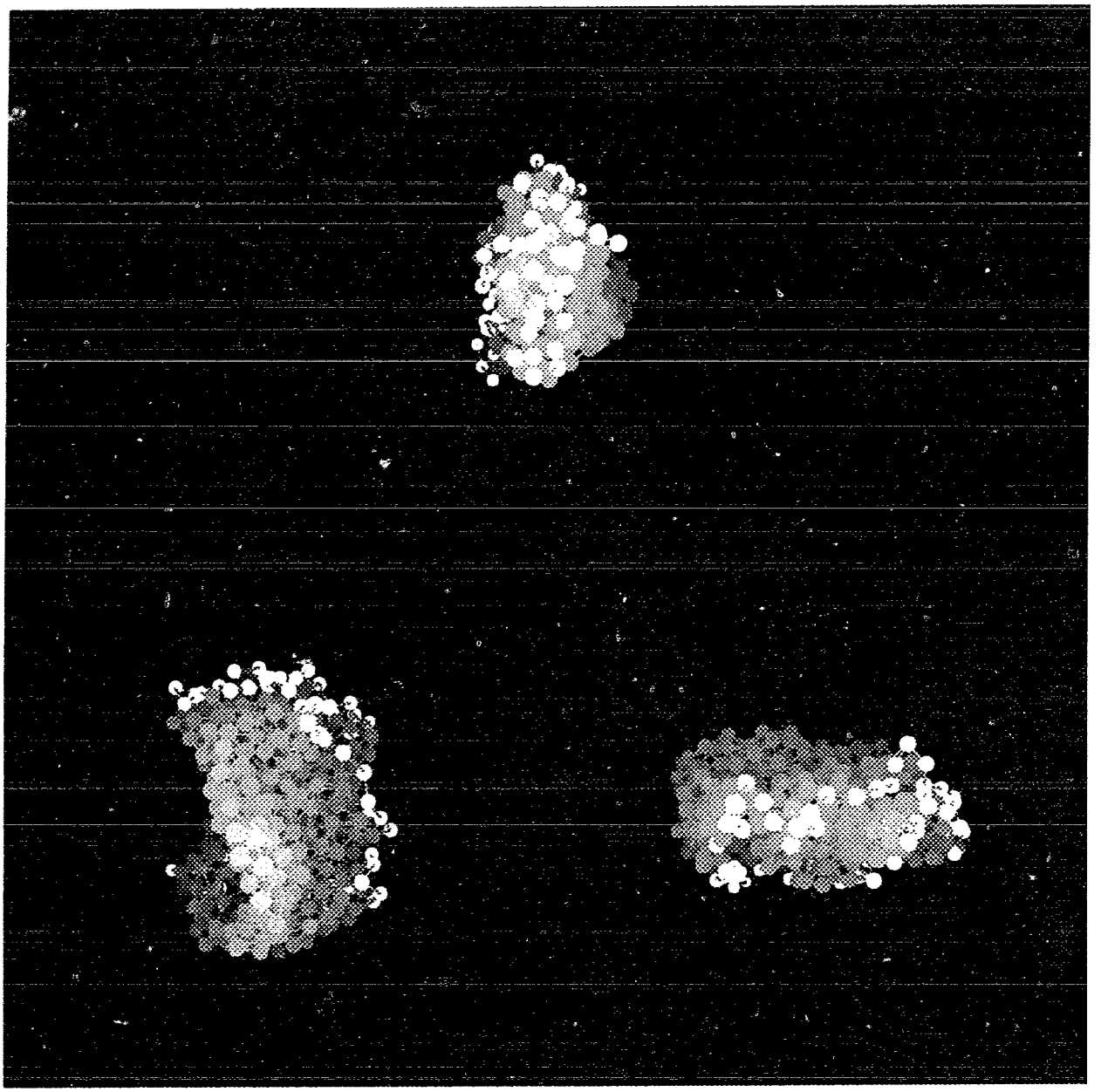

Figure 5.13: A configuration of a membrane of size $L = 25$ at $\tilde{\beta} = 0.25$, viewed from the three directions of the principal axes. The unshaded particles are on the perimeter of the membrane.

the repulsive entropic interactions between membranes [53], or parts of a membrane, tends to keep a certain distance between parts of the membrane. Consequently, the particles can not fully take advantage of the attractive potential. It is this competition that creates the crumpled phase in our model.

Although the model I have studied is similar to that used in Ref. [28], the phase diagram seems to be different. The authors of Ref. [28] carried out molecular dynamics calculations for a different model and concluded that the collapsed and flat phases are separated by one or more folded phases. However, they conjectured that a different sequence of transitions namely flat→crumpled→collapsed might also exist and, as stated above, we believe that this is the sequence in our model. A direct comparison of our results to those of Ref. [28] is difficult, as the scaling behavior of the principal moments and structure factor in the folded phase were not reported. It is, of course, conceivable that in a folded phase the radius of gyration, the principal moments and the structure factor are all characterized by an exponent $\nu \approx 0.8$. If this were the case, a distinction between crumpled and folded phases would become experimentally difficult and theoretically moot.

In summary, we have observed a transition from the flat phase of self-avoiding tethered membranes to an isotropically crumpled phase as function of temperature. We have also found that at still lower temperatures the equilibrium state is collapsed rather than crumpled. Our results are consistent with recent light-scattering experiments on suspended graphite-oxide sheets, in which a crumpled phase was observed over a range of the control parameter and a collapsed phase was also found [30, 31].

Bibliography

[1] *Statistical Mechanics of Membranes and Surfaces*, edited by D. R. Nelson, T. Piran and S. Weinberg (World Scientific, Singapore, 1989)

[2] Reinhard Lipowsky, Nature **349**, 475–481(1991)

[3] Stanislas Leibler, in Ref. [1]

[4] P. G. de Gennes and C. Taupin, J. Chem. Phys. **86**, 2294(1982)

[5] W. Helfrich, J. Phys. (Paris) **46**, 1263

[6] L. Peliti and S. Leibler, Phys. Rev. Lett. **54**, 690(1985)

[7] A. Baumgärtner and J.-S. Ho, Phys. Rev. A **41**, 5747–5750(1990)

[8] David H. Boal and Madan Rao, Phys. Rev. A **45**, R6947(1992)

[9] D. M. Kroll and G. Gompper, Science (in press)

[10] Theodore L. Steck, *Cell shape : determinants, regulation, and regulatory role,* edited by D. Stein Wilfred and Felix Bronner (Academic Press, San Diego, 1989)

[11] D. R. Nelson and L. Peliti, J. Physique **48**, 1085–1092(1987)

[12] P. G. de Gennes, *Scaling Concepts in Polymer Physics* (Cornell University Press, Ithaca, 1979)

[13] P. J. Flory, *Statistics of Chain Molecules* (Interscience Publishers, New York, 1969)

[14] B. Nienhuis, Phys. Rev. Lett. **49**, 1062(1982)

[15] Y. Oono, Advances in Chemical Physics **61**, 301(1985)

[16] Mehran Kardar and David R. Nelson, Phys. Rev. A **38**, 966–982(1988)

[17] Y. Kantor, M. Kardar, and D. R. Nelson, Phys. Rev. A **35**, 3056–3071(1987)

[18] S. F. Edwards, Proc. Phys. Soc. (London) **85**, 613(1965)

[19] Y. Kantor and D. R. Nelson, Phys. Rev. Lett. **58**, 2774(1987); Phys. Rev. A **36**, 4020–4032(1987)

[20] M. Plischke and D. H. Boal, Phys. Rev. A **38**, 4943(1988)

[21] F. F. Abraham, W. E. Rudge, and M. Plischke, Phys. Rev. Lett. **62**, 1757(1989)

[22] J.-S. Ho and A. Baumgärtner, Phys. Rev. Lett. **63**, 1324(1989)

[23] D. Boal, E. Levinson, D. Liu, and M. Plischke, Phys. Rev. A **40**, 3292–3300(1989)

[24] Edward Levinson, thesis, Simon Fraser University (1992)

[25] Gary. S. Grest, J. Phys. I France **1**, 1695–1708(1991)

[26] G. S. Grest and M. Murat, J. Phys. France **51**, 926(1990)

[27] Michael Plischke and Bertrand Fourcade, Phys. Rev. A **43**, 2056–2058(1991)

[28] Farid F. Abraham and Mehran Kardar, Science **252**, 419–422(1991)

[29] Damin Liu and Michael Plischke, Phys. Rev. A **45**, 7139–7144(1992)

[30] Terence Hwa, Etsuo Kokufuta, and Toyoichi Tanaka, Phys. Rev. A **44**, 2235(1991)

[31] Xin Wen, Carl W. Garland, Terence Hwa, Mehran Kardar, Etsuo Kokufota, Yong Li, Michael Orkisz, and Toyoichi Tanaka, Nature **355**, 426–428(1992)

[32] Terence Hwa, thesis, Massachusetts Institute of Technology (1990)

[33] Y. Kantor, M. Kardar, and D. R. Nelson, Phys. Rev. Lett. **57**, 791(1986)

[34] M. Kardar and D. Nelson, Phys. Rev. Lett. **58**, 1289(1987); Phys. Rev. Lett. **58**, 2280(E)(1987); J. A. Aronowitz and T. C. Lubensky, Europhys. Lett. **4**, 395(1987); B. Duplantier, Phys. Rev. Lett. **58**, 2733(1987)

[35] Bertrand Duplantier, in Ref. [1]

[36] J. Ambjorn, B. Dunrhus, and T. Jonsson, Nuclear Phys. **B316**, 526(1989)

[37] P. E. Rouse, J. Chem. Phys. **21**, 1272(1953)

[38] Farid F. Abraham and David R. Nelson, Science **249**, 393(1990)

[39] R. Lipowsky and M. Girardet, Phys. Rev. Lett. **65**, 2893(1990); Phys. Rev. Lett. **67**, 1670(1991)

[40] F. F. Abraham, Phys. Rev. Lett. **67**, 1669(c)(1991)

[41] G. Gompper and D. M. Kroll (unpublished)

[42] C. F. Schmidt, K. Svoboda, N. Lei, I. B. Petsche, L. E. Berman, C. R. Safinya, and G. S. Grest (unpublished)

[43] Farid F. Abraham and David R. Nelson, J. Phys. France **51**, 2653–2672(1990)

[44] K. Kremer, A. Baumgärtner, and K. Binder, Z. Physik B **40**, 331–341(1981)

[45] S. F. Edwards, J. Non-Cryst. Solids **4**, 417(1970)

[46] I. M. Lifshitz and I. M. Groberg, Soviet Phys. JETP **38**, 1198(1974)

[47] M. Nierlich, J. P. Cotton, and B. Farnoux, J. Chem. Phys. **69**, 1379(1978)

[48] C. F. Schmidt, K. Svoboda, N. Lei, C. R. Safinya, S. M. Block, and D. Branton (unpublished)

[49] F. F. Abraham and M. Goulian, Europhys. Lett. **19**, 293–296(1992)

[50] K. Kremer, A. Baumgärtner, and K. Binder, J. Phys. A: Math. Gen. **15**, 2879(1981)

[51] A. Baumgärtner, J. Phys. I France **1**, 1549(1991)

[52] A. Baumgärtner and W. Renz, Euro. Phys. Lett. **17**, 381(1992)

[53] S. Leibler and A. C. Maggs, Phys. Rev. Lett. **63**, 406(1989); S. Leibler in Ref. [1]